Role of Phosphatidylinositol 3-Phosphates and Their Regulators in Skeletal Muscle Development and Disease

by

Aaron N. Reifler

A dissertation submitted in partial fulfillment
of the requirements for the degree of
Doctor of Philosophy
(Neuroscience)
in the University of Michigan
2013

Doctoral Committee:

Associate Professor James Dowling, Co-Chair, SickKids Hospital, Toronto
Professor Eva L. Feldman, Co-Chair
Professor John Y. Kuwada
Professor Michael D. Uhler
Professor Lois S. Weisman
Associate Professor Haoxing Xu

To me, truth *is not some vague, foggy notion.* Truth *is real. And, at the same time, unreal. Fiction and fact and everything in between, plus some things I can't remember, all rolled into one big 'thing'. This is* truth*, to me.*

— Jack Handey, 1992

2013

Dedication

To my wife, Bach-Tuyet Tammy Nguyen, who has paradoxically grounded me and given me every reason to strive to reach new heights. *Anh yêu em nhiều lắm*.

To my other two best friends, Xander and Tian, for while we may have a little gap in experience, their vim for life brings continual excitement to my own.

Acknowledgements

If the well used quote, “it takes a village…” has any bearing on my own development, then my time in the Dowling and Feldman labs epitomizes that sentiment beyond description. From the top down in the labs, there was always the feeling of cooperation and camaraderie.

First and foremost, I thank Jim, for picking me up and believing in me when I was counting myself out, for doing all of the things a mentor could be asked to do to motivate and coax the best out of me, and for never holding back words of advice to help me grow. Equally, I thank Eva for jumping in to my defense to give me solid ground, when it seemed like the firmament was moving under my feet.

Thank you to the many lab mates from the Dowling and Feldman labs. I owe a great deal of thanks to Xingli, with whom a vast portion of my dissertation work was accomplished: Her care of the mice (thanks to them, too), her adept surgical skills, her beautiful westerns, and her enthusiasm to always press forward with whatever experiments we had to do. Thanks to Carey and Crystal for their enormous help with the final push to the finish line, not to mention their efforts to keep me calm. Thanks to Stacey, for helping with the writing and organization of my dissertation, and being the eyes and ears for Eva at times. Thanks to Angela, for help with all of my work with the zebrafish, and for making injection days filled with music. Thanks to Trent for helping with all the little things that made the lab run. Thanks to Annie and Eric, who provided helpful discussions on my projects, and helped me with my writing. Thanks to Sam for his cheerful attitude and delicious honey. Thanks to BT for being a great lab mate. Thanks to Elizabeth for giving me inspiration and helping me get started in the lab.

Thanks to my collaborators on campus and at other institutions. Thank you Miriam, for giving me the basis for my first publication. Thank you Bob and Sue for your labs’ contributions. Thank you Carol, Guy, and Linda for all the support and help with

experiments for my first data chapter. Thank you Dan, for putting up with Jim and me for the work on the PI3-kinase mutants. We wouldn't have gotten nearly as far without you and your team, including Ashley, Steve and of course, Joel, who put out a heroic effort to find a membrane repair defect in those FDB's.

Thanks goes to Mike, for being with me from my first day in the program, when I rotated in his lab, through the trials and obstacles of candidacy, always ready to write a recommendation letter or lend me helpful advice, and for staying in my committee to the end. I would like to thank John, for sticking with me and supporting me as a committee member from the start. Thank you to Lois and Haoxing, for providing colorful conversations about PtdIns(3)*P*, PtdIns(3,5)P_2, and on occasion, PtdIns(5)*P*. I would also like to thank Lois for taking me under her wing in San Fransisco, and making sure I didn't get left out.

I would also like to thank all of the faculty members who mentored me and guided me through my time in my program. I had a strong relationship with Hisashi, from our time working together during my rotation and on my NS700 talk. I had a very enjoyable, however brief, rotation with Brian that I will cherish. I also had numerous occasions to interact with faculty across campus, in a variety of mentorship situations.

I want to thank Dan and all of the members of the Goldman lab for three years that were filled with many memories and exciting discoveries. I am able to look back on how much I learned about myself, about the field of retinal regeneration, and almost everything I know about zebrafish. I thank Curtis for being an incredible support for me since he joined the program, always ready to engage in deep intellectual discussions about our work, or have spiritual conversations late at night, or swap tales of our adventures exploring the great wilderness, and for all the rest that makes him a dear friend. Thanks to Rajesh and Pete for being great friends and teachers. Rose, Jin, Xiao-Feng, Mike and many others who passed through the lab were great colleagues.

Thank you Valerie and Rachel, for helping me and others through many challenging times, as well as keeping the program running as smoothly as it does. Thank you Ed, Rachael, Jill, Steve, Peter, and Les for your official roles as leaders in the Neuroscience Program during my tenure.

Thank you to my classmates, colleagues, and particularly, my cohort: Amber, Adam, Agnes, Alaina, Austin, Sam, Yoshi, Matt, Cole and Mel, who shared in many of the same experiences of graduate school, and have always inspired me to follow my own path. There are so many others in my program and at the school who made a significant impact on my time in graduate school, but will unfortunately go unnamed in this section.

Thinking back over the years, I have been fortunate to have many exemplary people make a significant impact on my life, helping to shape me into who I am. Of my many teachers, two of my science teachers Mr. VonEhr and Mr. Bixler deserve particular mention for instilling a greater sense of accomplishment and empowerment in becoming a scientist.

I have had many close friends who hopefully know who they are without their names in writing, but Eric, Jarod and Jon will always be the first among the many, since my college days.

Lastly, and without a doubt, most importantly, are my loved ones and family, who are not chosen, but would be chosen in a heartbeat, for their unconditional support and love through many challenging times, and for ultimately who I am today. My mother and father, my stepmother, my grandparents, my brother and sister, and my many aunts, uncles and cousins are all amazing people, and I am always amazed at how fortunate I am to have their love. I have infinite gratitude towards my wife, Tammy, whom I absolutely did choose, and do choose again and again, and her very large family, who have always made me feel as welcome and integral as my own kin. And of course, the two people who will always have my undying love, for whom I would give up anything I had to give, my true friends, conspirators and partners, Xander and Tian, on whom I have already placed the heavy burden of expectation and nachas.

Preface

I think that a preface is a very nice thing to have in a personal work of writing. It makes the transition from the dedication and acknowledgements to more heady topics, in that it begins to introduce the intellectual content, rather than the [extensive] emotional content of my graduate work, yet allows a more casual voice. Here is a brief introduction to my background, my interests and my thoughts on this work, to give the reader an opportunity to put this writing into a frame of reference. Many of the goals of this research have a clinical application, or at least in the rationale, and while my mentors are physicians, I am by no means a medical doctor. I have a degree and teaching certification in secondary education, with a major in French. How that leads to a Ph.D. in Neuroscience is anyone's idea.

Even after joining the graduate program, I did not come to study the role of phosphatidylinositols (PtdIns) in muscle by a linear path. I spent a great deal of time exploring the identity and development of neurons, or neuronal precursors, in the laboratories of Drs. Mike Uhler, Hisashi Umemori and Dan Goldman. This exciting field led me to the investigation of stem-cell properties of Müller glia and their role in retinal regeneration of the zebrafish. I spent three years working on various paradigms and models in the zebrafish, working on ways to track and manipulate cell identity. When that time was over, I did not intend to dramatically switch fields.

In fact, after joining Dr. Jim Dowling's laboratory, I planned on working specifically with zebrafish, albeit in a somewhat new paradigm of muscle development, at least with an organism I knew fairly intimately. We primarily used morpholinos to silence translation or splicing of gene products, injecting them directly into zebrafish embryos at a single-cell stage post-fertilization. My first project in the zebrafish involved targeting a PtdIns 5-kinase, aptly named PIKfyve (Fab1 in yeast).

Not long after starting the zebrafish work, the opportunity to work on a mouse project with a fairly large scope became too enticing, especially when some hiccoughs in the zebrafish work hampered my progress. It was in this way that I began my studies of mouse muscle.

We had initiated a project to directly test the hypothesis that myotubular myopathy (MTM) was caused by a dysregulation—namely, a buildup—of PtdIns(3)*P* in cells, due to mutations in MTM1. The strategy for manipulating the system seems imminently simple on paper: reduce production of PtdIns(3)*P* on the MTM background, and cure the disease. Regulation of PtdIns(3)*P* is a highly dynamic and integral component of many cellular processes, involving many proteins that act as regulators or effectors of the lipid. Therefore, there are many targets (proteins) to choose from when aiming to shift the balance of PtdIns(3)*P* synthesis or metabolism.

This dissertation introduces and explains some of the targets of our manipulations, and provides insight in regard to the role of selected regulators of phosphatidylinositol 3-phosphate in skeletal muscle. The first chapter is an introduction to many of the topics covered in my studies, including the (difficult to say) phosphoinositides, or more specifically (and more difficult to say), phosphatidylinositol phosphates. The second, third and fourth chapters introduce unique lines of mice harboring genetic mutations targeted to skeletal muscle: (mainly) *Sac3/Fig4, Vps34/Pik3c3* and *PI3K-C2β/Pik3c2β*, respectively. The final chapter proposes work for the future, and some of the challenges awaiting future basic research and clinical practice.

Table of Contents

List of Figures

List of Tables

List of Abbreviations

AVM	autophagic vacuolar myopathies
CK	(serum) creatine (phospho-)kinase
CNM	Centronuclear myopathy
CMT	Charcot-Marie-Tooth
DNA	deoxyribonucleic acid
EEA1	early endosome antigen 1
EBD	Evan's blue dye
EGF(R)	epidermal growth factor (receptor)
ELISA	enzyme-linked immunosorbent assay
E/ANTH	epsin/AP180 N-terminal homology (domain)
FERM	Four-point one, Ezrin, Radixin, Moesin
FYVE	Fab1p, YOTB, Vac1p and EEA1 domain
GAPDH	glyceraldehyde-3-phosphate dehydrogenase
GLUT4	glucose transporter type 4
GRAM	glucosyltransferases, Rablike GTPase Activators and Myotubularin domain
GroP	Glycerophosphoinositol phosphates
H&E	hematoxylin and eosin
HEAT	Huntington, EF-3, PR65/A and mTOR domain
HPLC	high-performance liquid chromatography
IGF1	insulin-like growth factor 1
IIHC	indirect immuno-histological chemistry
Ins	*myo*-inositol
KO	knockout (mutant animal with genetic deletion)
LAMP1	lysosomal-associated membrane protein 1
LPA	lysophosphatidic acid
MD	muscular dystrophy

MTM	X-linked (centronuclear) myotubular myopathy
MTM1	myotubularin 1
MTMR2	myotubularin related protein 2
mTORC1	mammalian target of rapamycin complex 1
MVB	multi-vesicular body
O.C.T.	Optimal Cutting Temperature embedding medium (TissueTek)
P	phosphate
PAS	Periodic Acid Schiff
(qRT-)PCR	(quantitative real-time) polymerase chain reaction
PH	pleckstrin homology (domain)
PHD	plant homeodomain
PI	phosphoinositide
PIK3C2α	phosphoinositide 3 position kinase class II alpha
PIK3C2β[1]	phosphoinositide 3 position kinase class II beta
PIK3C3 (Vps34)	phosphatidylinositol three position kinase class III
PIKfyve	phosphoinositide kinase for five position containing a FYVE finger domain
PKB (also known as Akt)	protein kinase B
PKD	protein kinase domain
plt	pale tremor mouse
Ptd	phosphatidyl
PtdIns	phosphatidylinositol
PtdIns(3)*P*	phosphatidylinositol 3- phosphate
PtdIns(3,5)P_2	phosphatidylinositol 3,5-bisphosphate
PX	phox homology (domain)
(m)RNA	(messenger) ribonucleic acid
r.p.m.	revolutions per minute
RyR1	ryanodine receptor 1
SDH	succinate dehydrogenase (stain)
SD	standard deviation

[1] In mice, nomenclature for genes is represented in italics, while protein products are fully capitalized in roman type. Human genes are capitalized in italics, and protein products are romanized.

s.e.m.	standard error of the mean
SNP	single-nucleotide polymorphism
SPR	surface plasmon resonance
SR	sarcoplasmic reticulum
TUNEL	Terminal deoxynucleotidyl transferase-mediated dUTP nick end labeling
(h)Vps	(human) vacuolar protein sorting
WD40	beta-propeller domain or betatransducin repeats
WT	wild type (black 6 mouse strain, herein)

Abstract

X-linked myotubular myopathy (MTM) is a severe centronuclear myopathy, characterized by profound weakness and hypotonia at birth, early mortality, and significant morbidities. MTM results from mutations in the phosphoinositide phosphatase myotubularin (MTM1), which dephosphorylates the lipid substrates phosphatidylinositol 3-phosphate (PtdIns(3)*P*) and phosphatidylinositol 3,5-bisphosphate (PtdIns(3,5)P_2). We propose that dysregulation of PtdIns(3)*P* and PtdIns(3,5)P_2 leads to the disease state in MTM, and that these lipids play a significant role in muscle development and homeostasis. To elucidate the effect of PtdIns(3)*P* dysregulation in MTM, we examined several mouse models with targeted inactivation of phosphoinositide phosphatases (*Mtm1* and *Fig4*) and kinases (*Pik3c3* and *Pik3c2β*).

Previous studies showed that tissue-specific neuronal rescue of the spontaneously occurring *Fig4* mutation of pale tremor (*plt*) mice prevented overt muscle weakness and the development of obvious muscle abnormalities. Our studies confirmed that the changes in skeletal muscle observed in the *plt* mice were primarily related to denervation. *Fig4* deletion had previously been shown to rescue aspects of Mtmr2-dependent neuropathy, so we evaluated the effect of *Fig4* haploinsufficiency on the myopathy of *Mtm1*-knockout mice. Compared with $Mtm1^{-/Y}$ males, mice with the genotype $Fig4^{+/-}/Mtm1^{-/Y}$ displayed no improvement in muscle histology, muscle size, or longevity, indicating that reduction of FIG4 does not ameliorate the *Mtm1*-knockout phenotype.

To further investigate the function of PtdIns(3)*P* in skeletal muscle, we focused on the primary kinase responsible for its production, and created a muscle-specific conditional knockout of the class III PI 3-kinase, *Pik3c3*. This resulted in progressive disease characterized by reduced activity and death by two months of age. Histopathology demonstrated changes consistent with a murine muscular dystrophy.

Mechanistic evaluations revealed significant alterations in the autophagolysosomal pathway with mislocation of known dystrophy proteins to the lysosomal compartment. We present the first analysis of *Pik3c3* in skeletal muscle, and report a novel association between deletion of *Pik3c3* and muscular dystrophy.

In contrast, muscle-specific deletion of *Pik3c2β* caused no overt physiological defects by 11 months of age, other than impaired glucose tolerance. These studies demonstrate the critical role of PIK3C3 in muscle physiology and give insight to some of the mechanisms disrupted in muscle diseases.

Chapter 1:
Introduction

The focus of this dissertation is to examine the role of phosphatidylinositol phosphates (PtdIns*P*s)[2] and the kinases and phosphatases that regulate them in the context of skeletal muscle health. For an introduction to the topic, there is an overview and description of PtdIns*P*, including their structure, regulation and functions. Next, the focus shifts to two isoforms in particular, PtdIns(3)-monophosphate and PtdIns(3,5)-bisphosphate, that are described in detail. The connection of PtdIns*P*s to muscle disease focuses on the X-linked centronuclear myopathy: myotubular myopathy (MTM). Last is the introduction to chapters two through four, which describe projects involving the use of mice with mutations in specific kinases and phosphatases that regulate the phosphorylation of the PtdIns*P*-isoforms.

1.1 PtdIns*P*s

1-(3-*sn*-Phosphatidyl)-D-*myo*-inositol, or more simply, phosphatidylinositol (PtdIns), is the base for a family of lipid-phosphates, collectively referred to herein as PtdIns*P*s. These molecules participate in a number of signaling pathways and serve crucial roles in the organization and trafficking of membranes in cells. PtdIns*P*s are of relatively low-abundance, but are present in almost all cell types across eukaryotic species (De Camilli, Emr et al. 1996, Lindmo and Stenmark 2006, Volpicelli-Daley and De Camilli 2007, Nicot and Laporte 2008, Balla, Wymann et al. 2012, Falasca 2012, Maffucci 2012). Dysregulation of PtdIns*P*s has been implicated in a number of human diseases, including Charcot-Marie-Tooth (CMT) (Bolino, Bolis et al. 2004, Nicholson, Lenk et al. 2011), amyotrophic lateral sclerosis (ALS) (Chow, Landers et al. 2009), and

[2] Nomenclature for phosphatidylinositol phosphates as "PtdIns*P*" in this dissertation is based on guidelines from IUBMB and IUPAC (www.iubmb.org; http://www.chem.qmul.ac.uk/iupac/misc/phos2t8.html#t4).

other neuropathies and myopathies (Amoasii, Hnia et al. 2012, Hakim, Bertucci et al. 2012).

The synthesis and localization of PtdIns*P*s are regulated by phosphoinositide (PI) kinases and phosphatases that reversibly phosphorylate PtdIns at the 3-, 4- and 5-positions of the *myo*-inositol (Ins)[3] head group. This results in a group of seven unique and dynamically inter-convertible PtdIns*P* isoforms (Michell, Heath et al. 2006) (Figure 1.1). Regulation of PtdIns*P* metabolism is a highly conserved process with many of the genes encoding regulatory enzymes having close homologues across species (Boss and Im 2012). In fact, much of the seminal and ongoing work to understand the interactions among the various kinases and phosphatases that regulate PtdIns*P*s come from studies using *Saccharomyces cerevisiae*, as yeast provide a simple representative model of many similar processes involved in membrane and vesicle dynamics in mammals (Weisman 2006, Strahl and Thorner 2007).

One of the challenges to this line of work is in the detection of these lipids. There is a great interest and an ongoing effort to develop new techniques for detecting the individual phospho-isoforms of PtdIns*P* *in vivo*, but many of the analyses contained herein utilize indirect approaches to measure PtdIns*P*s. Some of these techniques take advantage of probes based on the recognition domains of proteins containing specific motifs for selecting a PtdIns*P* isoform. These domains are reviewed in detail (Lemmon 2003, Maffucci 2012), and allow for proper trafficking of proteins to membranes, and the membranes to their destinations.

While our understanding of the biology of PtdIns*P*s is constantly expanding, the scope of my work focuses primarily on the conversions of PtdIns to Phosphatidylinositol 3-phosphate (PtdIns(3)*P*) and of PtdIns(3)*P* to Phosphatidylinositol 3,5-bisphosphate (PtdIns(3,5)P_2), with some consideration of Phosphatidylinositol 5-phosphate (PtdIns(5)*P*) (Figure 1.2). The various PtdIns*P*s, and the mono-phosphorlyated forms, in particular, are very short lived, and can be metabolized within minutes under normal physiologic conditions (Michell, Heath et al. 2006). Of the PtdIns*P*s, PtdIns(3,5)P_2 is one

[3] The use of Ins for *myo*-inositol (Agrinoff's "turtle": see Fisher, S. K., J. E. Novak and B. W. Agranoff (2002). "Inositol and higher inositol phosphates in neural tissues: homeostasis, metabolism and functional significance." J Neurochem **82**(4): 736-754.) is not meant to diminish the importance of the other eight sterioisomers of inositol found in nature. For example, *scyllo*-inositol is one of the more aesthetically pleasing arrangements from a pure symmetry perspective.

of the least abundant, comprising only ~0.05% of the total population of PtdIns*P*s (Shen, Wang et al. 2011). Flux between PtdIns(3)*P* and PtdIns(3,5)P_2 regulates processes including endocytosis, endosomal trafficking, and autophagy (Itoh and Takenawa 2002, Payrastre 2004, Di Paolo and De Camilli 2006, Michell, Heath et al. 2006, Lecompte, Poch et al. 2008).

PtdIns(3)*P* is critical in the initiation of autophagosome formation, recruiting and organizing effectors that elongate and close the membrane (Vergne and Deretic 2010). PtdIns(3)*P* has been shown to be localized to the limiting membranes of early endosomes, and is also seen to be internalized in the yeast vacuole (Gillooly, Morrow et al. 2000). When individual regulators of PtdIns(3)*P* are mutated or inhibited, negative consequences have been observed including abnormal vacuolization in cells, defective autophagy, neurodegeneration, and muscle diseases among others (Vergne and Deretic 2010, Rommel, Vanhaesebroeck et al. 2011). Some genetic mutations, as in the case of *Pik3c3*, are embryonic lethal in mice (Zhou, Takatoh et al. 2011).

PtdIns(3)*P* is created primarily through phosphorylation of PtdIns at the 3 position by PI 3-kinases (PI3Ks) (Backer 2008, Meijer and Klionsky 2011), or through dephosphorylation of PtdIns(3,5)P_2 by FIG4 (Jin, Chow et al. 2008). In yeast, there is only one kinase known to produce PtdIns(3)*P*, and that is *Vps34*, the Class III PI3K known as *Pik3c3* in mammals. There are three classes of mammalian PI3Ks that are capable of producing PtdIns(3)*P* from PtdIns *in vitro*, with varying tissue expression and substrate specificity (Foster, Traer et al. 2003, Yan and Backer 2007, Vanhaesebroeck, Guillermet-Guibert et al. 2010). The Class I PI3Ks contribute specifically to the formation of PtdIns(3,4,5)P_3 *in vivo,* while PIK3C3 and the α- and β-forms of the Class II PI3Ks are responsible for PtdIns(3)*P* in mammalian cell types.

A group of related 3-phosphatases that convert PtdIns(3)*P* to PtdIns and also PtdIns(3,5)P_2 to PtdIns(5)*P* is a subset of the myotubularin related (MTMR) protein family, including MTM1, MTMR1, MTMR2, MTMR3, MTMR4, MTMR6, MTMR7, MTMR8 and MTMR14 (Vergne and Deretic 2010). Mutations in *MTM1* result in X-linked myotubular myopathy, with *MTMR14* playing a significant role as a disease modifier (Dowling, Low et al. 2010). Mutations in *MTMR2* and *MTMR13* result in forms of CMT neuropathies (Amoasii, Hnia et al. 2012). As the interconversion of PtdIns(3)*P*

to PtdIns(3,5)P_2 is highly important in regulating autophagic pathways, MTMRs have been shown to play an important role in activation and control of autophagy under both normal and starvation conditions (Dowling, Low et al. 2010, Vergne and Deretic 2010). Many of the MTMRs are capable of forming dimmers with other family members, increasing specificity and activity of the phosphatases (Clague and Lorenzo 2005). Additionally, it has been shown that certain MTMRs, such as MTM1 and MTMR2, bind with the regulatory subunit (PIK3R4) of the primary 3-kinase responsible for creating PtdIns(3)*P*, and thereby act as an inhibitor of phosphorylation in addition to their function as phosphatases (Cao, Laporte et al. 2007, Vergne and Deretic 2010). Extensive studies of the relationship between MTM1 and MTMR14 in zebrafish showed a significant deleterious effect on skeletal muscle, recapitulating features of the disease state seen in humans with MTM1 mutations (Dowling, Low et al. 2010).

Since its first reports in 1997 (Dove, Cooke et al. 1997, Whiteford, Brearley et al. 1997), PtdIns(3,5)P_2 has gained appreciation for its ever-increasing number of proposed roles, including the initiation of autophagy and other processes involved in cellular trafficking (Ho, Alghamdi et al. 2012, McCartney, Zhang et al. 2013). One of the most consistent phenotypes from PtdIns(3,5)P_2 dysregulation is the formation of enlarged vacuoles, indicating a failure to properly regulate membrane trafficking between endosomes and lysosomes. Deletion of key components that regulate interconversion between PtdIns(3)*P* and PtdIns(3,5)P_2 in yeast results in vacuoles with lower acidity than in wild type vacuoles (Yamamoto, DeWald et al. 1995, Bonangelino, Catlett et al. 1997). PtdIns(3,5)P_2 also plays a role in cytosolic assembly of nuclear-translocating factors such as Cti6-Cyc8-Tup1 complexes by way of a binding motif in Tup1 (Han and Emr 2011). In addition, work from the Xu lab has discovered a very important role for PtdIns(3,5)P_2 in the activation of lysosomal ion channels (Shen, Wang et al. 2011). Several studies have also described a role of PtdIns(3,5)P_2 in the activation of the ryanodine receptor in cardiac (Touchberry, Bales et al. 2010) and skeletal muscle (Shen, Yu et al. 2009).

PtdIns(3,5)P_2 is primarily generated from PtdIns(3)*P* by the action of PIKfyve, a PtdIns 5-kinase that functions in a complex of proteins in yeast that includes the PtdIns 5-phosphatase, Fig4, and regulatory proteins such as Atg18, Vac14, and Vac7 (Gary, Sato et al. 2002, Duex, Tang et al. 2006, Jin, Chow et al. 2008, Zolov, Bridges et al. 2012).

PtdIns(3,5)P_2 is metabolized by FIG4 (Sac3) to regenerate PtdIns(3)*P*, and by a family of three-position phosphatases, collectively known as myotubularin-related (MTMR) proteins, to generate PtdIns(5)*P* (Robinson and Dixon 2006, Tosch, Rohde et al. 2006, Dyson, Fedele et al. 2012, Hakim, Bertucci et al. 2012). Reduced abundance of FIG4 protein destabilizes PIKfyve, resulting in a threefold reduction of PtdIns(3,5)P_2 relative to total PtdIns levels (Chow, Zhang et al. 2007).

1.2 PtdIns*P*s are regulators of muscle development and homeostasis

Development of proper skeletal muscle mass and function depends on a signaling axis involving the insulin like growth factor (IGF), protein kinase B (PKB or Akt), and mammalian target of rapamycin complex 1 (mTORC1) (Hamilton, Philp et al. 2010). While the exact process of muscle growth is still not completely clear, there is a direct pathway from PtdIns(3,4,5)P_3 dependent activation of Akt that leads to signaling pathways to increase muscle mass (Bodine, Stitt et al. 2001). Inhibition of phosphorylation or activity of the kinases in the pathway result in muscle atrophy and prevent muscle growth (Bodine, Stitt et al. 2001).

Muscle atrophy has been shown to be regulated by ubiquitin ligases such as MuRF1 and Atrogin-1, which target thick filament components of sarcomeres for degradation by the proteasome (Glass 2010). FoxO transcription factors are responsible for the activation of these ubiquitin ligases by transcriptional signaling pathways, but their activity is neutralized by Akt-dependent phosphorylation, causing the factors to be excluded from the nucleus (Glass 2010). This shows that Akt control of muscle growth is accomplished through up-regulation of hypertrophy and down-regulation of atrophy pathways.

The FoxO transcription factors also play a significant role in other aspects of muscle homeostasis. Following starvation, muscle begins a process of autophagy in order to shut down certain elements of the cell to reduce energy expenditure and recycle other elements for additional sources of energy. Some of the genes induced in muscle following starvation include Bnip3 and Bnip3l, which are directly activated by FoxO3 binding to enhancers (Mammucari, Milan et al. 2007). Constitutively active Akt is

sufficient to abrogate the effects of starvation on transcriptional up-regulation of these genes, as well as other genes that are central to autophagic pathways, such as Cathepsins, Atrogin-1 and LC-3, indicating yet another role for PtdIns(3,4,5)P_3 regulated Akt activity (Mammucari, Milan et al. 2007). As the network of PtdIns*P* isoforms is highly interconnected, disruption in any of their regulators could potentially have an effect on muscle development or homeostasis.

In addition to regulation of muscle mass, insulin sensitive glucose transport is another area that relies upon PtdIns*P* signaling cascades (Bridges and Saltiel 2012). PtdIns*P* isoforms directly control various aspects including recycling, translocation and fusion of GLUT4-containing vesicles that enable the clearing and uptake of blood glucose into the muscle (Bridges and Saltiel 2012). Much of this regulation is accomplished through PtdIns(3,4,5)P_3 activation of Akt and important control of exocytosis and endocytosis by PtdIns(4,5)P_2 (Di Paolo and De Camilli 2006).

As GLUT4 continually traffics between the plasma membrane and vesicles that are internalized, recycled and pre-exocytic, PtdIns(3)*P* is also an important isoform in the processeses (Bridges and Saltiel 2012). PtdIns(3)*P* appears to be present in various locations within the cell, and numerous studies have shown the presence of accumulated pools of PtdIns(3)*P* at the plasma membrane is co-incident with increased GLUT4 trafficking and glucose transport in response to insulin (Bridges and Saltiel 2012). However, PtdIns(3)*P* appears to be involved in the localization of GLUT4 to points of fusion, and not in the actual process of fusion, which is dependent on other PtdIns*P* isoforms (Bridges and Saltiel 2012). These findings and others suggest that specific PtdIns 3-kinases may serve different functions depending on subcellular localization as well as other signaling cascades (Maffucci 2012).

In addition to the PI3Ks' importance in regards to regulation of insulin signaling, another kinase regulating PtdIns*P* also has a significant impact on insulin regulation: the PtdIns 5-kinase, PIKfyve, known as Fab1 in yeast (Duex, Tang et al. 2006). PIKfyve has a very complicated relationship with the phosphatase FIG4 (sometimes referred to as Sac3 (Sbrissa, Ikonomov et al. 2007)), and the two proteins form a complex with the scaffolding protein, VAC14, to regulate the interconversion between PtdIns(3)*P* and PtdIns(3,5)P_2 (Duex, Tang et al. 2006). In this way, FIG4 can be thought of as a sort of

amphibious enzyme, catalyzing both production and turnover of PtdIns(3,5)P_2. Nonetheless, mutations in the two genes result in highly deleterious outcomes, with *Fig4*$^{-/-}$ resulting in numerous neurological defects in a form of CMT and early mortality and *Pikfyve*$^{-/-}$ resulting in early embryonic lethality (Chow, Zhang et al. 2007, Ikonomov, Sbrissa et al. 2011).

As null mutations in *pikfyve* are not viable, Shisheva and colleagues created a mouse with a muscle-specific deletion using a floxed gene of *pikfyve* (Ikonomov, Sbrissa et al. 2011). These mice exhibited significant glucose intolerance and muscle insulin resistance at an early age, followed by increased body weight and adiposity (Ikonomov, Sbrissa et al. 2013). Levels of PtdIns(3,5)P_2 and PtdIns(5)*P* were shown to be reduced by *in vitro* lipid kinase activity assays only in skeletal muscle and heart lysates. The increases in body weight and adiposity are curious due to the lack of increased fasting blood glucose levels by 6 months of age. However, by 10 weeks of age, the knockout mice showed significantly increased levels of insulin measured from plasma in fasting animals, becoming more prominent by 6 months. Therefore, hyperinsulinemia without increased blood glucose could play a role in these observed effects (Ikonomov, Sbrissa et al. 2013).

Studies of myotubularins suggest additional important roles for PtdIns(3)*P* and PtdIns(3,5)P_2 in regulation of skeletal muscle health (Laporte, Bedez et al. 2003, Gibbs, Feldman et al. 2010, Romero-Suarez, Shen et al. 2010). The mammalian MTMR family contains 15 members encoding phosphatases that primarily dephosphorylate PtdIns(3)*P* and PtdIns(3,5)P_2 (Hnia, Vaccari et al. 2012). Mutation of *MTM1*, the canonical member of this gene family, causes myotubular myopathy (MTM), a severe congenital onset muscle disease associated with altered muscle structure and profound muscle weakness (Laporte, Hu et al. 1996). Analyses of lipid content in affected muscle reveals increased levels of PtdIns(3)*P* and possibly PtdIns(3,5)P_2 in skeletal muscle (Pierson, Dulin-Smith et al. 2012). Mutation of *MTM1* compromises multiple aspects of muscle function (Amoasii, Hnia et al. 2012), most notably, excitation-contraction (EC) coupling (Dowling, Vreede et al. 2009), the process by which neuronal stimulation to muscle is translated into calcium dependent muscle contraction. Specifically, *MTM1* mutations lead

to severe abnormalities in the structure of the EC coupling machinery (Al-Qusairi, Weiss et al. 2009, Dowling, Vreede et al. 2009).

In addition, MTM1 plays a significant role in numerous aspects of muscle physiology including regulation of autophagy (Vergne and Deretic 2010), proper function of the neuromuscular junction (Dowling, Joubert et al. 2012), desmin intermediate filament architecture (Hnia, Tronchere et al. 2011), and other aspects of muscle activity such as EC coupling (Dowling, Vreede et al. 2009). Autophagy is robustly induced in skeletal muscle following periods of fasting or denervation, and can be maintained at much higher levels and longer durations than in many other cell types (Sandri 2010). When autophagy is blocked, muscle wasting is accelerated during periods of fasting and denervation (Masiero, Agatea et al. 2009).

Proper function of the neuromuscular junction can be evaluated through tests of fatigability and exercise intolerance. Knock-in (KI) of a MTM1 missense mutation (p.R69C) in adult mouse skeletal muscle results in significant exercise intolerance and fatigable weakness (Dowling, Joubert et al. 2012). Furthermore, treatment with an acetylcholinesterase inhibitor, pyridostigmine, reversed the effects of the KI by modest gains in grip strength and larger increases in treadmill endurance, suggesting a link between disease pathogenesis seen in myotubular myopathy due to the lack of phosphatase activity and the overall condition of the neuromuscular junction (Dowling, Joubert et al. 2012).

Another critical role for MTM1 in muscle is found in the interactions between the phosphatase and desmin, an intermediate filament essential for positioning and movement of organelles, structural support throughout the cytoplasm and nucleus of the cell, and a means to reduce mechanical and nonmechanical stress such as during muscle contraction (Hnia, Tronchere et al. 2011). MTM1 interacts with desmin *in vitro* and in muscle, and plays a significant role in mitochondrial dynamics and motility, accounting for some of the disease characteristics of myotubular myopathy (Hnia, Tronchere et al. 2011).

MTMR14 is another myotubularin family member that is important for muscle function (Shen, Yu et al. 2009). Loss of MTMR14 in mice results in spontaneous leakage of calcium from sarcoplasmic reticulum and causes impaired EC coupling (Shen, Yu et

al. 2009). Further studies in zebrafish revealed that unlike mutations in MTM1, loss of MTMR14 alters EC coupling without significantly changing the underlying structure of the EC coupling machinery (Dowling, Low et al. 2010).

Direct application of PtdIns(3,5)P_2 increases calcium release from microsomes containing the intracellular ryanodine receptor calcium release channel (RyR1), a critical component of the EC coupling apparatus (Touchberry, Bales et al. 2010). Thus, direct regulation of RyR1-dependent stimulated calcium release may represent one important role of PtdIns(3,5)P_2 and MTMR14.

1.3 Muscle diseases

Muscle is a highly specialized, highly ordered and highly demanded organ that requires precisely coordinated activation. In addition, muscle plays significant roles in metabolic processes such as glucose processing and glycogen storage. Due to the particular needs of muscle cells, there are many processes that are unique in muscle, in terms of structural components and membranes. Furthermore, over the course of development, muscle tissue goes through stages of maturation that can be compromised by genetic mutations that result in numerous diseases with etiologies deriving from neuronal connectivity, extra-cellular matrix components, integral membrane composition or any number of signaling pathways (Grounds and Shavlakadze 2011). Some of the diseases that affect children include the congenital myopathies and muscular dystrophies, which are broad categorizations of numerous disorders, many of which have unknown genetic origin (North 2008, Rahimov and Kunkel 2013).

1.3.1 Congenital myopathies

Congenital myopathies are characterized by a constellation of distinctive morphological abnormalities in muscle biopsies that are detected perinatally after diagnosis with certain muscle weaknesses, such as in stereotypic facies and respiratory difficulties (North 2008). The individual classes of congenital myopathies are primarily diagnosed by features in muscle pathology, and there is a great deal of heterogeneity in

genetic etiologies (North 2008). Additionally, mutations in the same gene can cause multiple pathologies, and in some cases even differences of classification within the same individual when biopsied at different ages (Jungbluth, Zhou et al. 2007). This is in contrast to muscular dystrophies, which are typically differentiated by gene or mechanism of disease (North 2008). The four primary groups by morphology include myopathies with centralized nuclei, myopathies with protein accumulation, myopathies with cores and myopathies with fiber size variation (North 2008).

The centronuclear myopathies (CNM) are a subset of congenital myopathies classified in accordance with symptoms including early-onset muscle weakness and muscle biopsies that reveal extensive internalized or centralized nuclei without evidence of degeneration or regeneration (Das, Dowling et al. 2011). The diseases have a range of severity, in part due to the heterogeneity of genetic factors, which include autosomal-dominant forms, such as in mutations of dynamin-2 (*DNM2*), autosomal-recessive forms, such as in amphyphysin-1 (*BIN1*) and *RYR1* mutations, and the X-linked form (MTM), due to mutations in *MTM1* (Jungbluth, Wallgren-Pettersson et al. 2008, Nance, Dowling et al. 2012).

As previously introduced, MTM is one of the most severe neurologic disorders to affect children, characterized by profound weakness and hypotonia at birth, persistent life-long disabilities including wheelchair and ventilator dependence, and early mortality (Jungbluth, Wallgren-Pettersson et al. 2008, Das, Dowling et al. 2011). The X-linked gene *MTM1* is a lipid phosphatase that has been shown *in vitro* to specifically target PtdIns(3)*P* and PtdIns(3,5)P_2 for dephosphorylation (Taylor, Maehama et al. 2000). As predicted by the preferred substrate for MTM1 being PtdIns(3)*P*, levels of PtdIns(3)*P* are significantly elevated in animal models of MTM, in which *Mtm1* is mutated or deleted (Amoasii, Hnia et al. 2012, Pierson, Dulin-Smith et al. 2012).

1.3.2 Muscular Dystrophies

Unlike the congenital myopathies, muscular dystrophies involve the progressive degeneration and weakening of muscle, and are closer tied to specific genes whose mutations lead to numerous muscle-wasting and neuromuscular disorders (Rahimov and

Kunkel 2013). One of the most common diseases affecting approximately 1 in 3500 boys is Duchenne Muscular Dystrophy (DMD), caused by mutations in the gene encoding dystrophin, located on the X chromosome (Rahimov and Kunkel 2013). Dystrophin sits on the intracellular membrane of muscle, and interacts with other intracellular proteins, transmembrane proteins and extracellular proteins, collectively known as the dystrophin-associated protein complex, to allow the cell to withstand the enormous mechanical stress generated by sarcomeres (Rahimov and Kunkel 2013).

While DMD is the result of a defect in proper connectivity between the cytoskeleton and the extracellular matrix, other dystrophies manifest from mutations in genes that affect glycosylation of α-dystroglycan, disruption in the extracellular matrix, impaired signaling at the sarcolemma, and defective sarcolemmal repair, among others (Rahimov and Kunkel 2013). These defects can be recapitulated in vertebrate animal models with a high degree of fidelity, and studies involving mutant mice and zebrafish are currently being used to examine the disease mechanisms and potential drug treatments (Gibbs, Horstick et al. 2013).

1.4 Directed interference of PtdIns3*P* regulation by gene knockout of selected kinases or phosphatases has mixed results

This dissertation project is focused on understanding the roles and functions in skeletal muscle of specific kinases and phosphatases that regulate the phosphorylation of PtdIns. The following sections describe the specific aims of this work, and include background and rationale for the projects.

1.4.1 Mtm1 knockout mice: a model of human Myotubular myopathy

Through the use of vertebrate model systems of MTM, the specific function(s) of myotubularin *in vivo* are beginning to be uncovered (Buj-Bello, Laugel et al. 2002, Dowling, Vreede et al. 2009, Beggs, Bohm et al. 2010). Of particular interest are two mouse models of MTM, the first created by targeted inactivation of the myotubularin gene (Buj-Bello, Laugel et al. 2002), and the second by a knockout mouse model (Al-

Qusairi, Weiss et al. 2009). The first mice exhibited a severe, progressive skeletal myopathy reminiscent of the human disease; they also displayed the pathognomonic histopathologic changes of MTM. The two major findings to emerge from this initial study were as follows: first, that diseased muscle develops normally and develops pathologic changes only after myogenesis is complete; and second, that disease pathogenesis is muscle cell autonomous (and not due to motor neuron dysfunction). Buj-Bello and colleagues later confirmed these findings with a knockout mouse model; they further uncovered the fact that tubulo-reticular abnormalities precede the formation of central nuclei and occur coincident with disease onset (Al-Qusairi, Weiss et al. 2009, Dowling, Vreede et al. 2009). Despite such new knowledge acquired from these model system studies, much remains to be understood about the function of myotubularin and the pathogenesis of MTM.

1.4.2 Aim 1: To determine a muscle specific role for FIG4

The second chapter is based on continuations in the characterization of a spontaneous mouse mutant ('pale tremor' or *plt*) with a homozygous recessive loss-of-function mutation in the *Fig4* gene (Chow, Zhang et al. 2007). The *plt* mice are characterized by severe and progressive neurodegeneration (Chow, Zhang et al. 2007) and increased vacuolization due to defective lysosomal function and impaired autophagy (Ferguson, Lenk et al. 2009). However, previous studies of FIG4 did not extensively examine its direct role in skeletal muscle development and homeostasis.

Examinations of three distinct lines of mice gave some results that were a bit surprising, based on assumptions of the importance of PtdIns(3,5)P_2 in muscle. The three lines included the original *plt* mice, which die before 2 months of age due to progressive neurodegeneration, as well as *plt* mice with restored FIG4 expression in neurons (Chow, Zhang et al. 2007, Ferguson, Lenk et al. 2012). In addition, we crossed the *plt* mice with mice carrying mutations in *Mtm1* to follow up on a previous report that haploinsufficiency of *Fig4* rescues the neuropathy associated with *Mtmr2* mutation (Bolino, Bolis et al. 2004, Vaccari, Dina et al. 2011). These studies support the findings

that FIG4 is required for skeletal muscle function, but not in a cell-autonomous role in either muscle development or activity.

1.4.3 Aim 2: To determine the effects of targeted deletion of Pik3c3/hVps34 in skeletal muscle

The third chapter introduces a line of mice with a mutation in the Class III PI3K, *Pik3c3*, known in yeast as vacuolar protein sorting protein 34 (Vps34). As mice with null mutations for *Pik3c3* are not viable, it was necessary to design a mouse with the gene ablated specifically in skeletal muscle. These mice with conditional knockout of *Pik3c3* in skeletal muscle were generated by combining floxed *Pik3c3* (Zhou, Wang et al. 2010) and *Cre* recombinase under the muscle creatine kinase promoter: Tg(*Ckmm-Cre*) (Bruning, Michael et al. 1998). The resulting mice had normal embryonic and early postnatal development, but died by 2 months of age, presumably from severe cardiomyopathy (Jaber, Dou et al. 2012). Examination of skeletal muscle in knockout animals revealed a previously unreported murine muscular dystrophy that we further characterized. In all, we report for the first time a requirement for *Pik3c3* in skeletal muscle homeostasis, and further identify loss of *Pik3c3* as a cause of muscular dystrophy in the mouse.

1.4.4 Aim 3: To determine the role of PIK3C2β in skeletal muscle

Mice were developed by crossing a line harboring the muscle creatine kinase promoter driving Cre recombinase, Tg(*Ckmm-Cre*), with a previously described line carrying a floxed *Pik3c2β* to result in skeletal muscle deletion of *Pik3c2β* (Harada, Truong et al. 2005). As reported of the mice having null deletion of *Pik3c2β*, our mice have normal survival and mobility, growth and observed functions. There were no apparent abnormalities in muscle strength or development. However, we observed significant changes in certain metabolic processes concerning glucose disposal. There are descriptions of our findings in regards to glucose transport and metabolism in the fourth chapter.

1.4.5 Summary

In all, here are several approaches to identify the consequences in skeletal muscle from dysregulation of the phosphorylation of PtdIns(3)*P* and PtdIns(3,5)P_2. Depending on the exact nature of the disruption in PtdIns*P* metabolism, we witness a variety of effects on skeletal muscle. From these studies, it can be inferred that MTM appears to be not a direct result of impaired PtdIns3*P* processing, but possibly something to do with over-accumulation of PtdIns(3)*P* or PtdIns(3,5)P_2. The link between MTM1 and kinases including PIK3C2β remains to be explored in more detail. The potential directions for future studies will be outlined in the concluding chapter.

1.5 Figures

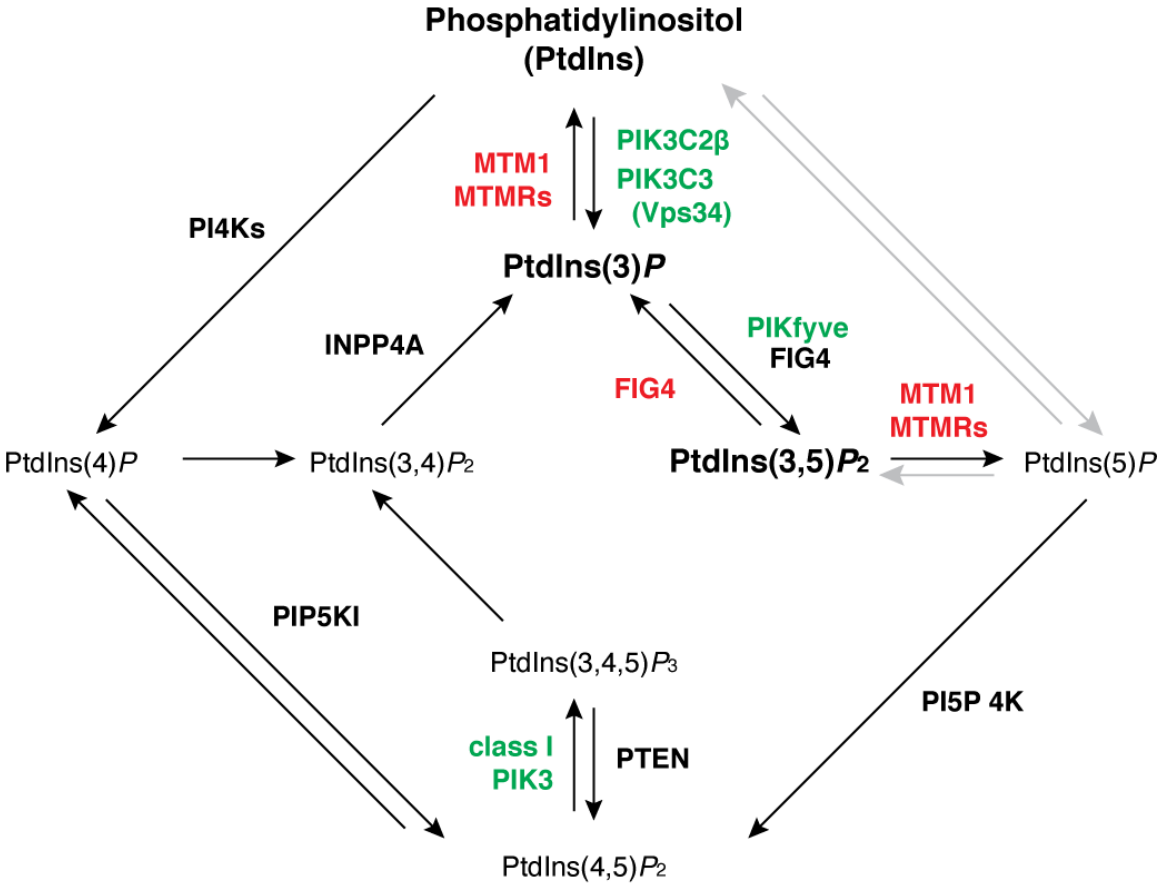

Figure 1.1 Phosphatidylinositol (PtdIns) and its seven phosphorylated isoforms

PtdIns*P*s play essential roles in numerous signaling pathways and metabolic functions. The individual phosphoisoforms are rapidly interconverted following activation of a variety of kinases (green) and phosphatases (red) upon cellular signals from sources such as G-protein coupled receptors (Kukkonen 2011), transcription factors (Mammucari, Milan et al. 2007), growth factors (Wheeler and Domin 2006) and insulin (Bridges and Saltiel 2012), among others.

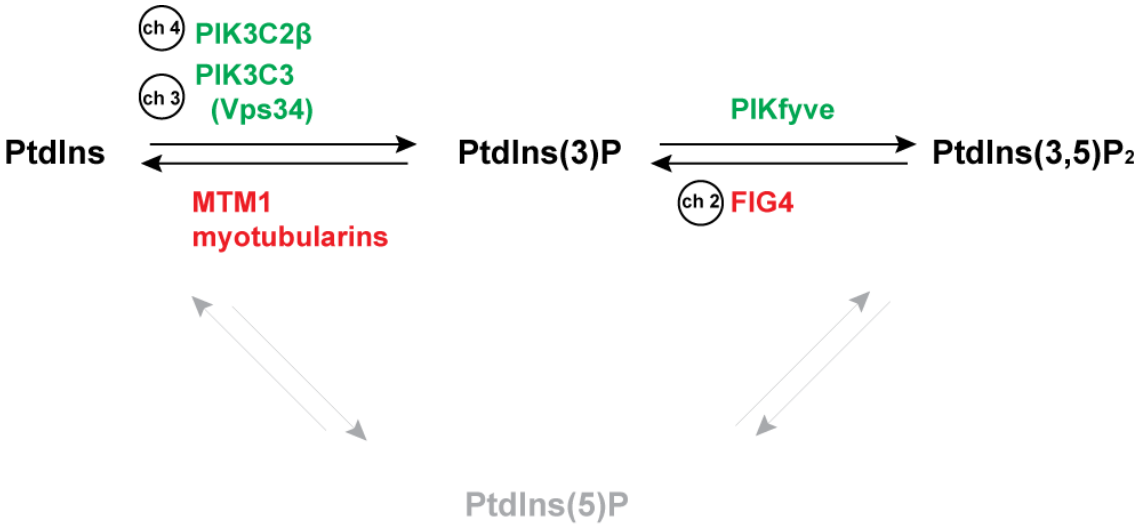

Figure 1.2 Interconversion among PtdIns, PtdIns(3)*P* and PtdIns(3,5)P_2.

This dissertation focuses on enzymes, both phosphatases (red) and kinases (green), that regulate the phosphorylation of phosphatidylinositol (PtdIns). These include a phosphatase, FIG4, responsible for converting phosphatidylinositol (3,5)-bisphosphate (PtdIns(3,5)P_2) to phosphatidylinositol 3-phosphate (PtdIns(3)*P*), as discussed in chapter 2; and two kinases, PIK3C3 and PIK3C2β, that use PtdIns as a substrate to form PtdIns(3)*P*, discussed in chapters 3 and 4, respectively.

Chapter 2:

Murine *Fig4* is dispensable for muscle development but required for muscle function[4]

2.1 Abstract

Background

Phosphatidylinositol phosphates (PtdIns*P*s) are low-abundance phospholipids that participate in a range of cellular processes, including cell migration and membrane traffic. PtdIns*P* levels and subcellular distribution are regulated by a series of lipid kinases and phosphatases. In skeletal muscle, PtdIns*P*s and their enzymatic regulators serve critically important functions exemplified by mutations of the PtdIns*P* phosphatase *MTM1* in myotubular myopathy (MTM), a severe muscle disease characterized by impaired muscle structure and abnormal excitation–contraction coupling. FIG4 functions as a PtdIns*P* phosphatase that participates in both the synthesis and breakdown of phosphatidylinositol 3,5-bisphosphate (PtdIns(3,5)P_2). Mutation of *FIG4* results in a severe neurodegenerative disorder in mice and a progressive peripheral polyneuropathy in humans. The effect of *FIG4* mutation on skeletal muscle has yet to be examined.

Methods

Herein we characterize the impact of FIG4 on skeletal muscle development and function using the spontaneously occurring mouse mutant pale tremor (*plt*), a mouse line with a loss of function mutation in *Fig4*.

Results

In *plt* mice, we characterized abnormalities in skeletal muscle, including reduced muscle size and specific force generation. We also uncovered ultrastructural

[4] This chapter was published as Reifler, A., G. M. Lenk, X. Li, L. Groom, S. V. Brooks, D. Wilson, M. Bowerson, R. T. Dirksen, M. H. Meisler and J. J. Dowling (2013). "Murine Fig4 is dispensable for muscle development but required for muscle function." Skelet Muscle **3**(1): 21.

abnormalities and increased programmed cell death. Conversely, we detected no structural or functional abnormalities to suggest impairment of excitation–contraction coupling, a process previously shown to be influenced by PtdIns(3,5)P_2 levels. Conditional rescue of *Fig4* mutation in neurons prevented overt muscle weakness and the development of obvious muscle abnormalities, suggesting that the changes observed in the *plt* mice were primarily related to denervation of skeletal muscle. On the basis of the ability of reduced FIG4 levels to rescue aspects of Mtmr2-dependent neuropathy, we evaluated the effect of *Fig4* haploinsufficiency on the myopathy of *Mtm1*-knockout mice. Male mice with a compound $Fig4^{+/-}/Mtm1^{-/Y}$ genotype displayed no improvements in muscle histology, muscle size or overall survival, indicating that FIG4 reduction does not ameliorate the *Mtm1*-knockout phenotype.

Conclusions

Overall, these data indicate that loss of *Fig4* impairs skeletal muscle function but does not significantly affect its structural development.

2.2 Introduction

Phosphatidylinositol phosphates (PtdIns*P*s) are low-abundance phospholipids that are implicated as regulators of a range of cellular processes, including cell migration, subcellular organelle trafficking and autophagy (De Camilli, Emr et al. 1996, Di Paolo and De Camilli 2006). Phosphatidylinositol 3,5-bisphosphate, or PtdIns(3,5)P_2, is a low-abundance PtdIns*P* whose function has recently come into focus (Ho, Alghamdi et al. 2012). PtdIns(3,5)P_2 is generated by the action of PIKfyve, a five-position phosphoinositide kinase (Zolov, Bridges et al. 2012). PtdIns(3,5)P_2 is metabolized by FIG4 (Sac3), a five-position phosphoinositide phosphatase, to regenerate phosphatidylinositol 3-phosphate (PtdIns(3)*P*), and by myotubularins, a family of three-position phosphatases to generate phosphatidylinositol 5-phosphate (or PtdIns(5)*P*) (Robinson and Dixon 2006, Tosch, Rohde et al. 2006, Dyson, Fedele et al. 2012, Hakim, Bertucci et al. 2012). Of note, maximal function of PIKfyve requires a complex of proteins that includes VAC14 and FIG4 (Gary, Sato et al. 2002, Duex, Tang et al. 2006, Jin, Chow et al. 2008). Reduced abundance of FIG4 protein destabilizes PIKfyve,

resulting in a threefold reduction of PtdIns(3,5)P_2 relative to total PtdIns$P$ levels (Chow, Zhang et al. 2007).

We recently identified and characterized a spontaneous mouse mutant ("pale tremor" or *plt*) with a homozygous recessive loss-of-function mutation in the *Fig4* gene (Chow, Zhang et al. 2007). *plt* mice exhibit severe and progressive neurodegeneration that involves both neurons and glia of the central and peripheral nervous system (Winters, Ferguson et al. 2011). The main subcellular phenotype is increased vacuolization due to defective lysosomal function and impaired autophagy (Ferguson, Lenk et al. 2009, Ferguson, Lenk et al. 2012). In addition, we (the Meisler group) have identified recessive *FIG4* mutations in patients with hereditary peripheral neuropathy (Charcot-Marie-Tooth Disease type 4J) (Ikonomov, Sbrissa et al. 2010, Lenk, Ferguson et al. 2011, Nicholson, Lenk et al. 2011) and motor neuron disease (amyotrophic lateral sclerosis, or ALS) (Chow, Landers et al. 2009). However, the role of FIG4 in skeletal muscle has yet to be extensively examined in detail.

Studies of myotubularins indicate a potentially important role for PtdIns(3,5)P_2 regulation in skeletal muscle (Laporte, Bedez et al. 2003, Gibbs, Feldman et al. 2010, Romero-Suarez, Shen et al. 2010). The mammalian myotubularin gene family contains 15 members encoding phosphatases that primarily dephosphorylate PtdIns(3)P and PtdIns(3,5)P_2 (Hnia, Vaccari et al. 2012). Mutation of *MTM1*, the canonical member of this gene family, results in increased levels of PtdIns(3)P, and possibly PtdIns(3,5)P_2, in skeletal muscle and causes myotubular myopathy (MTM), a severe congenital muscle disease associated with altered muscle structure and profound muscle weakness (Pierson, Dulin-Smith et al. 2012). Mutation of *MTM1* compromises multiple aspects of muscle function (Amoasii, Hnia et al. 2012), most notably excitation–contraction coupling (EC coupling) (Dowling, Low et al. 2010), the process by which neuronal stimulation to muscle is translated into calcium-dependent muscle contraction. Specifically, *MTM1* mutations lead to severe abnormalities in the structure of the EC coupling machinery (Al-Qusairi, Weiss et al. 2009).

MTMR14 is another myotubularin family member that is important for muscle function (Shen, Yu et al. 2009). Loss of MTMR14 function in zebrafish and mice causes aberrant autophagy and impaired EC coupling (Shen, Yu et al. 2009, Dowling, Low et al.

2010). Unlike MTM1, loss of MTMR14 alters EC coupling without significantly changing the underlying structure of the EC coupling machinery. Direct application of PtdIns(3,5)P_2 increases calcium release from microsomes containing the intracellular ryanodine receptor 1 calcium release channel (RyR1), a critical component of the EC coupling apparatus. Thus, direct regulation of RyR1-dependent stimulated calcium release may represent one important role of PtdIns(3,5)P_2 and MTMR14 (Touchberry, Bales et al. 2010).

Given the potential importance of PtdIns(3,5)P_2 in skeletal muscle, we sought to understand the impact of FIG4 mutation on muscle development and homeostasis. To address this issue, we examined skeletal muscle structure and function in the *plt*-null mouse model of FIG4 dysfunction. We examined *plt* mice, which die before 2 months of age as a result of progressive neurodegeneration, as well as *plt* mice with restored FIG4 expression in neurons (Chow, Zhang et al. 2007, Ferguson, Lenk et al. 2012). The latter mice have no overt phenotype and survive for more than 18 months. Our data reveal that *Fig4* mutation is associated with skeletal muscle changes (atrophy and increased apoptosis) and impaired muscle force generation, but not with abnormalities in the structure or function of the EC coupling machinery. The changes are likely the consequence of impaired neuronal input because phenotypic rescue is largely provided by neuronal expression of FIG4. In addition, we found that haploinsufficiency of *Fig4* does not ameliorate effects of *Mtm1* mutation in muscle, in contrast to a previous report that haploinsufficiency of *Fig4* rescues the neuropathy associated with *Mtmr2* mutation (Bolino, Bolis et al. 2004, Vaccari, Dina et al. 2011). Together, our results support a requirement for FIG4 in skeletal muscle function, but not a cellular autonomous role in either muscle development or EC coupling.

2.3 Results

2.3.1 FIG4 is expressed in skeletal muscle

We wanted to establish that FIG4 protein was present in skeletal muscle. We therefore performed Western blot analysis using anti-FIG4 antibody (NeuroMab). We first used a premade multitissue Western blot antibody (IMGENEX) and found that FIG4 was present in most tissues examined, including skeletal muscle (Figure 2.1A). To

determine if FIG4 expression was regulated with maturation of skeletal muscle, we examined protein extracts from skeletal muscle of various postnatal ages (Figure 2.1B) as well as from differentiating C2C12 myocytes (Figure 2.1C). We detected no obvious variability in FIG4 levels at different mouse ages or different developmental stages *in vitro*; thus we conclude that FIG4 is a ubiquitously expressed component of skeletal muscle. Of note, we verified that FIG4 expression was absent in *Fig4*-null (that is, *plt*) skeletal muscle as compared to WT littermates (Figure 2.1D).

2.3.2 Fig4-null myofibers are reduced in size and exhibit ultrastructural abnormalities

We began our analysis by examining both light and electron microscopic features of skeletal muscle from *Fig4*-null mice. We examined muscle at 5 weeks of age, since these mice do not survive beyond 6 weeks of age (Lenk and Meisler 2013). We also studied a limited number of animals with expression of a Fig4 cDNA transgene under control of the neuron-specific enolase (NSE) promoter (Ferguson, Lenk et al. 2012). These animals were examined at 4, 8 and 20 months of age.

Routine histopathological analysis of quadriceps, gastrocnemius and diaphragm using H&E and SDH stains did not reveal any obvious abnormalities in *plt* skeletal muscle compared to the WT (Figures 2.2A through 2.2D). However, the CSA of *plt* myofibers was significantly smaller than that of their WT counterparts. Quantitation of cross-sectional fiber area revealed that *plt* myofibers were 55.3% smaller than WT fibers (n = 400 total fibers counted from quadriceps in three mice per condition) (Figure 2.2E). This reduction in size corresponds with the observation that overall muscle mass in *plt* animals was similarly significantly reduced compared to that of age-matched WT littermates (Figure 2.11). Of note, overall mass of the body (which is largely dictated by muscle weight) at 6 weeks of age was also significantly reduced in *plt* mice (Figure 2.10).

Ultrastructural analyses were performed on quadriceps muscle from age-matched WT and *plt* mice using transmission electron microscopy (n = 4 per condition). Overall, muscle ultrastructure in *plt* mice resembled that of controls (Figures 2.3A and 2.3B), though swollen and enlarged mitochondria were occasionally observed in muscle from *plt* mice (M in Figure 2.3C). We did not, however, detect consistent abnormalities in the

triad, the location of the EC coupling machinery, in any *plt* mouse examined (arrow in Figure 2.3B).

2.3.3 Increased apoptosis in skeletal muscle and primary myocytes from Fig4-deficient mice

The combination of reduced muscle fiber size and ultrastructurally abnormal mitochondria led us to examine whether there was increased cell death in *plt* muscle. TUNEL staining of muscle sections revealed few positive cells in the WT tissue but several positive cells in the mutant tissue (Figure 2.4A). To better evaluate this finding, we studied isolated myocytes from neonatal WT and *plt* mice. As with primary cells from other organ systems of the *plt* mice, cells derived from *plt* muscle demonstrated abundant vacuolization. We measured cell death in these primary cell cultures using a TUNEL assay. We observed a significant increase in TUNEL-positive cells in *Fig4*-mutant myocytes, consistent with decreased cell survival (Figure 2.4B). Of note, despite the vacuolization and impaired survival, *Fig4*-null myocytes were able to successfully differentiate into myotubes upon serum withdrawal (data not shown). There was also no change in the ability of *plt* myocytes to proliferate, as determined by bromodeoxyuridine (BrdU) labeling of cells (64% of cells BrdU-positive in control (116 of 182 cells counted) vs 64% of cells positive in *plt* (151 of 235 cells counted).

2.3.4 FIG4-mutant skeletal muscle has impaired force generation

To determine the potential functional effects of *Fig4* deficiency in skeletal muscle, we measured force generation from intact muscle fibers. Testing both EDL and soleus muscles revealed statistically significant reductions in specific force generation (12% to 24% decrease when adjusted for CSA), indicating mild muscle weakness and impaired force generation in the *plt* animals (Figure 2.5).

2.3.5 FIG4-mutant myocytes have normal intracellular calcium dynamics

Given the previous association between PtdIns(3,5)P_2 and EC coupling and the fact that FIG4 is a known regulator of PtdIns(3,5)P_2 levels, we interrogated intracellular calcium dynamics. We used whole-cell voltage patch-clamping of isolated neonatal mouse myocytes to simultaneously measure voltage-gated L-type calcium currents and

intracellular calcium transients. We did not detect abnormalities in either orthograde or retrograde coupling or in L-type calcium currents in *plt* myocytes (Figure 2.6 and Table 2.1). Taken in conjunction with the normal histological appearance of the triad, these data suggest that loss of *Fig4* is not associated with impaired bidirectional dihydropyridine receptor (DHPR)–RyR1 coupling.

Table 2.1 Parameters of fitted current-voltage and fluorescence-voltage (ΔF/F-V) curves.[a]

	Gmax (nS/nF)	VG1/2 (mV)	kG (mV)	VREV (mV)	(ΔF/F)max	VF1/2 (mV)	kF(mV)
WT (n = 11)	219 ± 14	9.8 ± 1.4	5.0 ± 0.5	65.3 ± 3.0	2.3 ± 0.4	−7.8 ± 1.9	4.4 ± 0.2
plt (n = 11)	194 ± 15	9.4 ± 1.3	4.0 ± 0.4	66.7 ± 2.7	2.1 ± 0.2	−5.8 ± 1.7	4.6 ± 0.3

[a]WT, wild type.

2.3.6 Neuronal expression of Fig4 in plt mice reduces skeletal muscle pathology

We previously reported that expression of FIG4 under the NSE promoter in *plt* animals prevents the development of typical phenotypic abnormalities (Ferguson, Lenk et al. 2012). In fact, the appearance of the transgenic (Tg) animals is indistinguishable from their WT littermates. We examined skeletal muscle in *Fig4*$^{-/-}$/TgNSE mice at 4, 8 and 20 months of age. There was no obvious difference in histological appearance between WT and *Fig4*$^{-/-}$/TgNSE mice, which is similar to what we observed in the *Fig4*-null mice. Unlike the null mice, however, *Fig4*$^{-/-}$/TgNSE mice exhibited only a very slight alteration in myofiber size (11% smaller than WT; $n = 5$ animals examined per genotype, $P = 0.02$) (Figures 2.7A and 2.7B). This reduction was statistically significant and occurred despite the fact that overall weight was the same between WT and *Fig4*$^{-/-}$/TgNSE animals. *Fig4*$^{-/-}$/TgNSE muscle did not display any of the ultrastructural changes seen in the *Fig4*$^{-/-}$ mice (Figure 2.7C) and did not exhibit evidence of increased apoptosis.

Last, to determine whether muscle function was altered in *Fig4*$^{-/-}$/TgNSE mice, we measured maximum isometric force in soleus and EDL muscles of 18-month-old animals. There was a small (approximately 10%) but statistically insignificant ($P > 0.1$) decline in force generation between *Fig4*$^{-/-}$/TgNSE mice and their WT littermates (Additional File 1, Figure S4). Taking all our data together, we conclude that expression of *Fig4* in neurons is sufficient to correct the development of significant muscle atrophy

and programmed cell death in *plt* skeletal muscle, but not to prevent subtle but reproducible changes in myofiber size *in vivo*. Of note, we verified by both RNA (reverse transcriptase polymerase chain reaction) and Western blot analysis that there was no appreciable Fig4 RNA or protein in muscle of $Fig4^{-/-}$/TgNSE mice (data not shown and Figure 2.1D).

2.3.7 Fig4 haploinsufficiency does not improve the Mtm1-knockout mouse phenotype

There is a complex interplay between the enzymes that regulate phosphoinositides. One potential avenue for treatment of diseases related to PtdIns*P* dysregulation is manipulation of other enzyme levels. This point has been demonstrated for the neurological abnormalities associated with *Mtmr2* mutation (Vaccari, Dina et al. 2011). Mice with a recessive mutation in *Mtmr2* exhibit peripheral neuropathy, and aspects of this neuropathy are reversed in the setting of *Fig4* haploinsufficiency. Since MTM1 and MTMR2 are highly homologous, we evaluated the effect of haploinsufficiency of *Fig4* (in $plt^{+/-}$ mice) on the severe muscle phenotype in knockout mice lacking expression of *Mtm1*. Generation of $Fig4^{+/-}/Mtm1^{-/Y}$ male mice revealed no difference from $Mtm1^{-/Y}$ mice, with comparable impairments of weight gain, motor function and survival and no statistically significant difference in weight or survival (Figures 2.8A and 2.8B).

By histopathological analysis, we demonstrated similar alterations between $Mtm1^{-/Y}$ mice and $Mtm1^{-/Y}/Fig4^{+/-}$ mice. We quantitated myofiber size because size is correlated with disease severity in patients with MTM (Pierson, Agrawal et al. 2007). There was no clear difference in this parameter (Figure 2.8B, consistent with the observed lack of functional improvement in the $Fig4^{+/-}/Mtm1^{-/Y}$ animals. In all, haploinsufficiency of *Fig4* did not appear to alter the *Mtm1* phenotype in any meaningful way.

2.4 Discussion

FIG4 exhibits an important role in central and peripheral nervous system development and homeostasis. The consequences of FIG4 deficiency on other organ systems are less well delineated. In this study, we defined the consequences of *Fig4*-null

mutation on skeletal muscle. We found that (1) global inactivation of *Fig4* in the *plt* mouse is associated with myofiber atrophy and/or hypotrophy, increased apoptosis and diminished specific force production; (2) loss of *Fig4* does not alter the structure, EC coupling apparatus or bidirectional DHPR–RyR1 coupling; and (3) reexpression of *Fig4* in neurons significantly reduces all observed muscle abnormalities. The implications of these findings are discussed below.

Perhaps the most striking aspect of this study is the fact that *Fig4* mutation did not result in a more deleterious direct effect on muscle development and function. In neurons and glia, loss of FIG4 results in severe structural and functional consequences. Given the previously recognized importance of phosphoinositide regulation in skeletal muscle (Al-Qusairi, Weiss et al. 2009, Dowling, Low et al. 2010), we predicted that *plt* mice would exhibit pronounced changes in muscle structure and function. However, effects of *Fig4* ablation on muscle were minimal and largely rescued following neuron-specific restoration of FIG4 expression ($Fig4^{-/-}$/TgNSE mice). Muscle alterations found to persist in $Fig4^{-/-}$/TgNSE mice (for example, 11% reduction in fiber size) could be explained by either a minor role for FIG4 expression in muscle fiber size determination or a small amount of residual neurogenic atrophy. It is of interest to note the dichotomy between the relatively normal appearance of adult *plt* muscle *in situ* and the extensive vacuolarization of *plt* myocytes *in vitro* (Figure 2.12). Similar effects of culturing have been observed in other cell types, including fibroblasts (Chow, Zhang et al. 2007) and osteoblasts (unpublished manuscript, Lenk GM and Meisler MH). The explanation for this difference is unclear and requires further experimentation.

There are several potential explanations for the lack of a more severe phenotype in skeletal muscle of *Fig4*-null mice. First of all, the partial reduction of PtdIns(3,5)P_2 likely caused by loss of *Fig4* may not be enough to result in significant consequences for muscle development and function. Alternatively, a different PIKfyve protein complex may compensate for the loss of FIG4 to provide sufficient levels of PtdIns(3,5)P_2 to maintain myofiber homeostasis. A third possibility is that PtdIns(3,5)P_2 may be generated in muscle by a different or complementary pathway. For example, a three-position kinase may generate PtdIns(3,5)P_2 from PtdIns(5)P. One current barrier to attempting to distinguish these possibilities is the lack of suitable approaches to measure PtdIns(3,5)P_2

in whole tissues such as skeletal muscle. Development of techniques to aid in measuring PtdIns(3,5)P_2 *in situ* are required to answer these questions more definitively.

Regardless of the explanation, the fact that there is little, if any, muscle-cell autonomous phenotype in *Fig4*-null animals indicates that *FIG4* mutations are unlikely to result in primary muscle disease. However, significant secondary neurogenically mediated myopathic features, such as those observed in *plt* mice, including reduced muscle fiber CSA and specific force generation, suggest that skeletal muscle changes may contribute to disease pathogenesis. In other words, the myopathic changes described herein may influence disease severity in patients with Charcot-Marie-Tooth disease type 4J and other disorders caused by *FIG4* gene mutation.

The lack of impairment in the structure of the EC coupling apparatus or of bidirectional triad coupling in *Fig4*-null mice was unexpected. Data from the MTMR14-knockout mice support the hypothesis that increased levels of PtdIns(3,5)P_2 impair calcium release from the ryanodine receptor (the core component of the EC apparatus), though the underlying mechanism is not clear. Our data imply that reduced levels of PtdIns(3,5)P_2 do not acutely impair voltage-gated triad calcium release. Furthermore, the chronic loss of FIG4 from muscle (with the potential implication of chronically reduced PtdIns(3,5)P_2 levels) does not alter the ultrastructural appearance of the triad (that is, the location of the EC coupling machinery). Thus, a requirement for normal levels of PtdIns(3,5)P_2 for EC coupling seems unlikely, though the present data do not completely exclude this possibility. In addition to more direct interrogation of EC coupling in FIG4-deficient mice, another potential future direction to address this issue would be to assess the impact on EC coupling of muscle-specific knockout of PIKfyve, the kinase required for PtdIns(3,5)P_2 generation. Again, however, this would necessitate confirmation of a specific reduction in PtdIns(3,5)P_2 levels in skeletal muscle.

The final significant observation in this study is that reduced *Fig4* expression via *plt* haploinsufficiency does not significantly alter the phenotype of *Mtm1*-knockout mice. Of note, the *MTMR2* gene encodes a protein that is highly homologous to *MTM1* (Robinson and Dixon 2006). In addition, we previously demonstrated that zebrafish *mtmr2* functionally compensates (at least in part) for loss of *mtm1*, suggesting that MTMR2 and MTM1 are functionally quite similar (Dowling, Vreede et al. 2009).

However, in contrast to our findings in *Mtm1*-null mice, Bolino and colleagues found that *plt* haploinsufficiency rescued neuropathy in *Mtmr2*-knockout animals (Vaccari, Dina et al. 2011). The reasons why reduction of FIG4 levels improved the MTMR2-related neuropathology, but not the muscle pathology, seen in *Mtm1*-null mice are not clear. This distinction may provide another indication of the nonessential role of FIG4 in skeletal muscle or may reflect different quantitative requirements for PtdIns(3,5)P_2 in neurons and muscle or specific differences between mammalian MTMR2 and MTM1.

2.5 Conclusions

We present data demonstrating that FIG4 is required for muscle function but is dispensable for muscle development. In addition, most abnormalities associated with Fig4 mutation appears to be secondary to the severe neuropathy documented in *plt* mice. Our results do not support a role for FIG4 in EC coupling. Future experiments are needed to more firmly establish the relationship between PtdIns(3,5)P_2 and EC coupling.

2.6 Methods

2.6.1 Animal care and husbandry

All animals were cared for per protocol under the guidance of, and with ethical approval from, the University Committee on Use and Care of Animals (UCUCA) and with the assistance of members of the University of Michigan's Unit for Laboratory Animal Medicine (ULAM), who carefully monitored the health of the rodent colonies. ULAM maintained proper environmental regulation, including temperature and light cycles, unlimited access to water, appropriate food supply and clean enclosures. The Fig4-null mutation *plt* is maintained on two congenic lines, C57BL/6J.*plt*/+ (N14) and C3H.*plt*/+ (N10) (Lenk and Meisler 2013). Experiments were carried out on homozygous *plt*/*plt* F1 mice obtained from crosses between the two congenic strains. Pups were weaned according to standard protocols, and tails were clipped for genotyping.

2.6.2 Western blot analysis

Western blot analyses were performed using the following antibodies: FIG4 (1:1,000 NeuroMab; UC Davis/NIH NeuroMab Facility, Davis, CA, USA) and

glyceraldehyde 3-phosphate dehydrogenase (1:1,000 GAPDH; Millipore, Billerica, MA, USA). Mouse multitissue Western blot antibody was obtained from IMGENEX (San Diego, CA, USA). Protein extracts were established from flash-frozen mouse skeletal muscle and brain using *T-PER tissue* protein extraction reagent and a Dounce tissue homogenizer (Pierce Biotechnology, Rockford, IL, USA). Approximately 50 μg of protein were loaded per sample, resolved by polyacrylamide gel electrophoresis on 11% gels, and transferred to polyvinylidene fluoride. Secondary antibodies were used at 1:2,000 (Santa Cruz Biotechnology, Santa Cruz, CA, USA), blots were developed using electrochemiluminescence reagent (GE Biosciences, Pittsburgh, PA, USA), and bands visualized using the Bio-Rad ChemiDoc XRS+ System illuminator (Bio-Rad Laboratories, Hercules, CA, USA).

2.6.3 Histopathology

Animals were killed by anesthetic injection, which was followed by cervical dislocation. Tissues were then isolated using sterile surgical methods without the use of laminar flow hoods. Muscle tissue from quadriceps and tibialis anterior muscles was dissected and mounted onto small balsa wood pieces that had previously been frozen with drops of Tissue-Tek O.C.T. compound (Sakura Finetek USA, Torrance, CA, USA) and then semithawed with light friction. The mounted muscle tissue was immediately submerged in a −55°C isopentane bath cooled by liquid nitrogen for flash-freezing.

Muscles were cut into 12-μm cross-sections and mounted on Superfrost Plus slides (Thermo Scientific, Waltham, MA, USA) using a Leica cryostat (Leica Biosystems, Buffalo Grove, IL, USA) at −20°C and dried at room temperature before storage at −80°C. Slides were stained with Mayer's hematoxylin and eosin (H&E) or succinate dehydrogenase (SDH) following standard protocols and mounted with Permount mounting medium (Thermo Scientific). Apoptotic fibers were visualized with the ApopTag Plus Peroxidase *In Situ* Apoptosis Kit (S7101; Chemicon International/EMD Millipore, Billerica, MA, USA). Photomicrographs were captured using an INFINITY*1* digital camera with eponymous software (Lumenera Corp, Ottawa, ON, Canada) visualized through an Olympus BX43 light microscope (Olympus America, Center Valley, PA, USA).

2.6.4 Ultrastructural analysis

Immediately following dissection, quadriceps and gastrocnemius muscles were carefully cut into approximately 1-mm × 2-mm fragments and incubated in Karnovsky's fixative overnight at 4°C. Fixed tissue was brought to the Microscopy and Imaging Laboratory (MIL) Core facility at the University of Michigan for processing. Ultrathin sections were analyzed for orientation, and grids were prepared for use on the Philips CM-100 transmission electron microscope (Koninklijke Philips N.V., Amsterdam, The Netherlands).

2.6.5 Myocyte isolation

Muscle was dissected from the shoulders and legs of dead mice and placed immediately into sterile phosphate-buffered saline. Muscle was then minced finely with a sterile razor, fully dissociated with a mixture of collagenase type I (0.1%) and trypsin (0.1%) in Ham's F-12 medium, then incubated at 37°C for approximately 1 h with periodic trituration. Cells were pelleted and resuspended in 1:1 Dulbecco's Modified Eagle *Medium*:Ham's *F-12* Nutrient Mixture (DMEM/*F-12*) (Gibco/Life Technologies, Grand Island, NY, USA) with 20% fetal calf serum (HyClone Laboratories, Logan, UT, USA), then filtered through 70- and 40-μm meshes and plated onto collagen-coated dishes (BD Biosciences, San Jose, CA, USA). Media were changed after a 1-h incubation at 37°C, and recombinant human fibroblast growth factor–basic (AA 10-155, Publication PHG0026; Gibco/Life Technologies) was added to a final concentration of 10 ng/ml. Cells were maintained at 37°C in a 5% CO_2 atmosphere with daily changes of fresh media. Cells were visualized using Hamamatsu ORCA-R2 camera and software (Hamamatsu Photonics, Hamamatsu-shi, Japan) on a Leica inverted microscope (Leica Microsystems). All experiments were performed on passages 2 through 4 myocytes. Terminal deoxynucleotidyl transferase-mediated dUTP nick end labeling (TUNEL) staining was performed per the manufacturer's recommendations on myocytes grown on coverglass coated with fibronectin and fixed with 4% paraformaldehyde prior to staining.

2.6.6 Muscle force measurement

Extensor digitorum longus (EDL) and soleus muscles were carefully isolated and removed from anesthetized mice. Muscles were immediately placed into a bath of Krebs mammalian Ringer solution with 0.25 mM tubocurarine chloride maintained at 25°C and bubbled with 95% O_2 and 5% CO_2 to stabilize pH at 7.4. Using 5-0 silk suture, the distal tendon of the muscle was attached to a servomotor (model 305B; Aurora Scientific, Aurora, ON, Canada), and the proximal tendon was attached to a force transducer (model BG-50; Kulite Semiconductor Products, Leonia, NJ, USA). Muscles were stimulated by square pulses delivered by two platinum electrodes connected to a high-power biphasic current stimulator (model 701B; Aurora Scientific). A personal computer running custom-designed software (LabVIEW 7.1; National Instruments, Austin, TX, USA) controlled electrical pulse properties and servomotor activity and recorded data from the force transducer. Stimulation voltage and optimal muscle length (L_o) were adjusted to give maximum twitch force (Brooks and Faulkner 1988). While held at L_o, muscles were subjected to trains of pulses 300 ms in duration for EDL muscles and 900 ms for soleus muscles, with increasing stimulation frequency until maximum isometric tetanic force (P_o) was achieved (Brooks and Faulkner 1988). L_o was measured with digital calipers, and muscle fiber lengths (L_f) were determined by multiplying L_o by previously established L_f-to-L_o ratios of 0.44 for EDL muscle and 0.71 for soleus muscle (Brooks and Faulkner 1988). Total muscle fiber cross-sectional area (CSA) was estimated by dividing the mass of the muscle by the product of L_f and 1.06 g/cm^3, the density of mammalian skeletal muscle. P_o was normalized by CSA to give specific P_o.

2.6.6 Simultaneous measurement of macroscopic L-type Ca^{2+} currents and voltage-gated Ca^{2+} transients in myotubes

Primary cultures of skeletal myotubes were generated from myoblasts derived from wild-type (WT) and *plt* mice as previously described (Avila, O'Brien et al. 2001). The whole-cell voltage-clamp technique in conjunction with a Ca^{2+}-sensitive dye (fluo-4) was used to simultaneously measure voltage-gated L-type Ca^{2+} currents (L-currents) and intracellular Ca^{2+} transients on individual myotubes from 8- to 11-day-old myotube cultures (Avila and Dirksen 2001, Avila, O'Brien et al. 2001). All voltage-clamp experiments were carried out after an approximately 5-min period of dialysis following

establishment of the whole-cell configuration. The external recording solution consisted of 145 mM tetraethylammonium chloride, 10 mM $CaCl_2$ and 10 mM 2-[4-(2-hydroxyethyl)piperazine-1-yl]ethanesulfonic acid (HEPES) (pH 7.4). The internal patch pipette solution consisted of 145 mM Cs-aspartate, 10 mM CsCl, 0.1 mM Cs_2-ethylene glycol tetraacetic acid, 1.2 mM $MgCl_2$, 5 mM Mg-ATP, 0.2 mM K_5-fluo-4 and 10 mM HEPES (pH 7.4). A 1-s prepulse to −30 mV delivered immediately before each test pulse was used to inactivate voltage-gated Na^+ and T-type Ca^{2+} channels without producing significant L-channel inactivation. L-currents and Ca^{2+} release were subsequently elicited by 200-ms test depolarizations from −50 mV to +70 mV in 10-mV increments and a 10-s interval between each test pulse. Capacitative currents were minimized to about 10% using the capacitance cancelation feature of the patch-clamp amplifier. Remaining linear components were leak-subtracted using a P/3 protocol delivered from a holding potential of −80 mV before each test pulse. Peak L-current magnitude was normalized to cell capacitance (pA/pF), which was plotted as a function of membrane potential (V_m) and fitted as $I = G_{max} (V_m - V_{rev})/(1 + \exp[(V_{G1/2} - V_m)/k_G])$, where G_{max} is the maximal L-channel conductance, V_m is test potential, V_{rev} is extrapolated reversal potential, $V_{G1/2}$ is the voltage for half-maximal activation of G_{max}, and k_G is a slope factor. Relative changes in intracellular Ca^{2+} during each test depolarization were measured following dialysis with K_5-fluo-4 salt. Fluo-4-dialyzed myotubes were excited at 480 nm and fluorescence emission measured at 535 nm was digitized at 10 kHz. A computer-controlled shutter was used to eliminate dye illumination during intervals between each test pulse. Relative peak changes in intracellular Ca^{2+} were expressed as $\Delta F/F$ ($[F_{peak} - F_{base}]/F_{base}$) at the end of each test pulse, plotted as a function of V_m, and fitted according to equation 2.1:

$$\frac{\Delta F}{F} = \frac{\left(\frac{\Delta F}{F}\right)}{\left(1 + e^{\left(V_{F1/2} - V_m\right)/k_F}\right)} \qquad \textbf{(Equation 2.1)}$$

where $(\Delta F/F)_{max}$ is the calculated maximal change in fluorescence, $V_{F1/2}$ is the voltage for half-maximal activation of $(\Delta F/F)_{max}$, and k_F is a slope factor. Pooled current-voltage (*I*-

V) and fluorescence-voltage (ΔF/F-V) data were expressed as means ± s.e.m. Statistical significance was determined using a two-tailed Student's *t*-test.

2.6.6 Statistical analyses

GraphPad Prism software (GraphPad Software, La Jolla, CA, USA) was used to calculate the significance of fiber size differences and TUNEL staining results with unpaired Student's *t*-tests and one-way analysis of variance with Tukey's *post hoc* multiple comparison test.

2.7 Figures

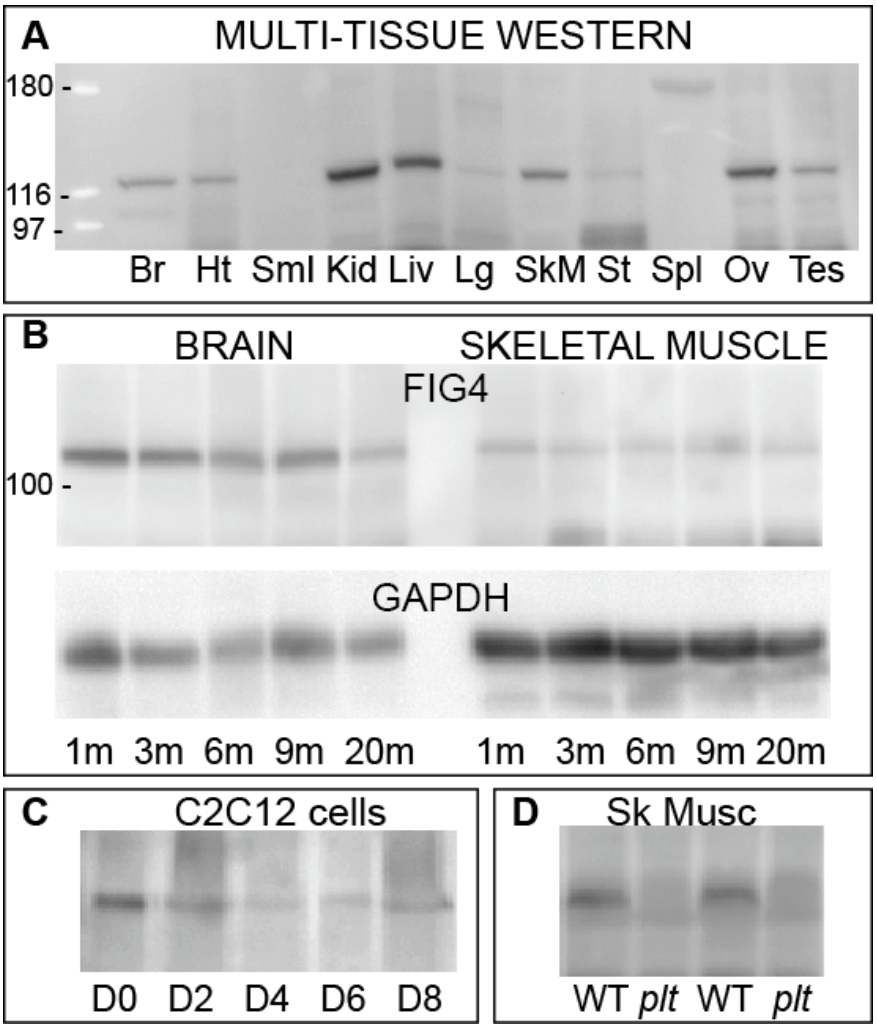

Figure 2.1 FIG4 is expressed in skeletal muscle.

Western blot analysis was performed to establish FIG4 expression using anti-FIG4 antibody. (A) Mouse multitissue Western blot reveals expression of FIG4 in a variety of tissues (Br = brain, Ht = heart, SmI = small intestine, Kid = kidney, Liv = liver, Lg = lung, SkM = skeletal muscle, St = stomach, Spl = spleen, Ov = ovary, Tes = testis). (B) FIG4 is expressed at multiple mouse ages in brain and skeletal muscle. Ages of mice tested were 1, 3, 6, 9 and 20 months. Left lanes are from brain, and right lanes are from quadriceps. The top blot was probed with anti-FIG4, and the bottom blot (loading control) was probed with glyceraldehyde 3-phosphate dehydrogenase (GAPDH). (C) Western blot of protein extracts from C2C12 cells at various stages of differentiation. Differentiation was induced by serum withdrawal. Cells were differentiated until long myotubes were obviously present (day 8 = D8). (D) Analysis of wild-type littermate and pale tremor (plt) mouse skeletal muscle reveals that FIG4 is absent from plt muscle.

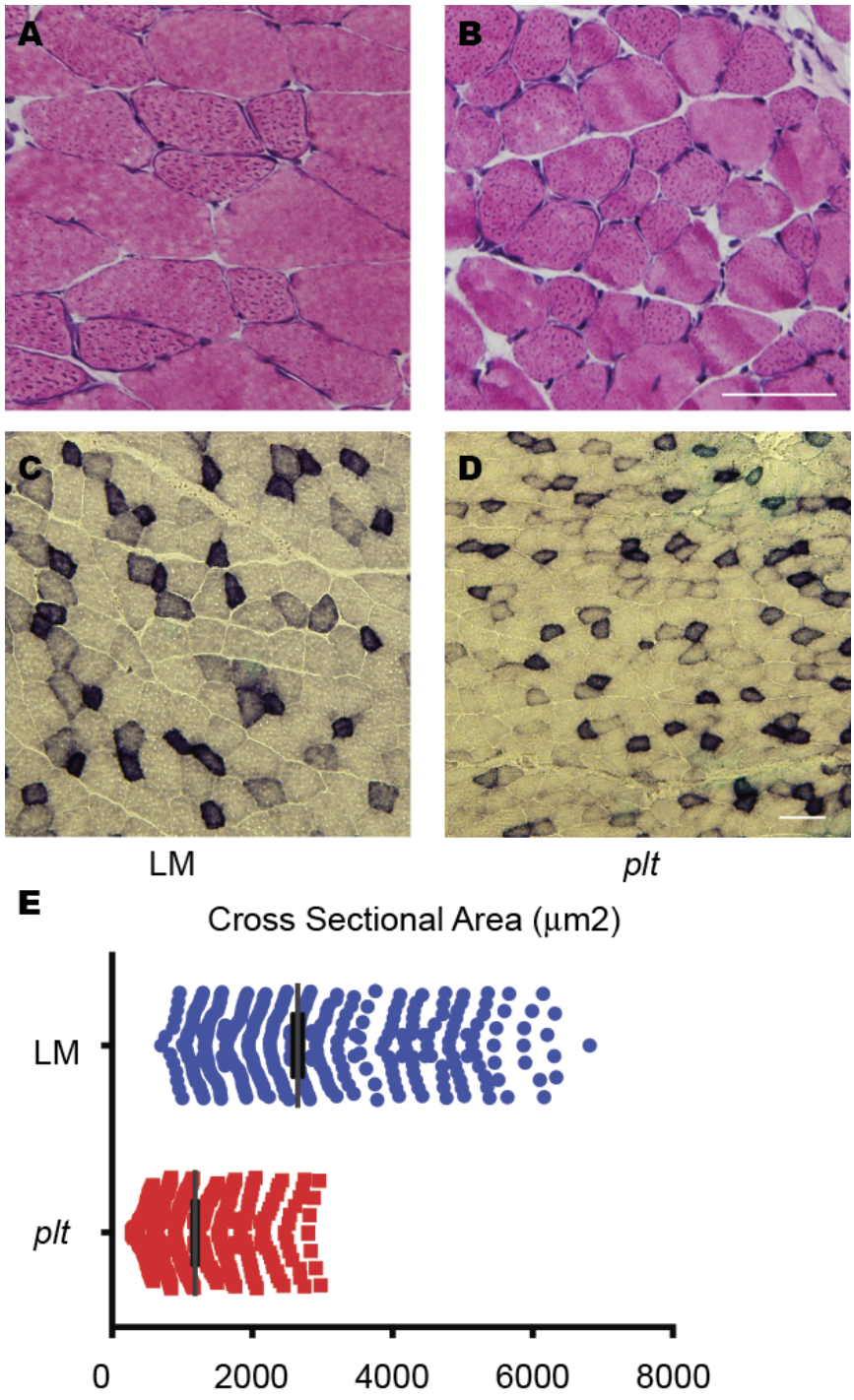

Figure 2.2 Histopathological analysis of pale tremor (*plt*) skeletal muscle.

Hematoxylin and eosin staining (A,B) and succinate dehydrogenase staining (C,D) of cryosections from quadriceps of control (wild type (WT)/littermate (LM)) and plt animals. Scale bars = 50 µm. (E) Quantitation of myofiber size from quadriceps muscle of 4-week-old plt and WT animals. There were significant reductions in myofiber size: 2,649 μm^2 ±70 for WT vs 1,185 μm^2 ± 32 for plt (n = 400 per condition, $P < 0.0001$).

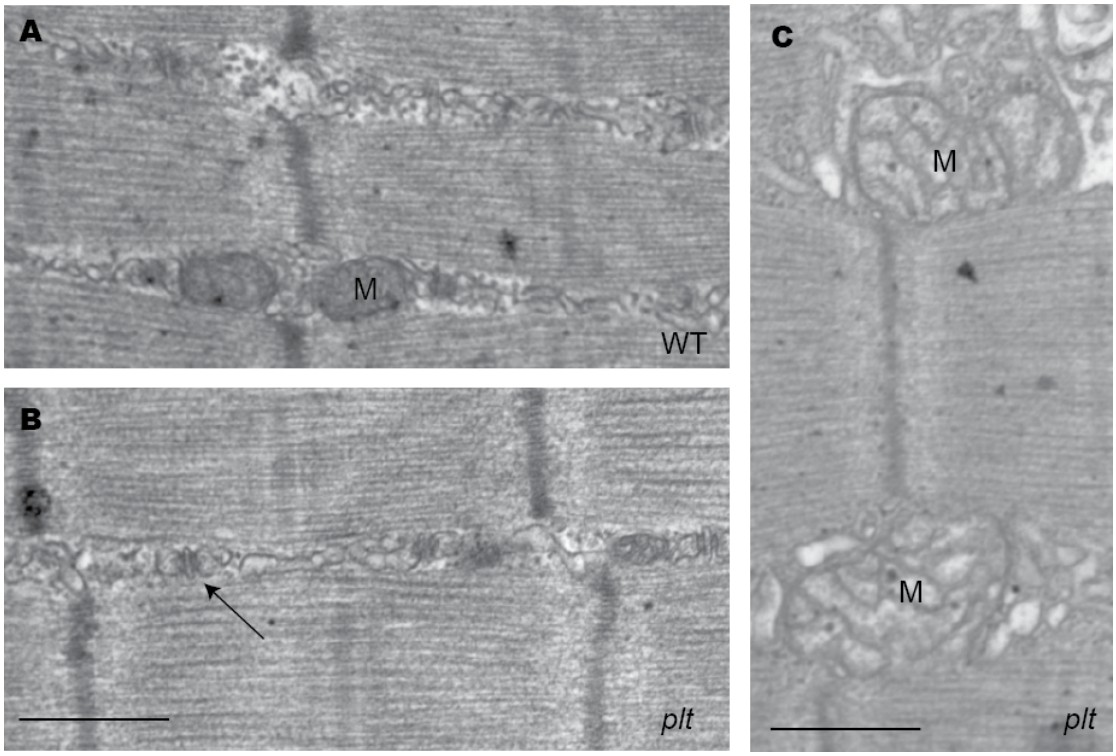

Figure 2.3 Ultrastructural analysis of pale tremor (*plt*) skeletal muscle.

Representative photomicrographs from transmission electron microscopic analysis of wild-type/littermate (WT, A) quadriceps and *plt* (B,C) quadriceps. Muscle ultrastructure was generally normal in *plt* muscle (B) with evidence of normal triads (arrow). There were infrequently observed areas of abnormalities that particularly included swollen and/or dilated mitochondria (M in C). Scale bars = 500 nm.

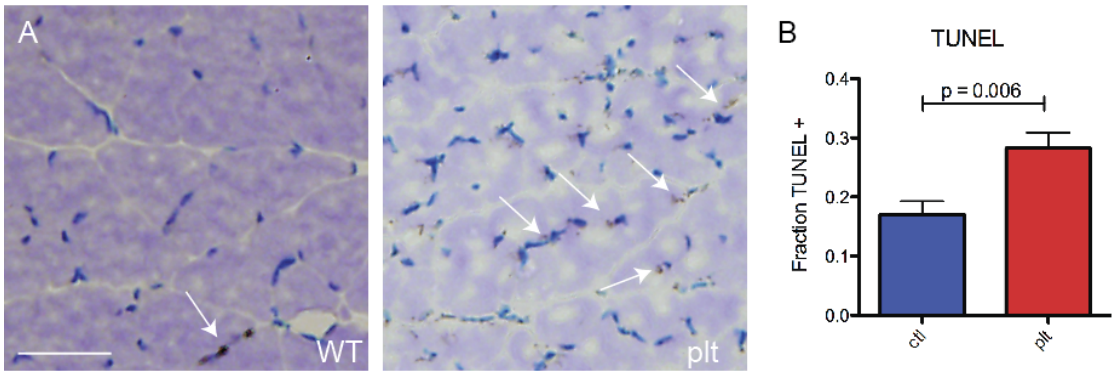

Figure 2.4 Increased apoptosis in *plt* skeletal muscle and skeletal myocytes.

(A) Terminal deoxynucleotidyl transferase-mediated dUTP nick end labeling (TUNEL) staining was performed on sections from wild-type (WT) and plt skeletal muscle. Arrows point to TUNEL-positive nuclei. There was a qualitative increase in TUNEL-positive fibers in plt muscle (experiment repeated with sections from three different mice per condition). (B) TUNEL staining was performed on myocytes. There was a significant increase in TUNEL-positive cells in plt myocytes vs WT myocytes. Data reflect fraction of 4′,6-diamidino-2-phenylindole-positive nuclei that were also TUNEL-positive. Numbers were 0.28 ± 0.06 for plt and 0.17 ± 0.05 for WT (P = 0.006). One hundred cells per experiment were counted, and each experiment was repeated five times (once for each culture derived with cells isolated from five different mice per condition).

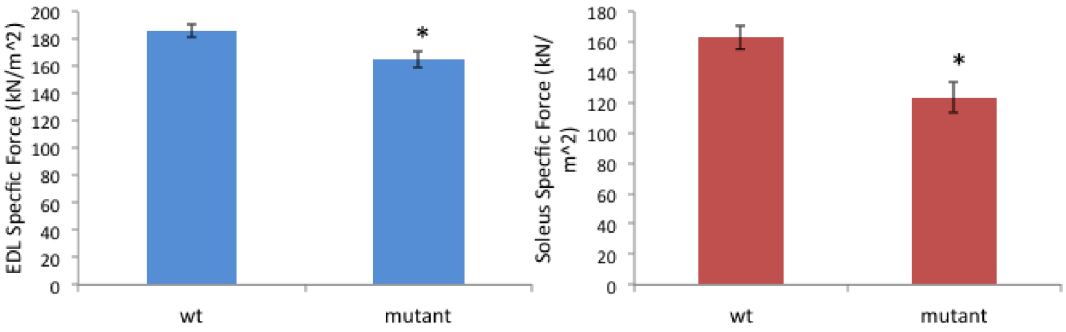

Figure 2.5 Diminished force production in pale tremor (*plt*) skeletal muscle.

Specific force (normalized to muscle and body weight) was measured for wild-type/littermate (WT) and plt (mutant) skeletal muscle (left panel = extensor digitorum longus, or EDL) (right panel = soleus). Normalized force was significantly reduced in plt muscles (n = 7 animals tested per condition). *P = 0.043 for EDL and P < 0.001 for soleus.

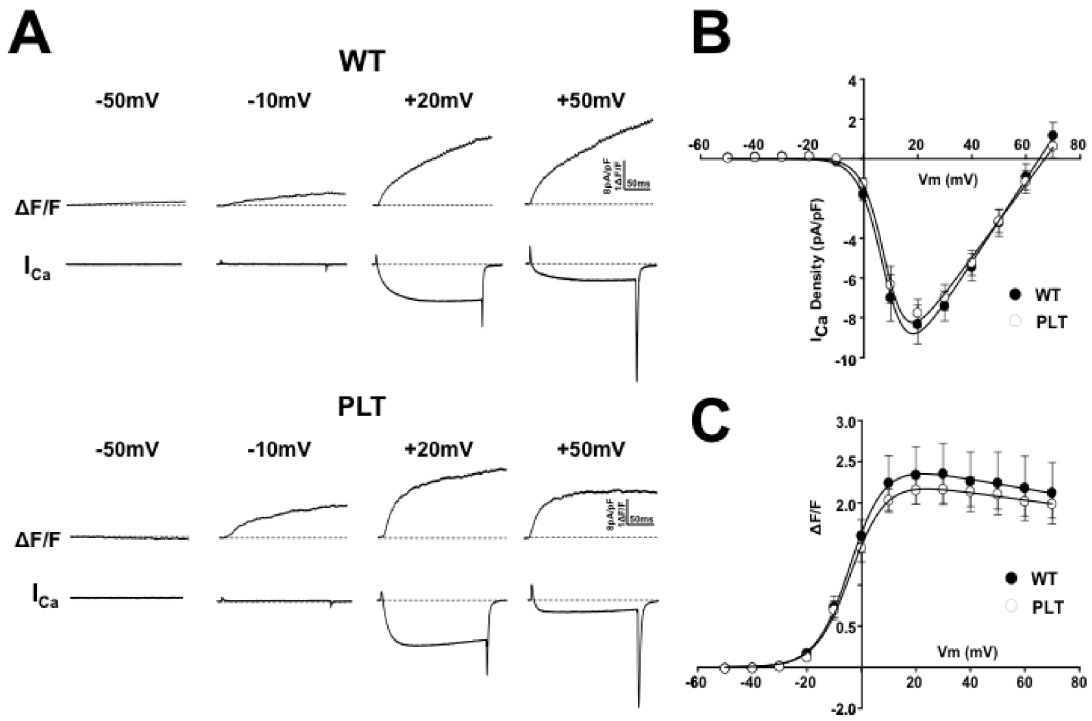

Figure 2.6 L-currents and voltage-gated Ca^{2+} release are unaltered in pale tremor (*plt*) myotubes.

(A) Representative whole-cell L-type Ca^{2+} currents (I_{Ca}) and intracellular Ca^{2+} transients (ΔF/F) obtained following 200-ms depolarizations to the indicated membrane potentials in myotubes derived from either wild-type (WT) mice (upper panel) or *plt* mice (lower panel). (B,C) Average (± s.e.m.) voltage dependence of peak L-type Ca^{2+} current density (B) and intracellular Ca^{2+} transients (C) for myotubes derived from either WT mice (filled circles) or *plt* mice (open circles).

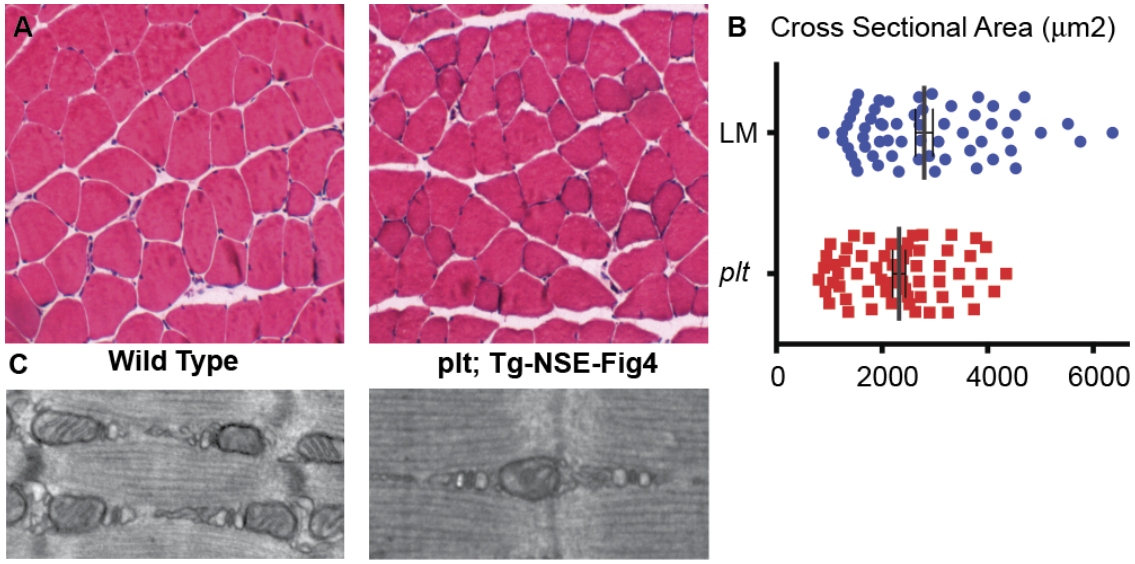

Figure 2.7 Transgenic (Tg) neuronal rescue of FIG4 expression largely restores *plt* myofiber size.

(A) Hematoxylin and eosin–stained sections of gastrocnemius muscle from wild-type (WT) and Fig4−/−/NSE-FIG4 (that is, plt with transgenic expression of Fig4 driven by the neuron-specific enolase (NSE) promoter). The plt muscle is essentially indistinguishable from WT, with the exception of mild reduction in fiber size. (B) Quantification of myofiber size from quadriceps muscles of 8-month-old Fig4−/−/NSE-FIG4 and WT animals. There was a small but significant reduction in total fiber area in transgenically rescued plt muscle: 2,799 μm^2 ± 165 for WT vs 2,322 μm^2 ± 121 for plt (n = 60, P = 0.02). (C) Transmission electron photomicrographs from tibialis anterior muscle. Normal triads and mitochondria were present in both WT and plt/Tg-NSE-Fig4 animals.

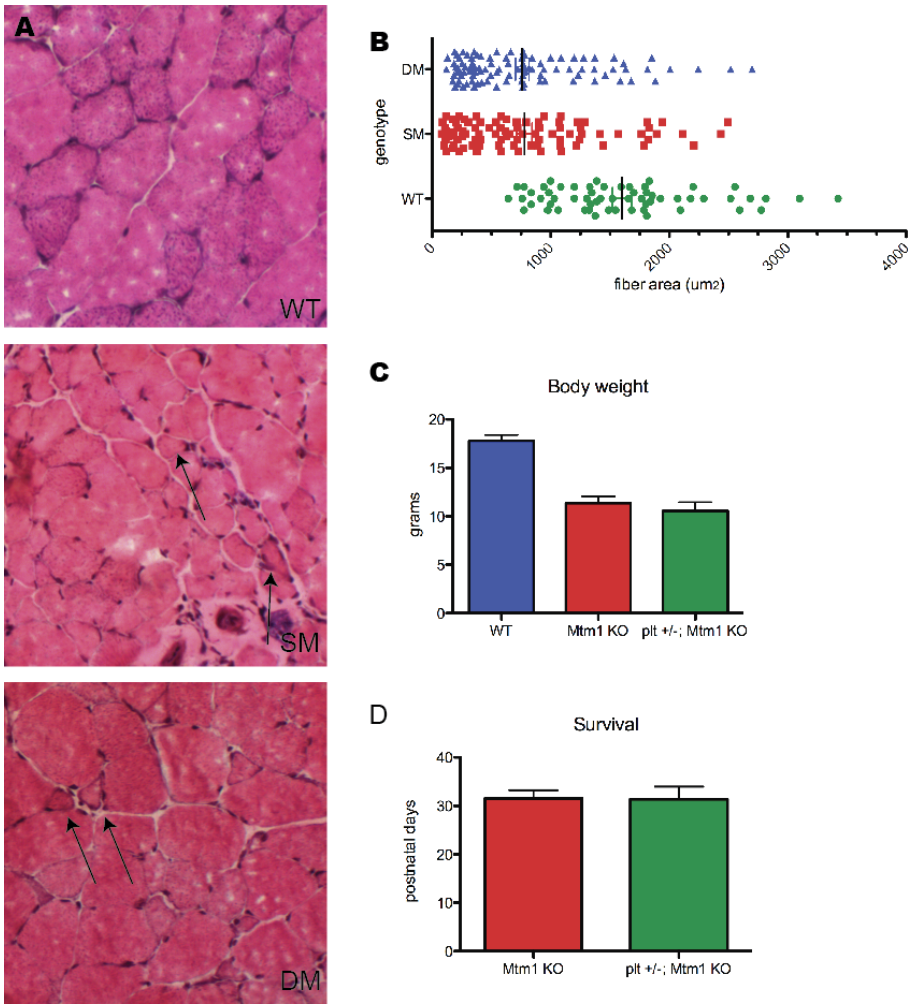

Figure 2.8 Fig4 haploinsufficiency does not improve the Mtm1-knockout phenotype.

(A) Hematoxylin and eosin stain of quadriceps muscle from wild-type (WT; $plt^{+/-}$) (top), Mtm1-knockout (Mtm1-KO) (SM, middle) and $plt^{+/-}$/Mtm1-KO (DM, bottom) animals. There was no obvious difference in the appearance of the muscle or in the number of abnormal fibers (arrows). (B) Distribution of fiber area. Fiber area was measured from WT; $plt^{+/-}$), single-mutant (SM; Mtm1-KO) and double-mutant (DM; $plt^{+/-}$/Mtm1-KO) skeletal muscles. Thirty fibers from each animal were measured (n = 4 for SM and DM, n =2 for WT). (C) Terminal body weight (measured in grams). There was significant reduction in the Mtm1-KO body weight compared to WT. There was no improvement in body weight in $plt^{+/-}$/Mtm1-KO animals. Average values were as follows: 17.8 ± 0.6 g for WT (n = 8), 11.4 ± 0.7 g for Mtm1-KO (n = 9, $P < 0.0001$ compared to WT) and 10.5 ± 0.9 g for $plt^{+/-}$/Mtm1-KO (n = 5, P = 0.48 compared to Mtm1-KO). (D) Haploinsufficiency of Fig4 did not provide any survival benefit. Average survival was 32 ± 2 days for Mtm1-KO (n = 9) and 31 ± 3 days for $plt^{+/-}$/Mtm1-KO (n = 5).

2.8 Additional Figures

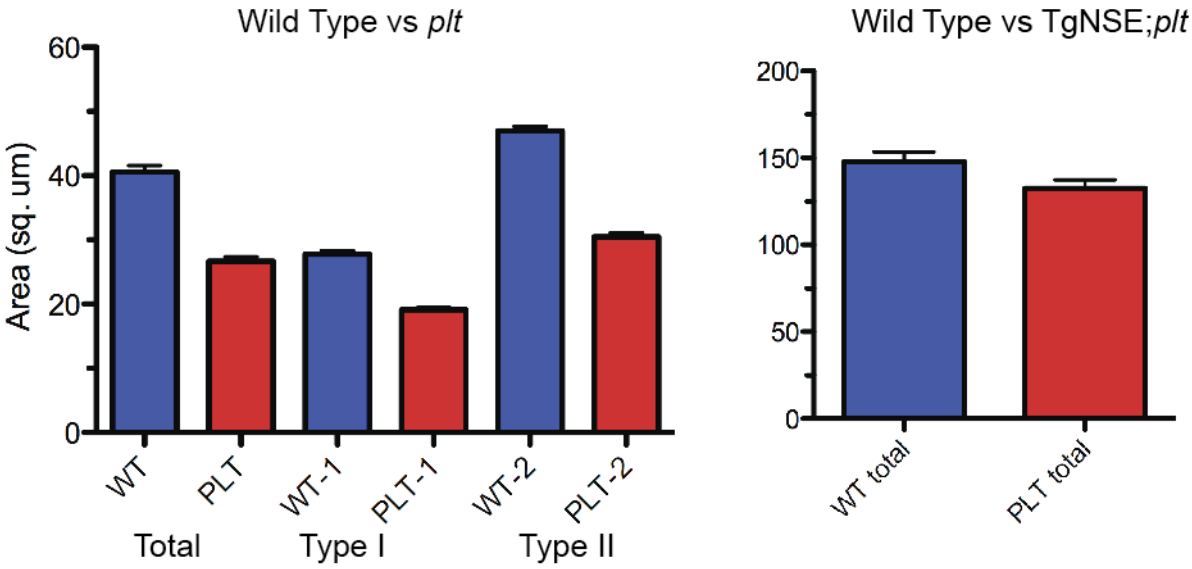

Figure 2.9 Myofiber size is reduced in *plt* skeletal muscle.

(Left panel) Quantitation of myofiber size from quadriceps muscle of 4 week of plt and wild type (WT) animals. There was significant reductions in the size of both type I and type II fibers. SDH staining was used to distinguish fiber types.

(Right panel) Quantification of myofiber size from quadriceps muscle of 8 month old TgNSEplt and wild type animals. There was a small but significant reduction in total fiber area in transgenically rescued plt muscle.

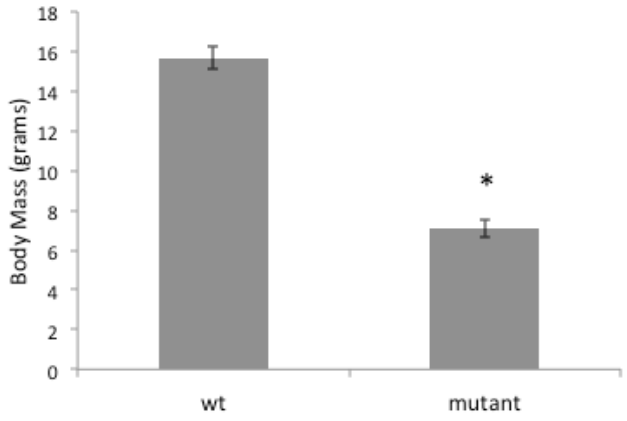

Figure 2.10 Body mass is reduced in *plt* animals.

Wild type (WT) and plt (mutant) animals were weighed just prior to muscle force measurements. There was a significant reduction in average body mass in *plt* animals.

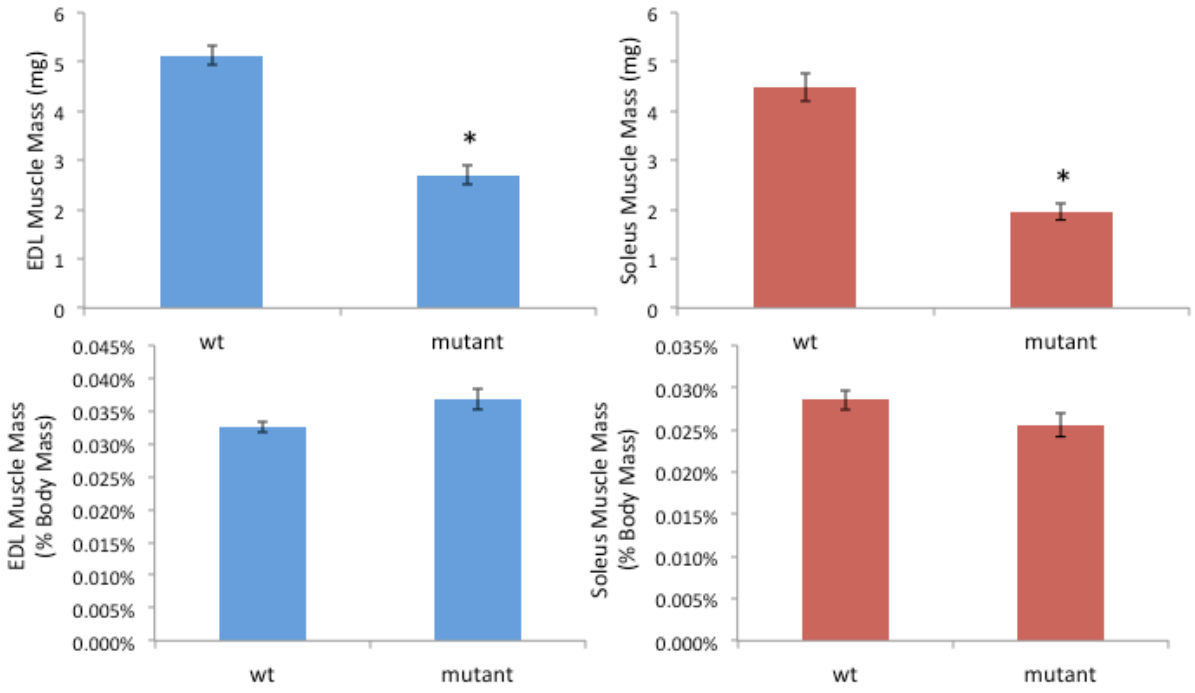

Figure 2.11 Muscle mass is reduced in *plt* animals

Muscle from wild type (WT) and *plt* (mutant) animals was weighed just prior to muscle force measurements. There was a significant reduction in average muscle mass in *plt* animals in both the extensor digitorum longus (EDL, left) and the soleus (right).

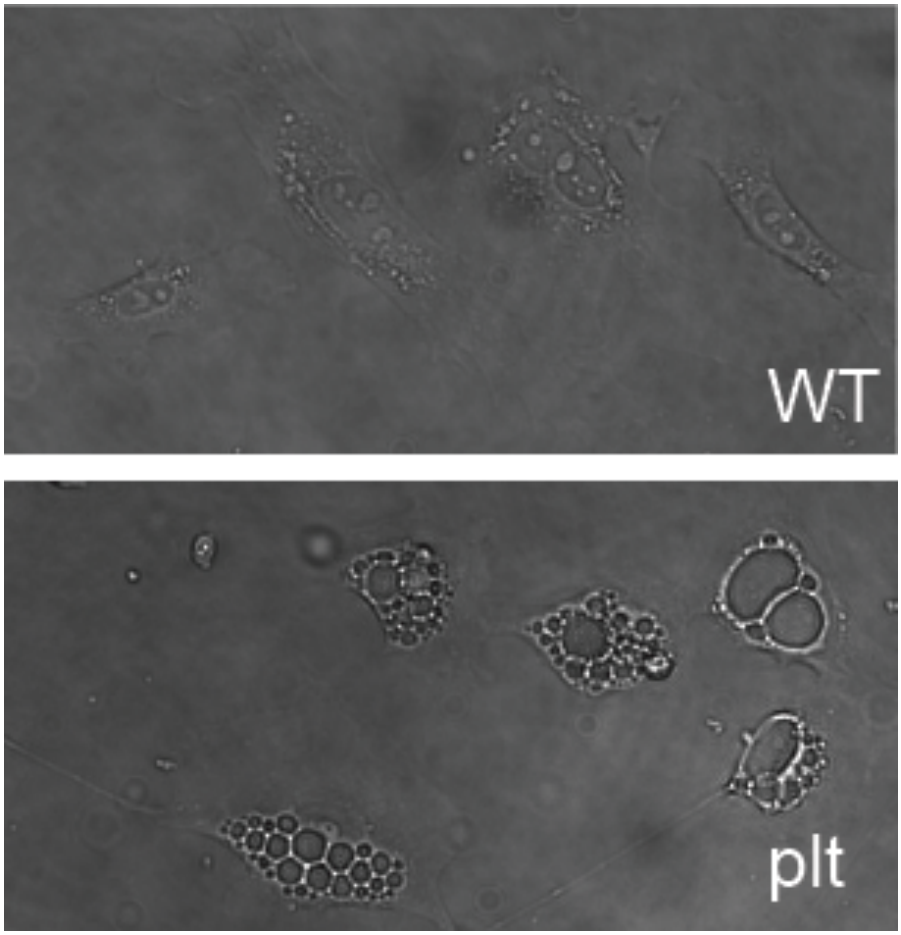

Figure 2.12 Vacuoles form in primary cultures from isolated muscle cells.

Muscle specific knockout of FIG4 results in the formation of vacuoles in isolated muscle cells, revealing abnormalities *in vitro*.

Chapter 3:
Conditional knockout of PIK3C3 causes a murine muscular dystrophy

3.1 Abstract

Abnormalities in phosphoinositide metabolism are an emerging theme in human neurodegenerative disease. Myotubular myopathy (MTM) is a prototypical disorder of phosphoinositide dysregulation that is characterized by profound muscle pathology and weakness and that is caused by mutations in *MTM1*, a phosphatase that targets 3-position phosphoinositides (PIs), and particularly phosphatidylinositol 3-phosphate (PtdIns(3)*P*). While the association between MTM1 and muscle disease has become more clarified, the normal role(s) of PtdIns(3)*P* metabolism in muscle development and homeostasis remain poorly understood. To begin to address the function of PtdIns(3)*P* in skeletal muscle, we focused on the primary kinase responsible for its production, and created a muscle-specific conditional knockout of the class III PI 3-kinase, *Pik3c3* (VPS34). Muscle specific deletion of *Pik3c3* did not disturb embryogenesis or early postnatal development, but resulted in progressive disease characterized by reduced activity and death by two months of age. Histopathological analysis demonstrated changes consistent with a murine muscular dystrophy. Examination for cellular mechanism(s) responsible for the dystrophic phenotype revealed significant alterations in the autophagolysosomal pathway with mislocation of known dystrophy proteins to the lysosomal compartment. In all, we present the first analysis of *Pik3c3* in skeletal muscle, and report a novel association between deletion of *Pik3c3* and muscular dystrophy.

3.2 Introduction

Phosphatidylinositols (PtdIns) comprise a group of low-abundance lipids with hydroxylated inositol head groups that are capable of receiving phosphates at any of the three outer positions. Dynamic phosphorylation of the inositol ring influences many cellular and metabolic processes including endocytosis, endosomal trafficking, and

autophagy (Itoh and Takenawa 2002, Payrastre 2004, Di Paolo and De Camilli 2006, Michell, Heath et al. 2006, Lecompte, Poch et al. 2008). The quantity and localization of different PtdIns*P*s are regulated by a group of phosphoinositide kinases and phosphatases that function as key regulatory gene products and that have been implicated in a number of human diseases, including especially oncologic and neurodegenerative diseases (De Camilli, Emr et al. 1996, Lindmo and Stenmark 2006, Volpicelli-Daley and De Camilli 2007, Nicot and Laporte 2008).

Myotubular Myopathy (MTM) is a severe childhood onset disease of skeletal muscle caused by mutations in the phosphoinositide phosphatase myotubularin (*MTM1*) (Laporte, Bedez et al. 2003, Dowling, Vreede et al. 2009). MTM is characterized by profound weakness and hypotonia at birth, persistent life-long disabilities including wheelchair and ventilator dependence, and early mortality (Das, Dowling et al. 2011). As predicted by the fact that MTM1 has been shown *in vitro* to be responsible for dephosphorylation of PtdIns(3)*P*, levels of PtdIns(3)*P* are significantly elevated in animal models of MTM (Dowling, Vreede et al. 2009, Pierson, Dulin-Smith et al. 2012, Amoasii, Hnia et al. 2013). Despite growing knowledge of disease pathogenesis, there are currently no available treatments for MTM. One significant barrier toward therapy development for MTM is the fact that the normal function(s) of PtdIns(3)*P* in skeletal muscle are unknown.

PtdIns(3)*P* is created through phosphorylation of PtdIns at the 3 position of the inositol ring by PtdIns 3-kinases (Backer 2008, Meijer and Klionsky 2011), or through dephosphorylation of PtdIns(3,5)P_2 by FIG4 (Jin, Chow et al. 2008). There are three classes of PtdIns 3-kinases that produce PtdIns(3)*P* in mammals, with varying tissue expression and substrate specificity (Yan and Backer 2007, Vanhaesebroeck, Guillermet-Guibert et al. 2010). In skeletal muscle, the primary sources of PtdIns(3)*P* are hypothesized (based on gene expression) to be the class III kinase, *Pik3c3* (*hVPS34*), and the class II kinase *Pik3c2β*, with PIK3C3 considered the major enzymatic regulator of its production (Herman and Emr 1990, Backer 2008, Meijer and Klionsky 2011). Previous studies of PIK3C3 have identified it as a regulator of several intracellular processes including endosome-to-golgi membrane traffic (Lindmo and Stenmark 2006),

endocytosis (Futter, Collinson et al. 2001, Johnson, Overmeyer et al. 2006), mTOR-S6K1 signaling (Nobukuni, Kozma et al. 2007, Nishida, Arakawa et al. 2009), and autophagy.

A homologue for the gene product of *Pik3c3* was initially discovered and characterized in yeast as vacuolar protein-sorting 34 (Vps34), with mutants exhibiting defective partitioning of the vacuolar membrane between mother and daughter cells (Herman and Emr 1990). It was later found to be present in a number of complexes with other kinases and regulatory proteins such as Vps15 (known as PIK3R4 in mammals) (Stack, Herman et al. 1993), Beclin1 (Furuya, Yu et al. 2005), and the GTPase, Rab7 (Stein, Cao et al. 2005). Early in the studies of Vps34/Vps15 in yeast, there were already suggestions of multiple complexes forming under circumstances promoting either autophagy or carboxypeptidase Y (Kihara, Noda et al. 2001), that eventually became known as complex I (Vps34, Vps15, Vps30/Atg6, and Atg14) and complex II (Vps34, Vps15, Vps30/Atg6, and Vps38), regulating autophagy and vacuolar protein sorting, respectively (Itakura, Kishi et al. 2008). Mammalian homologues were characterized forming similar complexes, with Vps34 known as hVps34 or PIK3C3, Vps15 known as PIK3R4, Vps30/Atg6 known as Beclin1, Atg14 known as Atg14l, and Vps38 known as UV irradiation resistance-associated gene (UVRAG) (Itakura, Kishi et al. 2008). Perhaps its best-studied function is in autophagy, where PIK3C3 and its regulatory subunit PIK3R4 form multiple complexes with other autophagy genes to regulate several steps of autophagosome formation and maturation (Funderburk, Wang et al. 2010, Miller, Tavshanjian et al. 2010, Jaber, Dou et al. 2012, Nemazanyy, Blaauw et al. 2013).

The goal of this study is to begin understanding the role of PtdIns(3)*P* in skeletal muscle by evaluating the function of PIK3C3. As previously reported, whole animal gene knockout of *Pik3c3* in the mouse results in early embryonic lethality (Zhou, Wang et al. 2010, Zhou, Takatoh et al. 2011). Therefore, to study PIK3C3 specifically in muscle we have utilized the Cre-lox system. Cre-lox mediated knockout of *Pik3c3* has been performed in kidney (Bechtel, Helmstadter et al. 2013), liver and heart (Jaber, Dou et al. 2012), sensory, cortical and hippocampal neurons (Zhou, Wang et al. 2010, Wang, Budolfson et al. 2011), and T-cells (Willinger and Flavell 2012), but *Pik3c3* has yet to be examined in skeletal muscle. We generated mice with conditional knockout of *Pik3c3* in skeletal muscle by combining floxed *Pik3c3* (Zhou, Wang et al. 2010) and Cre

recombinase under the muscle creatine kinase promoter: Tg(Ckmm-Cre) (Bruning, Michael et al. 1998). The resulting mice had normal embryonic and early postnatal development, but died by 2 months of age, presumably from severe cardiomyopathy (Jaber, Dou et al. 2012). Somewhat surprisingly, examination of skeletal muscle in knockout animals revealed a murine muscular dystrophy. We present the comprehensive characterization of this dystrophic phenotype. In all, we report for the first time a requirement for *Pik3c3* in skeletal muscle homeostasis, and further identify loss of *Pik3c3* as a cause of muscular dystrophy in the mouse.

3.3 Results

3.3.1 Generation and verification of muscle specific Pik3c3 knockout mice

We generated muscle specific *Pik3c3* knockout mice by breeding mice harboring a conditional null mutant allele, in which exons 17 and 18 of *Pik3c3* are flanked by *LoxP* sites (*Pik3c3*$^{flox/+}$) (Zhou, Wang et al. 2010), with previously characterized transgenic mice expressing Cre recombinase under the muscle creatine kinase (Ckmm) promoter (*TgCkmm-Cre*) (Bruning, Michael et al. 1998). Heterozygous animals (*Pik3c3*$^{flox/+}$*;TgCkmm-Cre*$^{+}$) were intercrossed to produce *Pik3c3* muscle specific knockout mice (*TgCkmm-Cre*$^{+}$*; Pik3c3*$^{flox/flox}$), referred to as *Pik3c3*-cKO or simply KO, and sibling mice, referred to as littermate controls or wild type (WT). An example of PCR based genotyping, using previously published primers (Zhou, Wang et al. 2010), from a representative cross is presented in Figure 3.1A.

To verify that we successfully achieved knockdown of *Pik3c3* expression, we compared both transcript and protein levels from skeletal muscle of knockout mice and age-matched littermates. Quantitative RT-PCR (qPCR) revealed an average reduction in skeletal muscle of (mRNA) *Pik3c3* levels of 82 ± 31% (s.e.m.) in knockout mice compared to wild types ($n = 4$, $p = 0.038$) (Figure 3.1B). Western blot analysis of extracts from quadriceps muscle demonstrated an average reduction of PIK3C3 protein levels to 11 ± 4% (s.e.m.) of wild type ($n = 3$, $p < 0.001$) (Figure 3.1C, D).

PIK3C3 is hypothesized to be the primary kinase that generates PtdIns(3)*P*. To determine the consequence of reduced PIK3C3 levels on PtdIns(3)*P* levels, we next examined PtdIns(3)*P* levels from quadriceps muscle of knockout animals and wild type

littermates. We did this using an established PtdIns(3)*P* ELISA (Pierson, Dulin-Smith et al. 2012). ELISA based analysis revealed a reduction of PtdIns(3)*P* levels in skeletal muscle of knockout animals to 50% of controls (n = 9) (Figure 3.1E). This level of reduction is in keeping with (though less than) the reduction of amount of PIK3C3 protein, and supports the previous assumption that PIK3C3 is the primary (but not sole) kinase responsible for PtdIns(3)*P* production in skeletal muscle.

3.3.2 Muscle specific knockdown of Pik3c3 resulted in premature lethality

Pik3c3-cKO animals appeared normal at birth, and are qualitatively similar to littermates through the first month of extra-uterine life (Figures 3.2A,B). This was revealed subjectively through animal appearance and activity, and objectively by analysis of body weight of gender-matched animals, as comparisons did not show significant differences (Figure 3.2A-C). In addition, skeletal muscle tissue taken from animals sacrificed within the first month appeared histologically normal (Figure 3.9).

However, between 40 and 60 days of age, KO animals began to exhibit an overt phenotype consisting mainly of reduced voluntary activity. The youngest animal observed in our cohort to demonstrate overt phenotypic changes did so at age 42 days (n = 27 KO animals). Shortly after first signs of disease, the *Pik3c3*-cKO animals displayed progressively reduced mobility as well as early mortality. The youngest age of death was 42 days old, while the oldest living knockout animal survived only to 62 days (Figure 3.2D). The exact cause of death in KO animals was not precisely known, though we strongly suspect it is related to cardiac disease (see below).

3.3.3 Pik3c3 knockout causes a severe dilated cardiomyopathy

Because the Ckmm promoter expresses in cardiac and skeletal muscle, we next examined the hearts of *Pik3c3*-cKO animals. We first analyzed levels of *Pik3c3* transcript from heart tissue by qPCR (Figure 3A), and showed an average reduction of 87±3% (s.e.m.). We next examined the gross anatomic phenotype of the hearts, and observed a dramatic increase in heart size, with the average knockout heart to body mass ratio measuring 250% of aged matched controls: (Figures 3.3B,C). Low magnification histopathologic analysis corroborated this anatomic observation, revealing qualitative

enlargement and thickening of both atrium and ventricle (n = 3) (Figure 3.3D). In addition, echocardiography showed evidence of significant cardiac hypertrophy and severe cardiac dysfunction (Table 3.1). While B-mode measurements of chamber dimensions were largely unchanged, all measurements of septal and posterior left ventricular wall thickness by M-mode were significantly increased in *Pik3c3*-cKO mice (Figure 3.3D), with estimated ventricular mass consistent with the morphological findings in isolated hearts. Indices of systolic function including ejection fraction and stroke volume and cardiac output were all decreased in *Pik3c3*-cKO, while resting heart rate was unchanged. Diastolic function was also impaired as indicated by an increase in isovolumic relaxation time and ratio of mitral valve E blood velocity to E' tissue Doppler velocity at the septal annulus. In all, our analysis supports a conclusion that *Pik3c3* deletion in the heart causes a severe cardiomyopathy. Of note, our results are consistent with a previously published study using cre-lox knockout of *Pik3c3* (Jaber, Dou et al. 2012).

3.3.4 Pik3c3 knockout results in a murine muscular dystrophy

As our primary interest in creating conditional knockouts of *Pik3c3* was to examine its requirement for skeletal muscle development and homeostasis, we focused all subsequent studies on skeletal muscle. We began our analysis by performing routine histopathology studies from quadriceps, gastrocnemius, and tibialis anterior muscles. Hematoxylin and eosin staining of fresh frozen, cryosectioned muscle from 42-60 day old animals revealed clearly abnormal areas with features that included inflammatory infiltrates (small blue cells, indicated by arrows), and degenerating and regenerating fibers (arrowheads) (Figure 3.4). Within these areas of abnormal muscle, there was a significant increase in myofibers with internalized nuclei (Figure 3.10A), consistent with muscle regeneration (Figure 3.4A,B). In total, the histopathological changes (inflammatory cells, increased internal nuclei and degenerating fibers) were consistent with a murine muscular dystrophy. These changes were seen in all muscle groups evaluated and in multiple different animals (n=5).

Of note, there were as well areas of relatively unaffected muscle next to areas with dystrophic changes. In addition, muscles harvested from older knockout animals had

more areas of aberrant fibers, while (as mentioned above) muscle analyzed before 1 month of age appeared normal (Figure 3.9). Also, average fiber size was not significantly different between knockouts and their littermates (Figure 3.10B). Lastly, we did not observe an increase in fibrosis in dystrophic muscle areas of the knockout animals (Figure 3.11).

To corroborate the histopathologic observation of dystrophic muscle in *Pik3c3* knockout mice, we used two additional strategies (Figure 3.5). The first was to measure serum creatine phospho-kinase (CK) levels. We obtained blood samples from the saphenous vein of animals that were not previously exposed to strenuous exercise or diet modifications. CK levels were significantly and highly elevated ($p = 0.0062$). The average level in 45 day-old mice was almost 20-fold higher in conditional knockout animals (5450 ± 1260, $n=4$) as compared to their littermate controls (230 ± 66, $n=4$, Figure 3.5A).

The second measure of muscular dystrophy was assessment of Evans blue dye uptake in skeletal muscle (Figure 3.5B). After systemic injection of Evans blue dye, damaged/dystrophic fibers demonstrate dye uptake, while healthy fibers do not. As compared to wild types, there was a visible increase in EBD positive fibers, indicating damaged muscle in the knockouts. Importantly, there was only a slight increase in EBD in the hearts of knockout animals (Figure 3.12), suggesting that the elevated CK levels found in the knockouts are most likely from skeletal (and not cardiac) muscle breakdown. In all, based on histopathology, serum CK levels, and EBD studies, we concluded that reduction of *Pik3c3* expression resulted in a murine muscular dystrophy.

3.3.5 Ultrastructural analysis reveals aberrant membrane structures

We performed analysis of skeletal muscle ultrastructure to look for clues related to muscle disease pathogenesis. Despite elevated CK levels and abnormal EBD uptake, no obvious membrane discontinuities or tears were observed in *Pik3c3* cKO muscle. However, there were widespread and striking abnormalities in several subcellular structures (Figure 3.6). Specifically, among the various abnormalities we observed, we detected frequent swellings associated with internal sarcolemmal membranes (Figure 3.6B, arrows) as well as aberrantly appearing mitochondria (Figure 3.6B, arrow-heads).

We also observed degradation compartments surrounded by double membranes, a finding consistent with aberrant autophagy (Figures 3.6C,E, arrows). Overall, these changes were consistent with a defect in membrane turnover (Millay, Maillet et al. 2009), and resemble changes seen in skeletal muscle with defective autophagy (Nishino 2003).

3.3.6 Autophagy genes had aberrant expression and localization in cKO animals

One of the functions of PIK3C3 *in vitro* is in the initiation of autophagy. Given that the ultrastructural changes were reminiscent of defective autophagy, we examined *Pik3c3* cKO muscle for evidence of aberrant autophagy. We examined autophagy using three approaches: (1) measurement of autophagy related gene expression changes by qPCR, (2) examination of autophagic markers by Western blot analysis, and (3) study of markers by immunocytochemistry. qPCR revealed significant increases in transcripts associated with autophagy, including upregulation of *p62* (4.5 ± 0.97 fold change) and *LC3* (3.3 ± 0.53 fold change) (Figure 3.7A). We also detected increased expression of gene products associated with muscle atrophy, such as ubiquitin ligases *atrogin-1* (7.0 ± 1.7 fold change) and *MuRF1* (3.1 ± 0.71 fold change). Similarly, we observed significant increases in levels of the lysosomal proteinase, *cathepsin L* (9.1 ± 1.8 fold change). While other reports (Mammucari, Milan et al. 2007) on muscle wasting have shown upregulation in *Bnip3* and *Bnip3l*, levels of these transcripts were unaffected by the Pik3c3 knockout: *Bnip3* had a 0.92 ± 0.2 fold change and *Bnip3l* gave a 0.86 ± 0.23 fold change when normalized to WT animals. This is consistent with the fact that we did not detect any corresponding alterations in overall muscle size or in the size of individual fibers (Figure 3.10).

We next examined autophagy by looking at protein markers of the pathway. Western blot analysis showed significant increases in total protein levels of LC3 and p62: LC3-I increased 604% ± 137% and LC3-II by 420% ± 118%, while ratios of LC3-I:LC3-II remained not significantly different (147% ± 12%) (Figure 3.7B-E); p62 antibody showed increases in KO muscle to 1593% ± 137% that of WT controls, using β-actin as internal control (n=3). These changes are consistent with defective autophagic flux and with the measurements of transcript levels. We performed immunocytochemical analysis using an antibody to p62, a protein associated with the initiation of autophagy that

accumulates when autophagic flux is impaired. We observed significant accumulation of p62 with fibers of KO animals, as compared to basically absent staining in age-matched control siblings (Figure 3.7F-H). In total, *Pik3c3*-cKO resulted in upregulation of markers of autophagy, but rather than showing turnover of key proteins, we witnessed an accumulation of the markers of autophagosome formation, consistent with an overall impairment in the initiation of autophagy.

3.3.7 Loss of PIK3C3 causes impairment in lysosomal function

Because aberrant autophagy alone is unlikely to explain the histopathologic changes we observed, we sought to uncover additional potential causes for dystrophic muscle pathology in the KO mice. Because elevated CK levels and increased EBD uptake were suggestive of compromised integrity of the muscle's external membrane, we analyzed expression and localization of integral membrane proteins using immunohistochemistry. We observed striking changes in the localization of both dystrophin and caveolin-3. In numerous muscle fibers from KO (but not wild type) animals, these proteins, while still present at the membrane, also accumulated within the myofiber (Figure 3.8B,C,E,F). The mislocalization of these proteins occurred without a change in their overall levels, as determined by western blot analysis (Figure 3.13).

Internal accumulation of membrane proteins has been previously reported in the setting of abnormal lysosomal function (Nemazanyy, Blaauw et al. 2013). We therefore sought to interrogate lysosomal function in our knockout animals. We examined LAMP1 staining, and found two important changes as compared to wild types (Figure 3.8A,D): accumulation of LAMP1 staining within myofibers as well as increased intensity of LAMP1 staining around the plasma membrane. Both findings have been observed in other models of lysosomal dysfunction (Malicdan and Nishino 2012). In order to quantitate a possible abnormality in lysosomal function, we looked at cathepsin-D processing by western blot analysis. Cathepsin-D processing is used as a marker for the normal functioning of the lysosome. We found a significant decrease in the mature forms of cathepsin-D, suggesting a significant abnormality in the ability of the lysosome to cleave cathepsin to its mature, active form (Figure 3.8G,H). Taken together with the immunostaining results for LAMP1, dystrophin and caveolin-3, these results are

consistent with impaired lysosomal function and suggest aberrant lysosomal processing is the cause of membrane protein mislocalization.

3.4 Discussion

In summary, we have generated muscle-specific knockout mice of *Pik3c3* (Vps34) and provided the first phenotypic description of the role of PIK3C3 in skeletal muscle. Knockout mice had reduced levels of *Pik3c3* mRNA and protein in striated muscle, and had significantly reduced levels of PtdIns(3)*P*, the phospholipid generated by PIK3C3. Using both morphological and functional analyses, we identified significant changes in skeletal and cardiac muscle structure and function and in the overall health of the animals, including premature lethality in the second postnatal month. Our results specifically identify PIK3C3 as a gene product required for normal muscle structural integrity and for the regulation of basal autophagy and lysosome function in skeletal muscle.

One of the most significant findings in our study was the appearance of dystrophic muscle pathology in affected mice. This observation was in contrast to our pre experiment prediction that loss of *Pik3c3* would be associated with abnormalities similar to those observed with myotubularin dysfunction, as both over expression and knockout of *Mtm1* cause significant disruption of the sarcotubular network and (at least for *Mtm1* knockout) a centronuclear myopathy phenotype. *Pik3c3*-cKO mice clearly did not have a centronuclear myopathy, but instead had changes consistent with a muscular dystrophy. The presence of a dystrophy was established based on histopathology, CK levels, and Evans blue dye staining, and our study thus provides a connection between dysfunction in PtdIns*P* regulation and dystrophic muscle pathology. Of note, a recent study described the muscle specific knockout of Vps15, which functions as a co-factor of PIK3C3 required for many aspects of its function. These mice similarly manifested a murine muscular dystrophy, a finding that corroborates the data from the present manuscript (Nemazanyy, Blaauw et al. 2013).

The appearance of dystrophic pathogenesis gives insight into the involvement of PIK3C3 in pathways other than canonical Beclin-complex-mediated autophagy. Based on previous knockout mice studies, it is unlikely that the defects in autophagy we observed

in *Pik3c3* KOs are sufficient to explain the severe muscular dystrophy seen in these animals. Specifically, disruption the essential components of autophagic machinery *Atg7* and *Atg5* does not result in dystrophic pathology, but instead a mild myopathy characterized by reduced myofiber size (Raben, Hill et al. 2008, Masiero, Agatea et al. 2009). Instead, we postulate that abnormalities in lysosomal function are more likely to be the cause of the dystrophic animals. This assertion is supported by two major observations. The first is that mutations in the lysosomal proteins LAMP2 and GAA both result in skeletal muscle disease (Danon Disease (Malicdan and Nishino 2012) and Pompe Disease (Raben, Roberts et al. 2007), respectively) with dystrophic features. The second is that lysosomal function (and in particular lysosomal exocytosis) has been implicated in the regulation of membrane repair (Chakrabarti, Kobayashi et al. 2003), and defective membrane repair is a well-established trigger for the development of muscular dystrophy (Shin, Tajrishi et al. 2013). Additional experimentation will obviously be necessary to specifically establish why the loss of PIK3C3 function causes a muscular dystrophy, and to parse out which of the many potential functions of the protein are responsible for regulating membrane integrity in skeletal muscle.

Of note, there are several independent studies of mice with conditionally deleted alleles of *Pik3c3* in neurons (Zhou, Wang et al. 2010), in T-cells (Willinger and Flavell 2012), in podocytes (Bechtel, Helmstadter et al. 2013), and in heart and liver (Jaber, Dou et al. 2012). Consideration of these studies reveals several common features of organs lacking PIK3C3 that are seen as well in our muscle-specific deletion. These include aberrant autophagy, disrupted cellular homeostasis, and overall degeneration of tissues. Also, there are some specific differences when comparing studies of different cell types, including controversy over which stages of autophagy are most affected by loss of PIK3C3 function (Jaber, Dou et al. 2012, Nemazanyy, Blaauw et al. 2013). It should be noted that there are still many aspects of autophagy initiation and regulation that are not well understood, such as the extent of non-canonical pathways (sans Beclin-1), and cells use multiple processes for sequestering and/or delivering targets to the lysosome (Codogno, Mehrpour et al. 2012), and future studies of the various knockout strains of PIK3C3 may help illuminate these issues.

Lastly, it should also be noted that PIK3C3 is not the only means for generating PtdIns(3)*P* in skeletal muscle. This assertion is supported by the fact that we observe a 50% reduction in PtdIns(3)*P* levels in the muscle of knockouts, despite achieving much higher levels of PIK3C3 reduction. One candidate for generating a fraction of PtdIns(3)*P* in skeletal muscle is PIK3C2B, a class II PI 3-kinase that is expressed in skeletal muscle and whose function is poorly understood. Experimentation addressing the role of PIK3C2B in muscle, and its interplay with the functions of PIK3C3, will obviously be important to best understand the role of PtdIns(3)*P* and its regulation in skeletal muscle.

3.5 Conclusions

To summarize, muscle-specific conditional knockout of PIK3C3 revealed a novel murine dystrophy with aberrant autophagy and lysosomal function. These novel knockout mice provide a useful animal model for the study of degradation pathways and their association to the pathogenesis of muscular dystrophy.

3.6 Materials and Methods

3.6.1 Care and treatment of animals

All care and treatment of animals was implemented through protocols carefully monitored by the University Committee on Use and Care of Animals (UCUCA). The University of Michigan's Unit for Laboratory Animal Medicine (ULAM) carefully monitored the health of the rodent colonies. ULAM maintained proper environmental regulation including temperature and light cycles, unlimited access to water, appropriate food supply, and clean enclosures. Pups were weaned from their mothers according to standard protocols, and tails were clipped for genotyping, as described.

3.6.2 Generation of mutant mouse strains

Floxed *Pik3c3* mice were a gift from Fan Wang lab, described in Zhou et al. (Zhou, Wang et al. 2010). Cre mice are of the strain: B6.FVB(129S4)-Tg(Ckmm-cre)5Khn/J, obtained from Jackson labs. Mice were crossed to make $Pik3c3^{fl/+}$; Cre^{+} heterozygous mice, and in-crossed to produce the double floxed allele: $Pik3c3^{fl/fl}$, resulting in the muscle-specific conditional knockout animals.

3.6.3 Genotyping of mutant mouse strains

Protocols and primers for genotyping mice were described previously (Zhou, Wang et al. 2010).

3.6.4 Quantitative PCR

Total mRNA was isolated from muscle homogenates using QIAGEN RNeasy kits, and qPCR was performed using cDNA reverse-transcribed by iScript (BioRad) on ABI equipment using SybrGreen reagents. Analysis was done by using the ΔΔCt method. Primers for transcripts analyzed were previously described (Mammucari, Milan et al. 2007).

3.6.5 Western blots

Protein was isolated from tissue from KO and littermate mice by mincing and homogenizing in T-PER buffer (Thermo) with proteinase inhibitors (Roche), with brief sonication on ice. Loading buffer was added to protein and run on 10%-15% acrylamide gels, followed by transfer to PVDF blots. Primary antibodies were applied overnight at 4˚C at 1:1000 dilution in 3%BSA, 0.5% TritonX-100, NaF.

Indirect analysis of protein expression was performed in ImageJ following procedures outlined by http://lukemiller.org/index.php/2010/11/analyzing-gels-and-western-blots-with-image-j/.

3.6.6 Histology

Animals were sacrificed by anesthetic injection followed by cervical dislocation, and tissues were isolated using sterile surgical methods without the use of laminar flow hoods. Muscle tissue from quadriceps and tibialis anterior was dissected and mounted onto small balsawood pieces that were previously frozen with drops of O.C.T. (Optimal Cutting Temperature, Tissue-Tek) and then semi-thawed with light friction. The mounted muscle tissue was immediately submerged in a -55˚C isopentane bath cooled by liquid nitrogen for flash freezing.

Muscles were cut in 12 µm cross-sections and mounted on SuperFrost Plus slides using a Leica cryostat at -20˚C, and dried at room temperature before storage at -80˚C.

Micrographs were captured with an Infinity1 camera with eponymous software visualized through an Olympus BX43 light microscope. Images were cropped in Adobe Photoshop and arranged for figures with Adobe Illustrator.

Standard techniques for indirect fluorescent immunohistology were used:

Snap-frozen tissues were cryosectioned and collected on superfrost slides. After allowing slides to dry, residual O.C.T. from mounting tissue on cryo-chuck was washed away with PBS. Slides were blocked for more than 30 minutes at room temperature in a solution of 0.25M KCl, 0.20mM HEPES with 1% BSA, 0.1% gelatin, 0.02% NaN_3 and 0.1% Triton X-100, pH 7.9. Slides were incubated overnight at 4˚C in Progen p62 anti-guinea pig, diluted 1:100 in blocking solution. After three washes in PBS, secondary antibodies (Alexa Fluor® 488 conjugated with goat anti-guinea pig IgG, Life Technologies) were applied for one hour at room temperature, diluted 1:1000 in blocking solution. Slides were washed several times to remove excess secondary and then mounted with ProLong® Gold (Life Technologies).

3.6.7 Bright-field imaging and fiber size analysis

Slides were stained with Mayer's Hematoxylin and eosin (H&E) following standard protocols, and mounted with Permount.

Post-capture analysis, including tests of statistical significance, was performed using Microsoft Excel 2008 and Graphpad Prism 5 for MacOSX.

3.6.8 TEM

Immediately following dissection, tips of quadriceps were carefully cut into ~1x2mm fragments, and incubated in Karnovsky's fixative overnight at 4˚C.

The fixed tissue was brought to the Microscopy and Imaging Laboratory (MIL) Core facility at the University of Michigan for processing. Ultrathin sections were analyzed for orientation, and grids were prepared for use on the Phillips CM-100 transmission electron microscope (TEM).

3.6.9 Measurements of serum CK

Serum was collected from the saphenous vein of restrained animals and stored at −80°C. Creatine kinase activity was measured in duplicate using CK NADP Reagent (Cliniqa, San Marcos, CA, USA).

3.6.10 Evans Blue Dye uptake assay

Evans Blue Dye was injected intraperitoneally, and allowed to infiltrate tissues over the course of 24 hours before mice were sacrificed and tissues sectioned as described above.

3.6.11 Echocardiographic analysis

Echocardiograms were taken of the mice as described previously.

3.6.12 PtdIns(3)P ELISA

Lipid analysis was performed by indirect analysis of whole muscle lysates using Echelon's PtdIns(3)*P* Mass ELISA kit (K-3300), as previously described (Pierson, Dulin-Smith et al. 2012).

3.7 Figures

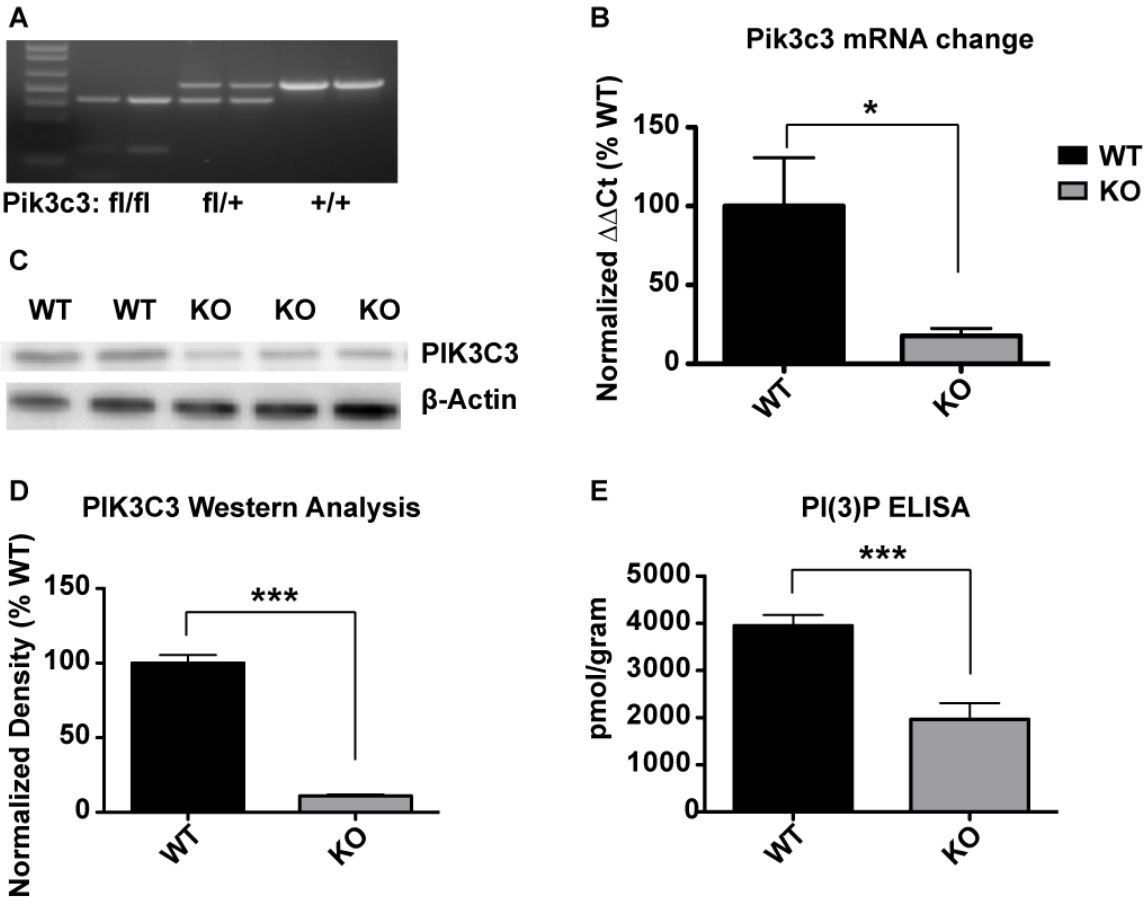

Figure 3.1 Muscle specific *Pik3c3* knockout causes significant decrease in PIK3C3 and PtdIns(3)*P* levels.

Muscle specific knockout of *Pik3c3* was confirmed through direct (DNA, mRNA, protein) and indirect (PtdIns(3)*P* levels) measures. Samples were obtained from quadriceps muscle isolated from 6-8 week old mice, with age-matched littermate controls, unless otherwise noted. (A) Genotyping of mice harboring homozygous floxed (fl/fl), heterozygous (fl/+), or wild-type (+/+) alleles. (B) As measured by quantitative RT-PCR, a significant decrease in *Pik3c3* transcript levels (17.7% ± 4.7%, n=4) was detected in skeletal muscle from knockout (KO) animals. Values were normalized to *Gapdh* transcript levels, with wild type (WT) average value set at 100% (± 31%, n=4). (C) Western blot analysis confirmed reduction of PIK3C3 levels in skeletal muscle from KO animals. (D) Quantitation of PIK3C3 protein levels as determined by densitometric

analysis, using β-actin protein levels as a loading control, showed a decrease from WT levels (100% ± 5.4%) to 11.0% ± 1.0%. (E) PtdIns(3)*P* levels are reduced in KOs, as determined by using a PtdIns(3)*P* ELISA kit (purified lipid (pmol)/mass (g) of muscle tissue) (WT: 3967 ± 225; n=9, KO: 1982 ± 334; n=8). Error bars are presented as s.e.m. Significance: *, $p<0.05$; ***, $p<0.001$.

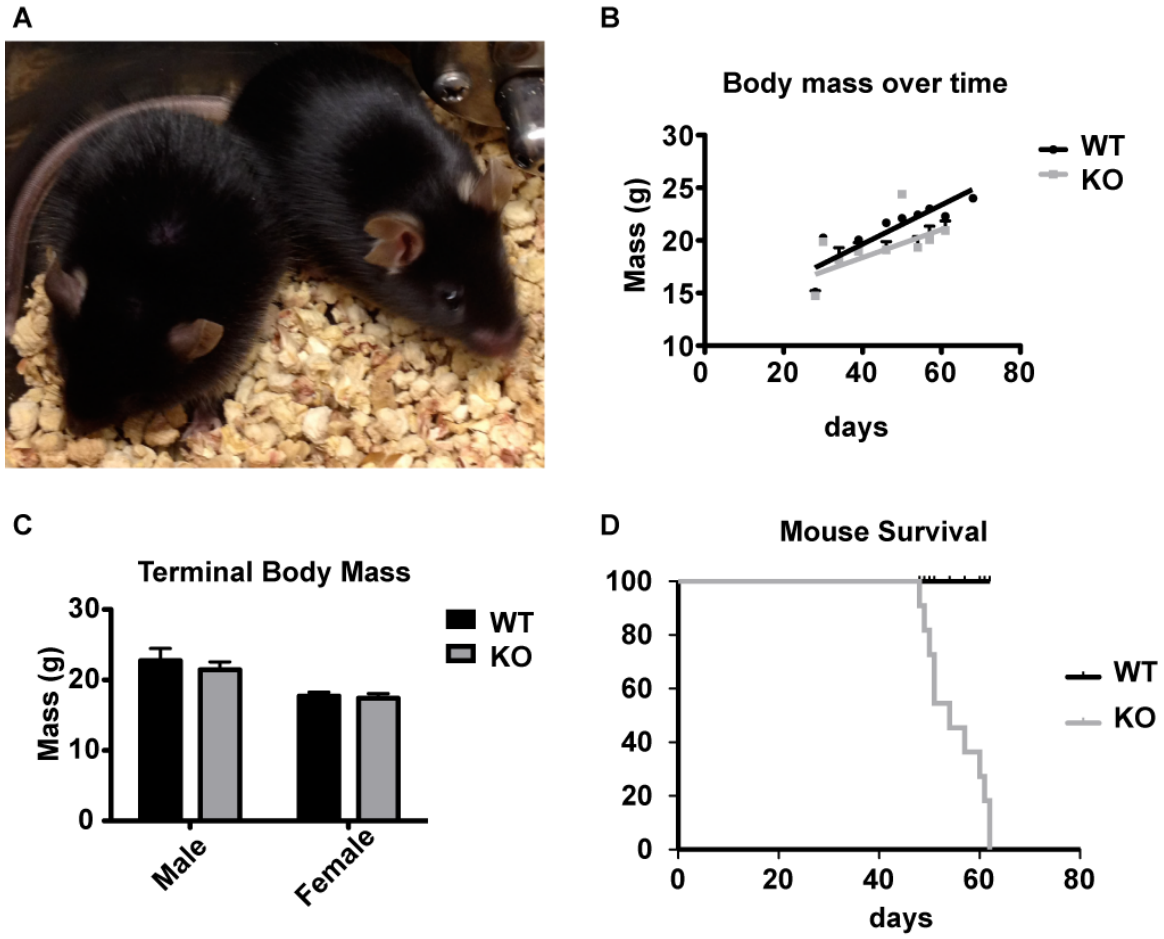

Figure 3.2 Muscle specific *Pik3c3*-cKO animals have reduced lifespan.

The disease phenotype of knockout (KO) mice develops after one month, and affected mice die rapidly after onset of symptoms. (A) Despite abnormal levels of activity, KO mice are difficult to distinguish by overall appearance from wild type (WT) littermates even at 6 weeks of age (KO is on the left). (C) Body mass of KO animals was not significantly different (slope p=0.21) than that of WTs, though weights trended smaller than age matched WT littermates towards the end of KO disease progression (lines represent linear regression WT n=3, KO n=4). (B) Terminal body mass of WT (22.7 ± 0.57 g for males and 17.7 ± 0.24 g for females) and KO animals (21.4 ± 0.38 g for males and 17.4 ± 0.29 g for females) are not significantly different (unpaired t-tests for males, p=0.075, n=9; for females, p=0.45, n=5). (D) KO mice die between 6 and 8 weeks of age, with median survival of 54 days (KO n=11, equal number of WT littermates were sacrificed to match age and gender).

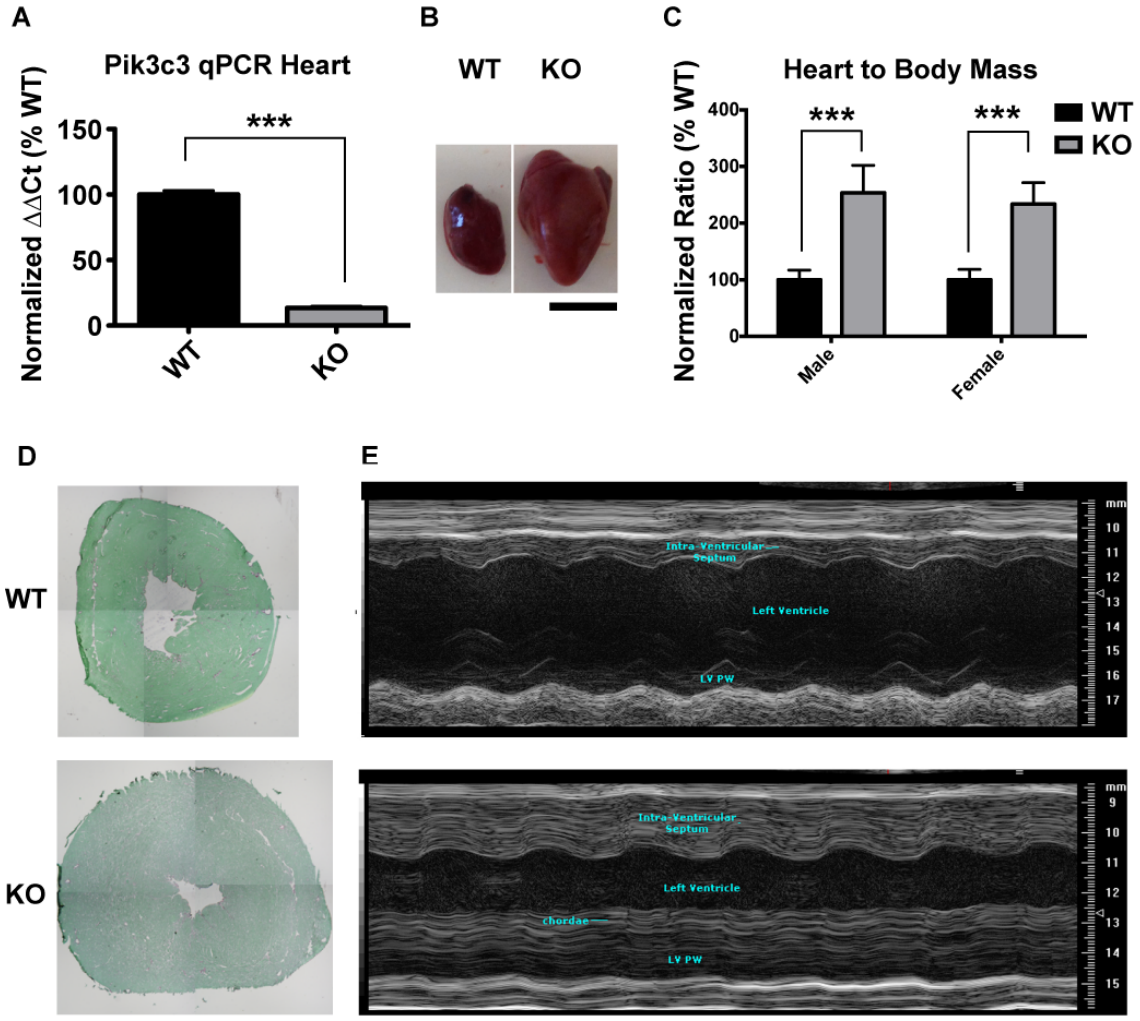

Figure 3.3 *Pik3c3*-cKO animals display cardiac abnormalities.

(A) As measured by qPCR, Ckmm driven cre expression in the heart leads to an 87% reduction in levels of *Pik3c3* transcript in KO (13.4 ± 1.2%) as compared to WT controls (100 ± 2.9%) (n=2, $p<0.001$). (B) Obvious cardiomegaly was observed in KO animals (scale bar = 50 mm). (C) Hearts in KO animals are 2-3 times the size of WT littermates. Increases in heart mass to body mass ratios are consistent in affected males (254 ± 16.1%) and females (234 ± 16.9%). (***, $p<0.001$). (D) Cross-sectional histology of hearts with sirius red stain demonstrates increased thickness of walls with no observable fibrosis (age = 45 days). (E) Representative M-mode echocardiograms from the left ventricle of KO mice show marked left ventricular wall hypertrophy compared to age-matched WT littermate mice.

Table 3.1 Echocardiographic analysis of VPSKO mice.

	WT	*Pik3c3*-cKO	P-value
BW (gm)	22.2 +/- 4.5	18.7 +/- 3.0	0.152
HR (bpm)	494 +/- 42	486 +/- 46	0.788
Chamber morphology			
LVDd (mm^2)	27.6 +/- 6.0	25.49 +/- 3.8	0.47
LVDs (mm^2)	17.6 +/- 3.5	19.2+/- 3.4	0.42
LVd length (mm)	7.36+/- 1.0	8.0 +/- 0.7	0.21
LVs length (mm)	6.25 +/- 0.9	7.2 +/- 0.7	0.06
LV Wall thickness			
IVSd (mm)	**0.73+/-0.05**	**1.19 +/- 0.15**	**<0.001**
IVSs (mm)	**0.99 +/- 0.08**	**1.47 +/- 0.26**	**0.001**
PWd (mm)	**0.68 +/- 0.04**	**1.2- +/- 0.16**	**<0.001**
PWs (mm)	**1.00 +/- 0.10**	**1.32 +/- 0.18**	**0.004**
LV mass (gm)	**0.11 +/- 0.02**	**0.19 +/- 0.03**	**<0.001**
Systolic function			
SV (ul/beat)	**46.4 +/- 17.1**	**25.1 +/- 4.7**	**0.016**
CO (ml/min)	**18.6 +/- 4.3**	**12.3 +/- 1.5**	**0.025**
EF (%) (B-mode)	**51.7 +/- 5.9**	**37.0 +/- 5.1**	**0.002**
EF (%) (M-mode)	**48.2 +/- 5.7**	**31.7 +/- 11.9**	**0.013**
Diastolic function			
IVRT (ms)	**17.58 +/- 2.83**	**30.05 +/- 10.7**	**0.021**
E/E'sa	**40.52 +/- 6.32**	**55.98 +/- 10.2**	**0.011**

Data are mean +/- SD, n=5 each genotype. Data in bold are statistically significant by Student's T-test. Abbreviations: BW, bodyweight; HR, heart rate; LVD left ventricular dimension; LV, left ventricular, IVS; intraventricular septum; PW, posterior wall; SV, stroke volume; CO, cardiac output; EF, ejection fraction; IVRT, isovolumic relaxation time; E/E'Sa, ratio of mitral valve E blood velocity to E' tissue Doppler velocity at septal annulus; lower case d and s, measurements made during systole (s) and diastole (d).

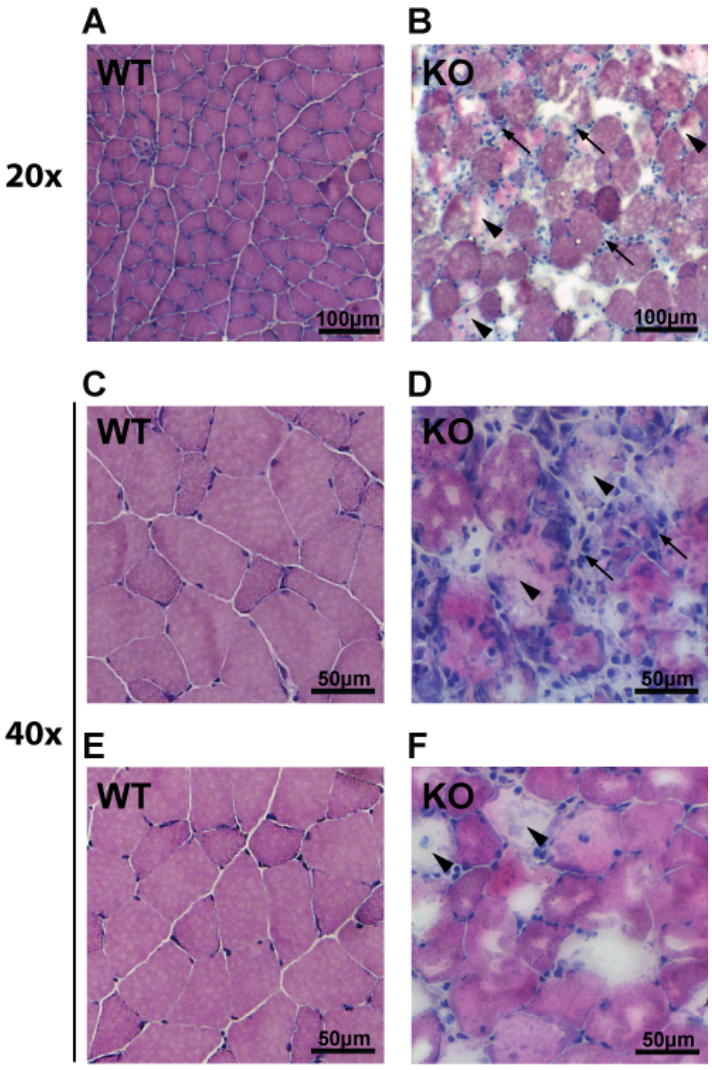

Figure 3.4 *Pik3c3*-cKO animals have aberrant histology.

Histological analysis of *Pik3c3*-cKO skeletal muscle shows signs of muscular dystrophy. Sections were taken from gastrocnemius muscle of 60-day-old wild type (WT) and knockout (KO) animals and stained with Hematoxylin and Eosin. (scale bar = 100 µm) (A) Low magnification images reveal inflammatory infiltrate (arrows) and changes consistent with degeneration and regeneration (arrowheads). (C-F) Higher magnification micrographs show changes as in (A,B) but also better reveal abundant internal nuclei. (scale bar = 50 µm).

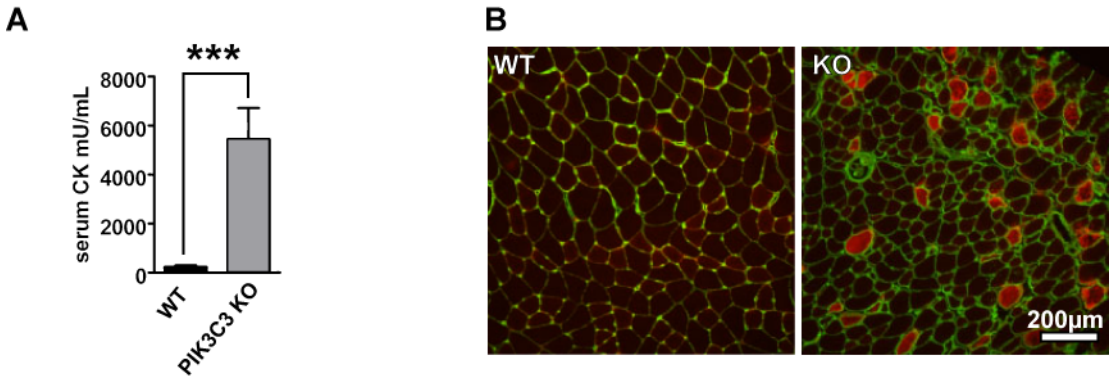

Figure 3.5 *Pik3c3*-cKO mice exhibit dystrophic muscle by independent measures.

(A) Creatine phosphokinase (CK) measurements of serum obtained from the distal saphenous vein showed increases of nearly 50 fold in excess when KO (avg = 5452 ± 1263 mU/mL, n=4) are compared to wild type littermates (avg = 233.3 ± 65.51 mU/mL, n=4). Significance: ***, $p<0.001$. (B) Evans Blue Dye (EBD) is taken up by dystrophic fibers after 24 hours of incubation following pertitoneal injection. EBD is shown in red and counterstained against the extracellular membrane protein Laminin in green. (Scale bar = 200 µm).

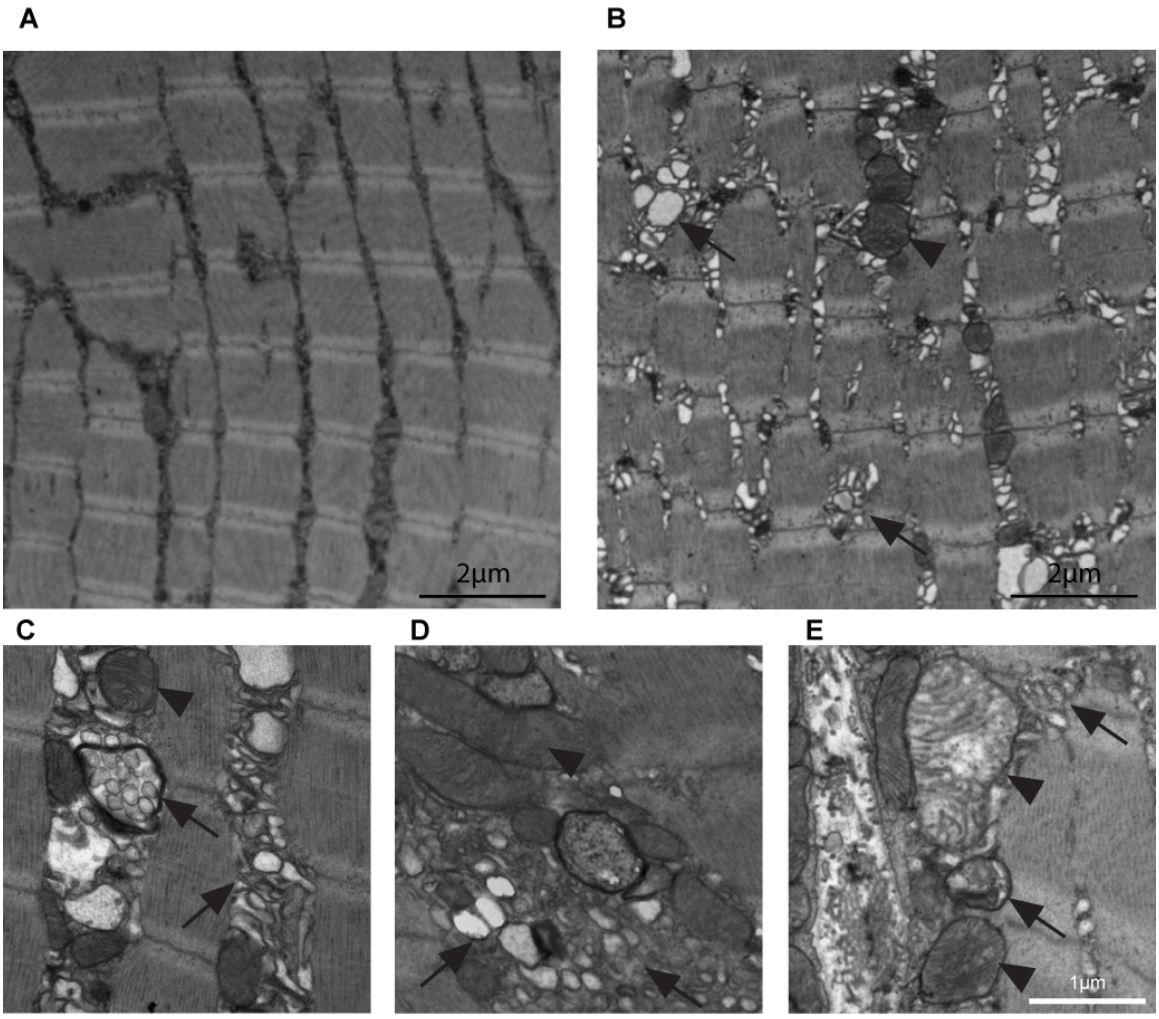

Figure 3.6 Ultrastructural analyses by TEM show aberrant features in *Pik3c3*-cKO mice.

Tissue from tibialis anterior muscle of six-week-old mice was prepared, mounted on slotted grids and imaged on a Phillips CM-100 transmission electron microscope. Analysis of TEM micrographs of wild type (WT) littermate controls (A) and *Pik3c3*-cKO (B-E) reveals numerous defects in muscle ultrastructure including sarcoplasmic swellings in addition to aberrant vacuoles (arrows) and mitochondria (arrowheads). Scale bar for (A,B) is 2 µm and for (C,D,E) 1 µm.

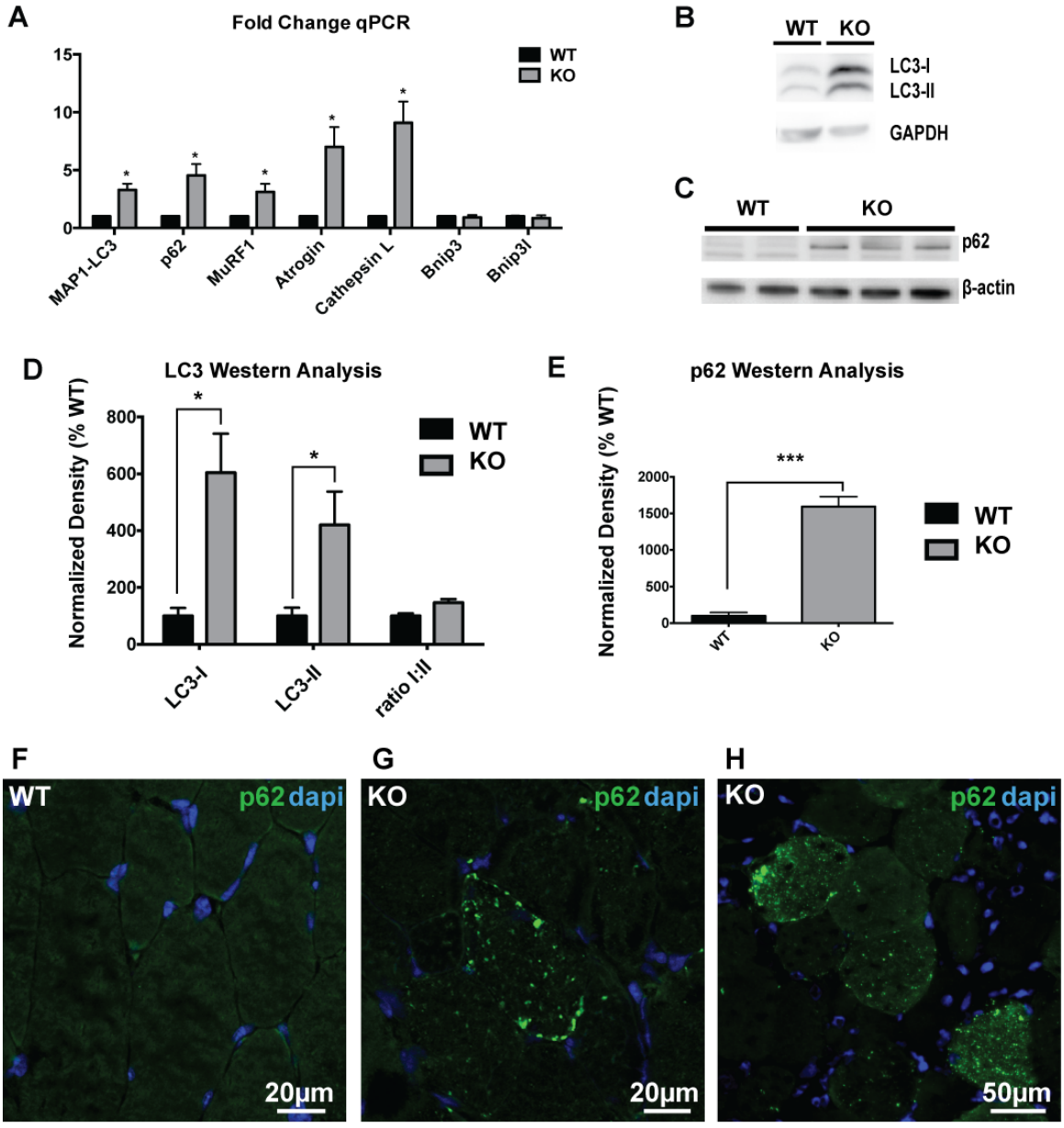

Figure 3.7 *Pik3c3*-cKO mice exhibit aberrant markers of basal autophagy.

(A) Transcript levels were measured from mRNA isolated from quadriceps of two-month-old *Pik3c3*-cKO (KO) and wild type (WT) littermates. Results using primers for *(Map1-)Lc3* (3.3 ± 0.53 fold change), *p62* (4.5 ± 0.97 fold change), *Murf1* (3.1 ± 0.71 fold change), *Atrogin1* (7.0 ± 1.7 fold change), *CathepsinL* (9.1 ± 1.8 fold change), *Bnip3* (0.92 ± 0.2 fold change) and *Bnip3l* (0.86 ± 0.23 fold change) were normalized to *Gapdh* internal controls. y-axis indicates fold increase normalized to littermate controls for ΔΔCt (n=3). (B, C) Protein was isolated from quadriceps of two-month-old KO and WT littermates for analysis by Western blot with antibodies against MAP1-LC3 and p62. (D) Densiometric analysis of LC3-I/II was performed using GAPDH as internal control (n=2), showing increases in LC3-I (604% ± 137%) and LC3-II (420% ± 118%), while

ratios of LC3-I:LC3-II remained not significantly different (147% ± 12%). (E) Densiometric analysis of blot probed with p62 antibody showed increases in KO muscle to 1593% ± 137% that of WT controls, using β-actin as internal control (n=3). Sectioned gastrocnemius muscle from 60-day-old animals stained using immunochemistry shows accumulation of p62/SQSTM1 (F, G, H). Scale bars are 20 μm for F and G, and 50 μm for H.

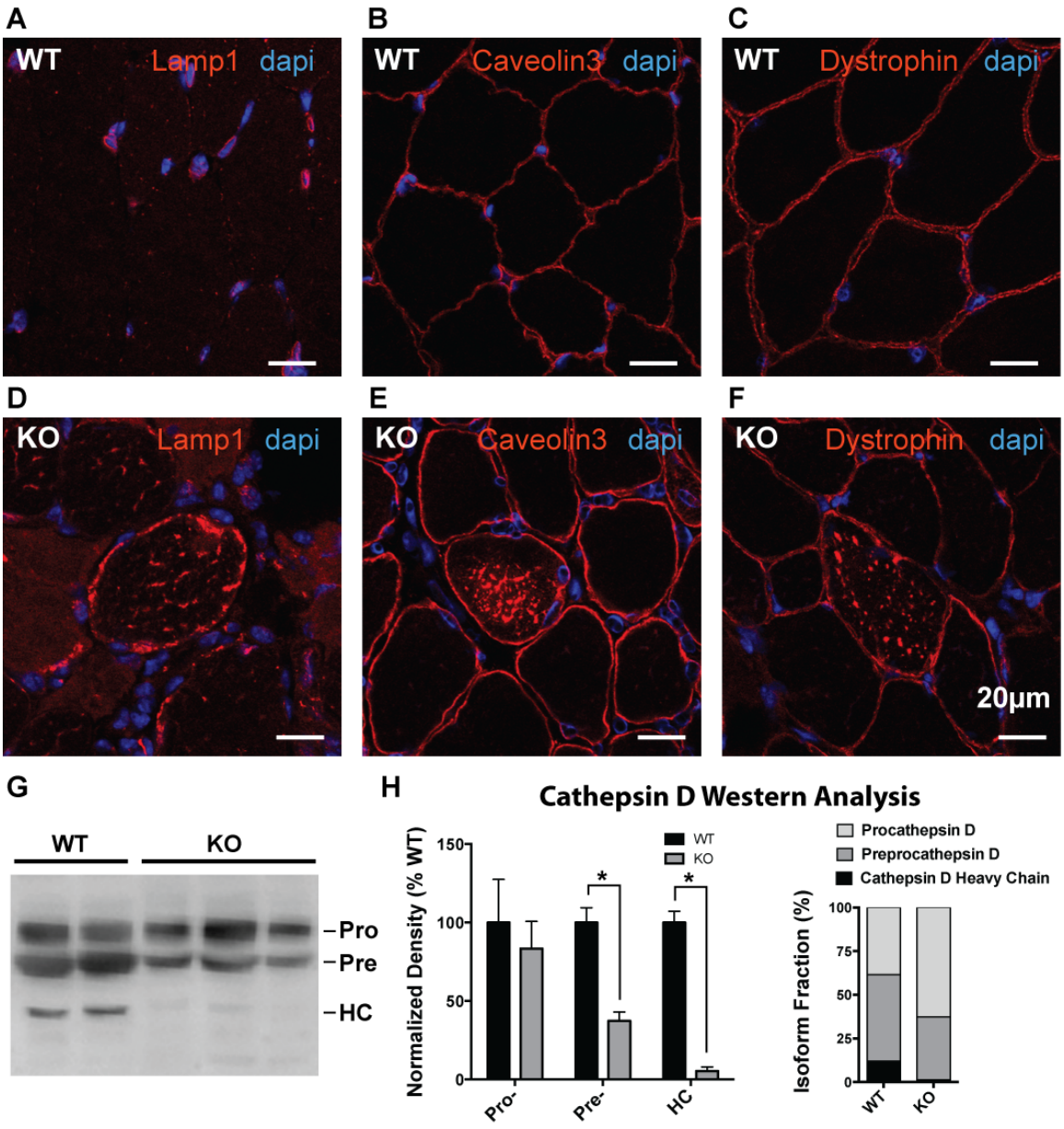

Figure 3.8 Aberrant accumulation of membrane-associated proteins indicates trafficking dysfunction.

Sectioned gastrocnemius muscle from 60-day-old animals stained using immunochemistry shows accumulation of LAMP1 (A and D), Caveolin-3 (B and E) and Dystrophin (C and F) in knockout (KO) animals compared to littermate controls. (G) Western blot of Cathepsin D reveals alterations in the processing of mature form in KO animals from Procathepsin D (Pro), Preprocathepsin D (Pre), and Cathepsin D heavy chain (HC) isoforms. (H) Densiometric analysis reveals significant decreases (p<0.01) in the levels of Pre and HC isoforms, demonstrated as overall levels normalized to β-actin at left, and as total fraction of Cathepsin D at right.

3.8 Additional Figures

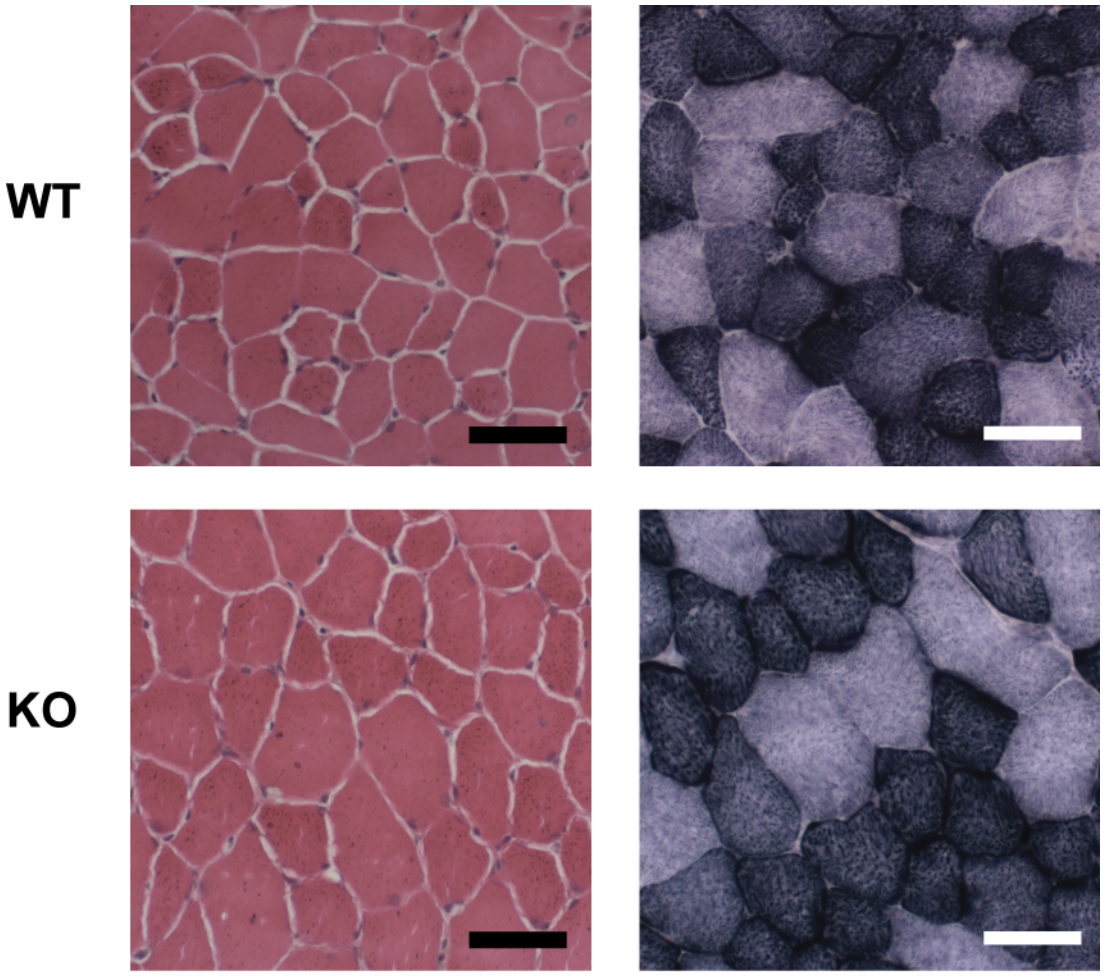

Figure 3.9 Muscle of young *Pik3c3* cKO animals appears normal by histological analysis.

Tibialis anterior muscle from animals harvested at 1 month of age appears normal. Top panels are from age matched littermate (WT) control. Bottom panels are from a *Pik3c3* knockout (KO) animal. Left panels are stained with H&E. Right panels are stained with SDH. Scale bars = 50 µm.

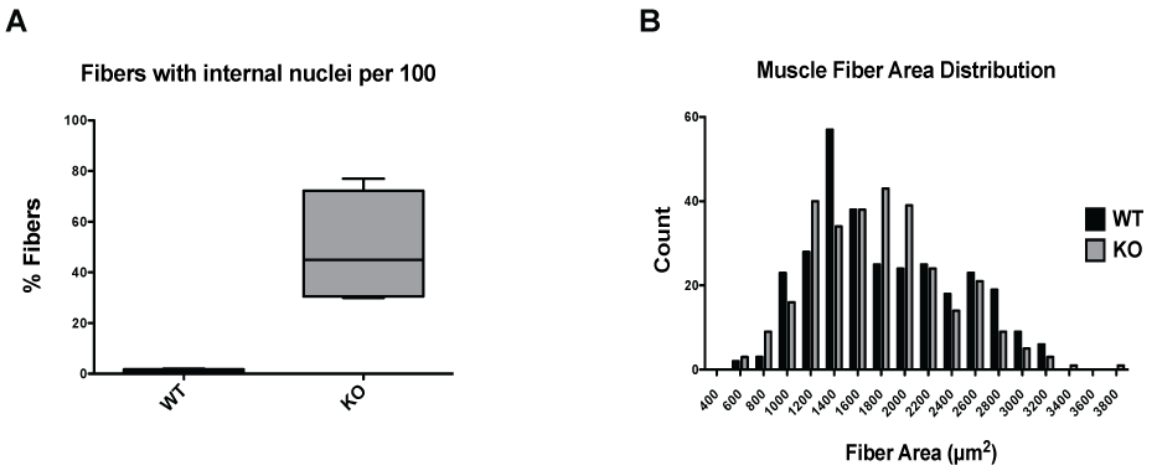

Figure 3.10 Cross-sectional muscle analysis is typical of a dystrophic phenotype.

(A) Concentrated areas of aberrant fibers contained elevated numbers of internalized nuclei in knockout (KO) animals (49 ± 11, n=4) compared to control littermates (WT) (1 ± 1, n=4). (B) Muscle fiber area distribution in knockout animals showed similar pattern to littermates (n=3).

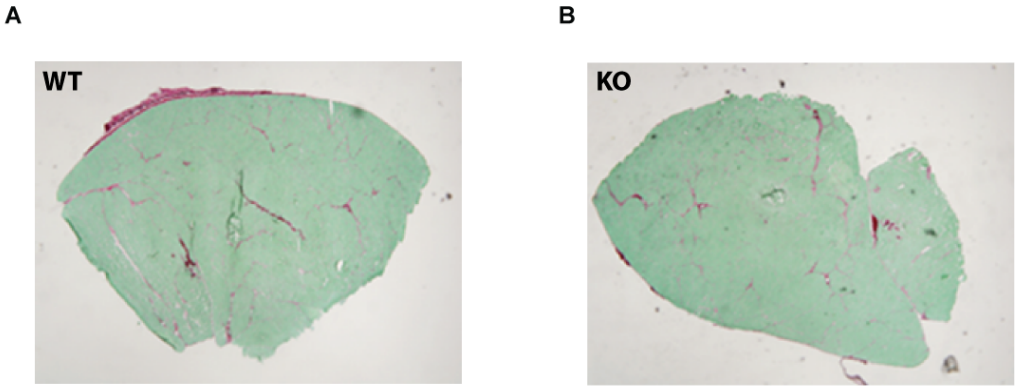

Figure 3.11 Fibrosis abnormalities are absent from muscle samples.

Representative level 3 tibialis anterior muscle of 48-day-old mice—control littermate (A), knockout (B)—stained with Gomori Trichrome as a test for fibrosis. There are no apparent differences between the controls and knockout animals.

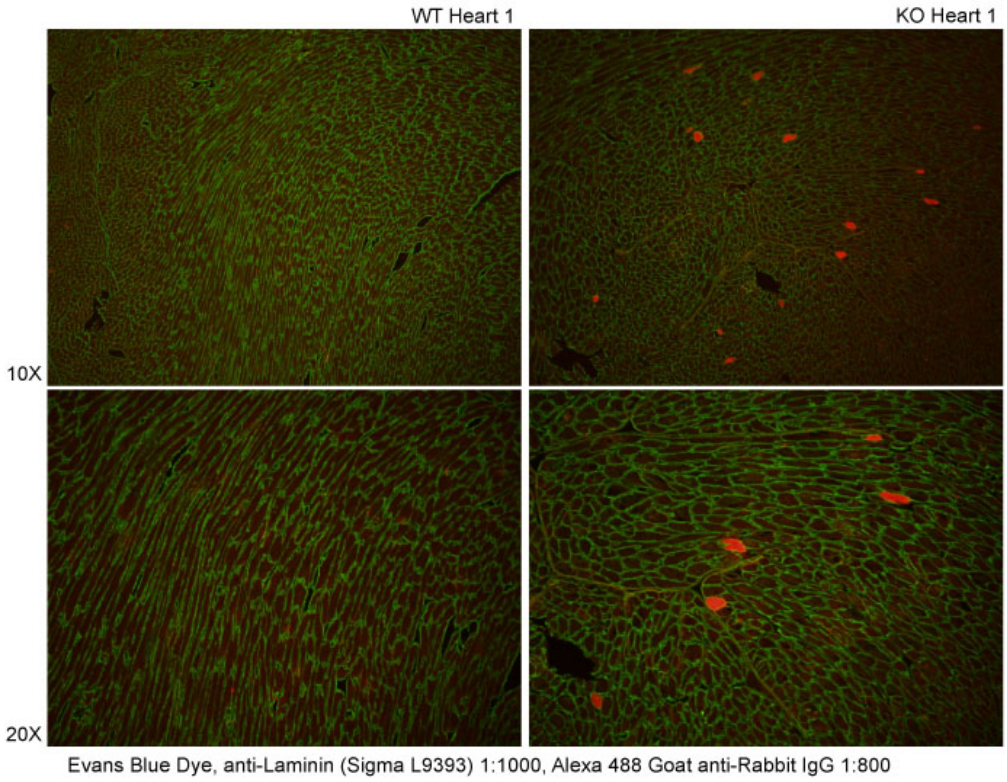

Figure 3.12 Hearts have limited loss of muscle integrity, as measured by Evans Blue Dye uptake.

48-day-old animals were injected with Evans Blue Dye (EBD) and sacrificed 24 hours later. Hearts were cryoprotected and sectioned at level 3. *Pik3c3* knockout (KO) animals showed sparse fibers containing EBD, counterstained with anti-laminin for visualizing individual fibers.

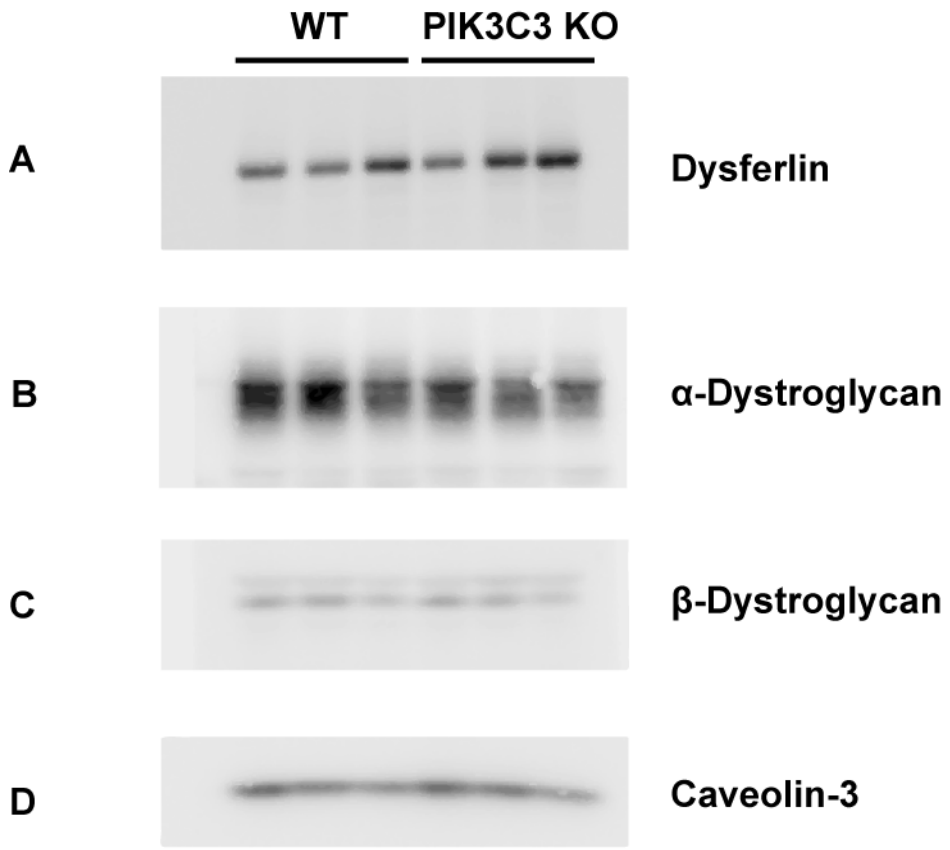

Figure 3.13 Overall levels of integral membrane proteins are unaffected by *Pik3c3* knockout.

Integral membrane proteins showed no appreciable differences in overall expression from skeletal muscle tissue samples isolated from 48-day-old mice.

Chapter 4:
Mice with conditional muscle knockout of *Pik3c2β* show glucose intolerance and loss of muscle integrity

4.1 Abstract

Phosphoinositide metabolism plays a role in many of the pathways responsible for a variety of human neurodegenerative diseases. One such prototypical disorder of phosphoinositide dysregulation is Myotubular myopathy (MTM), characterized by profound muscle pathology and weakness, and caused by mutations in *MTM1*, a phosphatase that primarily targets PtdIns(3)*P*. While the association between MTM1 and muscle disease has become more clarified, the normal role(s) of PtdIns(3)*P* metabolism in muscle development and homeostasis remain poorly understood. Following up on our recent study of muscle-specific conditional knockout of the class III Phosphatidylinositol 3-kinase, *Pik3c3* (*h*Vps34), we generated mice with conditional muscle deletion of a class II Phosphatidylinositol 3-kinase: *Pik3c2β*. Muscle specific deletion of *Pik3c2β* caused no overt physiological defects or decreased survival by 11 months of age. Histopathological analysis of skeletal muscle from knockouts appeared normal. Exploration for aberrant cellular mechanism(s) revealed potential roles for PIK3C2β in glucose trafficking and cell membrane dynamics. Of note, blood glucose levels were significantly elevated in knockout animals at time points following injection of glucose, but not following insulin. There were significant increases in resting serum CK in KO animals. In all, we present the first analysis of PIK3C2β in skeletal muscle, and report significant changes in some metabolic processes, with little to no discernable effect on muscle force output.

4.2 Introduction

The regulation of phosphatidylinositol phosphates (PtdIns*P*s) by its dynamic phosphorylation plays a significant role in cellular signaling pathways and membrane trafficking (Di Paolo and De Camilli 2006, Maffucci 2012). Mutations in several of the phosphatases that regulate PtdIns*P*s have been implicated in neurological diseases (Amoasii, Hnia et al. 2012). One such disease is myotubular myopathy (MTM), an X-linked centronuclear myopathy (CNM) that is characterized by significant disability and early mortality in boys carrying mutations in the gene myotubularin (*MTM1*) (Jungbluth, Wallgren-Pettersson et al. 2008, Das, Dowling et al. 2011). MTM1 is a PtdIns*P* 3-phosphatase, that primarily targets PtdIns(3)*P* (Taylor, Maehama et al. 2000) as well as PtdIns(3,5)P_2 (Tronchere, Laporte et al. 2004). Levels of these particular PtdIns*P*s are elevated in animal models of the disease (Dowling, Vreede et al. 2009, Pierson, Dulin-Smith et al. 2012).

PtdIns(3)*P* is created primarily through phosphorylation of PtdIns at the 3 position by PI 3-kinases (PI3Ks) (Backer 2008, Meijer and Klionsky 2011), or through dephosphorylation of PtdIns(3,5)P_2 by FIG4 (Jin, Chow et al. 2008). There are three classes of PI3Ks that are capable of producing PtdIns(3)*P* in mammals, with varying tissue expression and substrate specificity (Yan and Backer 2007, Vanhaesebroeck, Guillermet-Guibert et al. 2010). The PI3Ks include eight specific isoforms containing a PI3K core with C2, helical and catalytic domains (Vanhaesebroeck, Guillermet-Guibert et al. 2010). The Class I PI3Ks primarily phosphorylate PtdIns(4,5)P_2 to form PtdIns(3,4,5)P_3, and so the primary sources of PtdIns(3)*P* in muscle are PIK3C3 and the class II PI3Ks: PIK3C2α and PIK3C2β. PIK3C3 is considered the major enzymatic regulator of its production (Herman and Emr 1990, Arcaro, Volinia et al. 1998, Backer 2008, Meijer and Klionsky 2011).

There is a single Class III PI3K (PIK3C3/hVps34), discussed in the previous chapter, that is associated with PIK3R4/hVps15, and forms numerous complexes with other regulatory proteins (Backer 2008). It has been extensively reviewed in the context of autophagy, vesicular trafficking and nutrient signaling (Workman and van Montfort 2010, Bechtel, Helmstadter et al. 2013, Chen 2013). Studies in muscle have shown that

PIK3C3 is essential for muscle integrity and proper trafficking in the endo-lysosomal pathways (see Chapter 3).

The Class II PI3Ks function as monomers, and have a higher molecular weight compared with other members of the PI3Ks (Falasca and Maffucci 2007). *In vitro*, the class II isoforms preferentially target PtdIns and PtdIns(4)*P,* and not PtdIns(4,5)P_2 (Arcaro, Volinia et al. 1998), and further studies have shown that PIK3C2α and PIK3C2β generate PtdIns(3)*P* at the plasma membrane of muscle following stimulation by insulin (Maffucci, Brancaccio et al. 2003). However, there remains a bit of controversy in regards to the specific contributions of the Class II PI3Ks in insulin signaling pathways (Soos, Jensen et al. 2001, Falasca, Hughes et al. 2007).

The different members of the Class II PI3Ks have unique expression patterns and different cation specificity *in vitro* (Arcaro, Volinia et al. 1998). Cell processes that are affected by levels of the Class II PI3Ks include cell mobility and adhesion (Domin, Harper et al. 2005), immune responses of T-cells through Ca^{2+}-activated K^+ channels (Srivastava, Di et al. 2009), and even malignant progression of human cancers through RhoA and Rac activation (Blajecka, Marinov et al. 2012).

The Class II γ isoform is not well characterized, and has low expression patterns (Rozycka, Lu et al. 1998), but one study has shown a link between PIK3C2γ and type 2 diabetes in humans, based on single-nucleotide polymorphism (SNP) analyses (Daimon, Sato et al. 2008). The primary differences between the Class II α and II β forms have to do with their sensitivity to inhibition by wortmannin (Soos, Jensen et al. 2001), and also differences in receptivity to insulin and other signals (Falasca and Maffucci 2007, Leibiger, Moede et al. 2010).

Previous studies of PIK3C2β have identified it as a target of epidermal growth factor (EGF), leading to nuclear translocation based on a C-terminal motif (Banfic, Visnjic et al. 2009). *In vitro* studies in A-431 cells have demonstrated that PIK3C2β forms an association with a multi-protein complex containing Shc, Grb2, Eps8 and Abi1 to allow stimulation through EGF receptors (Katso, Pardo et al. 2006). PIK3C2β also contributes to lysophosphatidic acid (LPA)-mediated cell migration, suggesting a specific signaling molecule for activation of PIK3C2β (Maffucci, Cooke et al. 2005).

The experiments described in this manuscript follow up on a mouse created by Khavari and colleagues that was null for *Pik3c2β* by means of a germ-line deletion with Cre recombinase (Harada, Truong et al. 2005). Their study of that mouse focused primarily on the epidermis, and they detected no effect on epidermal growth, differentiation, wound healing or barrier function. Likewise, the mice were viable and fertile, indicating that PIK3C2β is dispensable for viability and epidermal homeostasis, and likely for most vital functions. The goal of the present study is to understand the role of PIK3C2β and PtdIns(3)*P* in skeletal muscle by evaluating a muscle-specific PIK3C2β conditional knockout mouse.

4.3 Results

4.3.1 Pik3c2β muscle conditional knockout mice are verified by molecular analyses.

Conditional knockout mice were generated that lack PIK3C2β in skeletal muscle, using Cre driven by the promoter/enhancer for muscle creatine kinase (Ckmm) to specifically excise a floxed allele of *Pik3c2β*, with loxP sites flanking exons 3-5. Mice were genotyped using primers described previously (Harada, Truong et al. 2005), and crossed to produce homozygous knockout animals. The animals are bred on the common BL/6 background. The *Pik3c2β* conditional knockout (KO) animals have no overt phenotypes to distinguish them from their wild-type littermates (WT), even by the end of their first full year of life.

In order to verify the knockdown of PIK3C2β from the Cre recombinase excision, we tested levels of *Pik3c2β* transcript and PIK3C2β protein by qPCR (Figure 4.1A) and Western blot (Figure 4.1C,D) respectively. We show a 63% reduction ($p < 0.01$) in levels of *Pik3c2β* transcript in the knockout mice (KO), normalized to wild type littermate controls (WT, Figure 4.1A).

The primary substrate for PIK3C2β is PtdIns, based on *in vivo* and *in vitro* analyses (Arcaro, Volinia et al. 1998), and activity of the kinase results in the production of PtdIns(3)*P*. Therefore, we measured PtdIns(3)*P* of rested animals by a Mass ELISA kit

(Echelon), and determined levels to be 951 ± 699 pmol/mg (n=4) for KO animals, compared with 5530 ± 1370 pmol/mg (n=7) for WT littermates (Figure 4.1B). This further confirmed the effectiveness of the knockout in our animals.

To assay protein levels of PIK3C2β, lysates were obtained from quadriceps muscles of the mice and the protein was analyzed by Western blots (Figure 4.1C). The predicted size of PIK3C2β should result in a band at approximately 180 kDa, and this band is reduced in the samples from knockout muscle lysates. Quantification of western blot by densitometry shows significant reduction (85.2% ± 20.0%, n=3, *:p=0.013) in the intensity of the bands at 180 kDa. PIK3C2β is normalized internally to Actin, and the KO animals are normalized to WT levels (Figure 4.1D).

4.3.2 Physiological tests show no overt muscular weakness in Pik3c2β knockout mice.

The transgenic *Ckmm-Cre* specifically targets the muscle, so we designed experiments to test for defects that might not be apparent by observation in 11-month-old KO mice and their littermates. For example, average body mass for the two groups of animals was not significantly different between KO (26.1 ± 1.0 g, SD, n=5) and WT littermates (27.4 ± 1.1 g, SD, n=5) (Figure 4.2A). Mice that had heterozygous deletions of *Pik3c2β* were included in WT groups for body weight, and analyses comparing the three groups (WT vs Het vs KO) also showed no significant differences among groups.

Next, tests of physical strength were performed to detect any weaknesses or subtle defects in the health of the muscle. We chose to use a test of grip strength and the rotorod test as basic physiological tests of muscle strength and balance. The KO mice performed equally as well as their WT littermates on both tests. Measurements of peak grip strength were measured to be 0.115±.028g (SD, n=5) for WT, and 0.104±0.020g (SD, n=5) for KO mice (Figure 4.2B). The results were not significantly different based on student's t-tests. For the rotorod test, KO mice achieved an average maximum speed of 6.5 ± 1.6 r.p.m. (SD, n=5) on the first day, while WT littermates reached 8.5 ± 2.4 r.p.m. (SD, n=5). On the second day of testing, KO mice improved to 10.5 ± 3.4 r.p.m. (SD, n=5), and WT averaged 9.9 ± 3.5 r.p.m. (SD, n=5) (Figure 4.2C). Results for rotorod

performance were not significantly different between any two groups, based on multiple student's t-tests or ANOVA.

In order to obtain better clarity of muscle force, we used more refined tests by isolating soleus and extensor digitorum longus (EDL) muscles from 11-month-old KO mice and WT littermates. The muscles were attached to force transducers while being maintained ex-vivo, and force was measured upon electrical stimulation directly to the muscles. We measured absolute force (Figure 4.2F,K), specific force (Figure 4.2G,L), and force deficit following lengthening contractions (Figure 4.2H,M) in both soleus (Figure 4.2D-H) and EDL (Figure 4.2I-M) muscles, normalizing to muscle mass of the individual muscles (Figure 4.2D,E,I,J). None of the measurements were significantly different between groups based on statistical analyses.

4.3.3 Muscle histology appears normal in knockout mice.

In order to assess the muscle for any histological indications of muscle disease, cross-sectional samples were examined from a selection of skeletal muscle to compare the *Pik3c2β* KO muscle fibers to that of WT littermates (Figure 4.3). Hematoxylin and eosin (H&E) stains enable visualization of nuclei and defects associated with muscle disease such as muscular dystrophy (Figure 3.4). There were no observable differences in the staining of gastrocnemius (Gast), tibialis anterior (TibA), or quadriceps (Quad) between the two groups, as shown in representative samples in Figure 4.3.

Succinate dehydrogenase (SDH) activity was used as a correlate of oxidative capacity, indicating the abundance of ER and mitochondria (Figure 4.3C,D,G,H,K,L). As with H&E stains, SDH activity did not appear to be different between KO and WT groups. Glycolytic activity was tested using a periodic acid-Schiff (PAS) stain and there were no differences when comparing KO to WT samples .

4.3.4 Pik3c2β KO mice have elevated serum levels of creatine kinase.

After the animals in the study were tested for muscle strength, serum levels of muscle creatine kinase (CK) were measured by drawing several drops of blood from the

saphenous vein. KO animals showed a small but significant increase in level of CK (258 ± 38 mU/mL, n=4) compared to WT animals (150 ± 18 mU/mL, n=4) (Figure 4.5A). This indicates mild muscle damage even in resting mice, independent of stress by exercise on treadmill. However, these numbers do not approach those of severely dystrophic muscle, which can be above 5000 mU/mL (Figure 3.5A).

4.3.5 Glucose metabolism is abnormal in Pik3c2β knockout mice.

PI3Ks play a significant role in insulin action and diabetes, through trafficking of the glucose transporter, GLUT4, and Akt pathways (Bridges and Saltiel 2012). The Class II PI3K, *Pik3c2α*, is highly regulated by insulin in skeletal muscle, and has a unique role in signaling, independent of pathways affected by wortmannin (Soos, Jensen et al. 2001). *Pik3c2β,* however, has not yet been examined in the context of glucose regulation. In order to determine the role of *Pik3c2β* in metabolic processes including glucose disposal, we administered a series of experiments to examine glucose levels and other lipids in the blood of *Pik3c2β* knockout mice. The mice were administered acute doses of glucose or insulin following a four-hour period without access to food, and drops of blood were taken from scratches to the tail.

KO animals had normal levels of glucose following the fast (185 mg glucose per dl blood) compared to WT (177 mg/dl), however there was a significant deficiency in their ability to dispose of blood glucose 30 minutes following acute injection (390 mg/dl KO compared to 216 mg/dl WT, n=2). Other time points suggested a trend towards significantly increased levels of blood glucose through two hours post injection (Figure 4.5B).

In order to determine whether the increase in blood glucose in KO animals was due to insulin resistance, we tested blood glucose levels of the mice following acute injection of 0.75U insulin per kg. Using a very small number of animals (n=2), we saw no significant differences in the response to insulin (Figure 4.5C).

Lastly, we sent blood samples to be tested for lipid analysis, including triglycerides, cholesterol and HDL/LDL levels, and we are awaiting results of those analyses as of the writing of this manuscript.

Table 4.1 Experimental mice

Animal #	Date of Birth	Gender	Genotype		BW (g) (7/29/13)	Data
55	8/24/12	♀	PIK3C2B$^{fl/fl}$; Cre^{+}	KO		RR, Gp, MF, P3, qP, W, HE, SDH
56	8/24/12	♀	PIK3C2B$^{fl/+}$; Cre^{-}	WT		RR, Gp, MF, P3, qP, W, HE, SDH
58 (“60”)	9/1/12	♀	PIK3C2B$^{fl/+}$; Cre^{+}	Het		RR, Gp, MF, P3, qP, W, HE, SDH
59	9/1/12	♀	PIK3C2B$^{fl/fl}$; Cre^{-}	WT		RR, Gp, MF, P3, qP, W, HE, SDH
60 (“6X”)	9/1/12	♀	PIK3C2B$^{fl/fl}$; Cre^{+}	KO	25.4	RR, Gp, MF, P3, qP, W, GTT
61	9/1/12	♀	PIK3C2B$^{fl/+}$; Cre^{+}	Het	26.3	RR, Gp, MF, P3
62	9/1/12	♀	PIK3C2B$^{fl/fl}$; Cre^{+}	KO	25.8	RR, Gp, GTT, ITT, BL, P3
63	9/1/12	♀	PIK3C2B$^{fl/fl}$; Cre^{+}	KO	25.1	RR, Gp, P3, qP, W, GTT, ITT, BL
97	10/22/12	♀	PIK3C2B$^{fl/+}$; Cre^{+}	Het	24.6	BL, ITT, P3, BL
98	10/22/12	♀	PIK3C2B$^{fl/+}$; Cre^{-}	WT	25.4	RR, Gp, MF, P3, qP, W, GTT
100	10/22/12	♀	PIK3C2B$^{fl/+}$; Cre^{-}	WT	26.3	RR, Gp, P3, GTT, BL, ITT
MPC 44	5/19/13	♀	PIK3C2B$^{fl/fl}$; Cre^{+}	KO		MC
MPC 45	5/19/13	♀	PIK3C2B$^{fl/+}$; Cre^{+}	Het		MC
MPC 46	5/19/13	♀	PIK3C2B$^{fl/+}$; Cre^{+}	Het		MC
MPC 53	6/9/13	♂	PIK3C2B$^{fl/fl}$; Cre^{+}	KO		MC

4.4 Discussion

In summary, we have generated muscle-specific *Pik3c2β* knockout mice and provided the first phenotypic description of the role of PIK3C2β in skeletal muscle. Knockout mice had reduced levels of *Pik3c2β* mRNA and (protein) in striated muscle, and had significantly reduced levels of PtdIns(3)*P*, the phospholipid generated by PIK3C2β. Using both morphological and functional analyses, we examined potential changes in skeletal muscle structure and function and in the overall health of the animals, including significant defects in glucose metabolism.

One of the most significant findings in our study was the discovery of glucose intolerance in affected mice. Elevated levels of blood glucose and insulin intolerance are some of the main diagnostic criteria for type 2 diabetes or pre-diabetes. Although the connection between PIK3C2β and glucose transporter protein 4 (GLUT4) trafficking has not previously been reported, one potential mechanism for this elevated blood glucose is through a failure of skeletal muscle to properly dispose of glucose. Another Class II PI3K, Pik3c2α, has previously been shown to play a role in insulin signaling through GLUT4 translocation (Falasca, Hughes et al. 2007, Dominguez, Raimondi et al. 2011). Reduction in PtdIns(3)*P* through overexpression of MTM1 also results in deficiencies in GLUT4 trafficking and activation in response to insulin (Chaussade, Pirola et al. 2003). These studies and ours would suggest that such a disruption in the PtdIns*P* pathway result in this condition.

Potential future directions that would address the role of PIK3C2β in metabolic disorders could involve altering exercise or dietary regimes, such as food restriction or high fat diets. Increased risk of obesity or mortality might indicate a predisposition for many of the complications of diabetes. Also, time course measurements of various signaling cascades following acute exposure to insulin or growth factors such as EGF could determine the role of PIK3C2β in other pathways. Much more will need to be learned about the exact effects from loss of PIK3C2β and PtdIns(3)*P* in regards to GLUT4 function and processing.

Finally, the relationship between PIK3C2β and MTM1 has been explored previously in cell culture studies (Razidlo, Katafiasz et al. 2011). Simultaneous knockdown of both genes seemed to alleviate some detrimental signaling pathways in the cells. In order to test the hypothesis that reduction in pools of PtdIns(3)*P* by elimination of PIK3C2β may counteract the effects seen from MTM1 knockout, we propose to cross knockouts of both genes in a single line of mice.

4.5 Conclusions

We present the first study of a mouse with conditional deletion of *Pik3c2β* in muscle. While these mice appear outwardly healthy and viable, we detected significant defects in important metabolic processes. Namely, muscle cells in these animals are deficient in their ability to dispose of extracellular glucose, indicating complications similar to those seen in diabetic and pre-diabetic individuals. Body weight and muscle mass relative to body, and specific force of individual muscles showed no significant differences in knockout animals from control littermates. We tested the strength and endurance of the affected mice, and saw no measurable deficiencies. Elevated levels of CK detected in blood serum from resting animals indicate defects in muscle integrity that will require further analysis. In all, these mice reinforce the importance of PtdIns(3)*P* regulation in metabolic homeostasis.

4.6 Materials and Methods

4.6.1 Care and use of animals

All animals were cared for under the guidance of the University Committee on Use and Care of Animals (UCUCA) protocols and assistance by the University of Michigan's Unit for Laboratory Animal Medicine (ULAM), who carefully monitored the health of the rodent colonies. Proper environmental regulation including temperature and light cycles, unlimited access to water, appropriate food supply, and clean enclosures were maintained for the duration of the study. Pups were weaned according to standard protocols, and tails were clipped for genotyping.

4.6.2 Generation and screening of transgenic lines

Generation of the mice with the floxed allele of *Pik3c2β*, obtained from Jackson labs (strain 005702), was described previously (Harada, Truong et al. 2005). The Cre mice are of the strain: B6.FVB(129S4)-Tg(Ckmm-cre)5Khn/J, obtained from Jackson labs (strain 006475). Mice were crossed to make $Pik3c2\beta^{fl/+}$; Cre^{+} heterozygous mice, and in-crossed to produce the double floxed allele: $Pik3c2\beta^{fl/fl}$, resulting in the muscle-specific conditional knockout animals. Primers used for verification of genomic incorporation of the transgenic cassettes were also described previously (Harada, Truong et al. 2005).

4.6.3 qRT-PCR

Total mRNA was isolated from muscle homogenates using QIAGEN RNeasy kits, and qPCR was performed using cDNA reverse-transcribed by iScript (BioRad) on ABI equipment using SybrGreen reagents. Analysis was done by using the 2^-(ΔΔCt) method. Primers for *Pik3c2β* transcripts analyzed include AACAAGGACACCTCTGGGAAACCT and GTCGGTTATTGCCAGGTGTTGCAT; and for Rpl4 include ACAACAGACAGCCCTATGCC and CGTCCCCCACGACACATATT.

.

4.6.4 Protein isolation and western analysis

Protein was isolated from tissue from KO and littermate mice by mincing and homogenizing in T-PER buffer (Thermo) with proteinase inhibitors (Roche), with brief sonication on ice. Loading buffer was added to protein and run on 10%-15% acrylamide gels, followed by transfer to PVDF blots. Primary antibodies were applied overnight at 4˚C at 1:1000 dilution in 3% BSA, 0.5% TritonX-100, NaF: Anti-PIK3c2β - #WH0005287M2 Sigma monoclonal mouse, Immunogen: NP_002637 αα1~111 GST tagged (total 185kDa). Anti-Class I PIK3 (p170) complex BD, #611046 mouse IgG1 170 kDa. Anti-Class II PIK3 type α (H-300): sc-67306 Santa Cruz, Rabbit polyclonal αα61~360 (N-term human 2α) 190 kDa. Anti-Vps34 – Thermo rabbit polyclonal PAI-46456.

Indirect analysis of protein expression was performed in ImageJ following procedures outlined by http://lukemiller.org/index.php/2010/11/analyzing-gels-and-western-blots-with-image-j/.

4.6.5 Lipid isolation and PtdIns(3)P analysis

Lipid analysis was performed by indirect analysis of whole muscle lysates using Echelon's PtdIns(3)*P* Mass ELISA kit (K-3300), as previously described (Pierson, Dulin-Smith et al. 2012). A Labscan Multiskan Ascent 96-well plate reader was used to measure optical readings of color change at 450 nm.

4.6.6 Histology

Animals were sacrificed by anesthetic injection followed by cervical dislocation and tissues were isolated using sterile surgical methods without the use of laminar flow hoods. Muscle tissue from quadriceps and tibia anterioralis was dissected and mounted onto small balsawood pieces that were previously frozen with drops of O.C.T. (Optimal Cutting Temperature, Tissue-Tek) and then semi-thawed with light friction. The mounted muscle tissue was immediately submerged in a -55˚C isopentane bath cooled by liquid nitrogen for flash freezing.

Muscles were cut in 12 µm cross-sections and mounted on SuperFrost Plus slides using a Leica cryostat at -20˚C, and dried at room temperature before storage at -80˚C. Slides were stained with Mayer's Hematoxylin and eosin (H&E) following standard protocols, and mounted with Permount. Standard protocols were used for succinate dehydrogenase reactions to show oxidative staining patterns. Sigma-Adlrich protocol for Periodic Acid-Schiff (PAS, procedure no. 395) was followed using the microwave procedure for tissue sections. Micrographs were captured with an Infinity1 camera with eponymous software visualized through an Olympus BX43 light microscope. Images were cropped in Adobe Photoshop and arranged for figures with Adobe Illustrator.

4.6.7 Rotorod test

Animals were tested using an accelerating rotorod (Economex, Columbus Instruments, Columbus, OH, USA). Mice were placed on the rod which remained stationary for 10 s, after which the speed was set at 5 r.p.m. After rotating at a constant

speed for 60 s, the rod began accelerating at a rate of 0.1 r.p.m./s and continued until the animal was unable to remain on the rod. Total time spent on the rod was recorded starting from the time the rod began rotating. Mice were given three trials daily for two consecutive days. In between daily trials, animals were returned to their cage for a minimum of 15 min. A total of five animals were tested for each genotype.

4.6.8 Measurements of serum CK

Analyses of CK activity were performed as previously reported (Gumerson, Davis et al. 2013). Briefly, serum was collected from the saphenous vein of restrained animals and stored at −80°C. CK activity was measured in duplicate using CK NADP Reagent (Cliniqa, San Marcos, CA, USA).

4.6.9 Muscle force measurements

Extensor digitorum longus and soleus muscles were carefully isolated and removed from anesthetized mice. Following the removal of all muscles, mice were euthanized with an overdose of anesthetic and induction of a pneumothorax. Muscles were immediately placed in a bath of Krebs mammalian Ringer solution with 0.25 mM tubocurarine chloride maintained at 25°C and bubbled with 95% O_2 and 5% CO_2 to stabilize pH at 7.4. Using 5-0 silk suture, the distal tendon of the muscle was attached to a servomotor (model 305B, Aurora Scientific, Aurora, ON) and the proximal tendon to a force transducer (model BG-50, Kulite Semiconductor Products, Leonia, NJ). Muscles were stimulated by square pulses delivered by two platinum electrodes connected to a high-power biphasic current stimulator (model 701B, Aurora Scientific). A personal computer running custom-designed software (LabVIEW 7.1, National Instruments, Austin, TX) controlled electrical pulse properties and servomotor activity and recorded data from the force transducer. Stimulation voltage and optimal muscle length (L_o) were adjusted to give maximum twitch force (Brooks and Faulkner 1988). While held at L_o, muscles were subjected to trains of pulses, 300 ms in duration for EDL muscles and 900 ms for soleus muscles, with increasing stimulation frequency until maximum isometric tetanic force (P_o) was achieved (Brooks and Faulkner 1988). L_o was measured with digital calipers and muscle fiber lengths (L_f) were determined by multiplying L_o by

previously established L_f-to-L_o ratios of 0.44 for EDL and 0.71 for soleus muscles (Brooks and Faulkner 1988). Total muscle fiber cross-sectional area (CSA) was estimated by dividing the mass of the muscle by the product of L_f and 1.06 g/cm^3, the density of mammalian skeletal muscle. P_o was normalized by CSA to give specific P_o.

4.6.10 Blood Glucose Measurements and Insulin Tolerance Tests

Blood spots were taken from the extreme distal end of the tail and blood glucose content was measured using a hand-held glucometer. Immediately following an initial baseline reading, either 1 mg/g D-glucose in saline or 0.75 U/kg insulin was injected intraperitoneally. Blood glucose (in mg/dl) was measured with AlphaTRAK2 glucometer and test strips (Abbott) from venous blood samples, and recorded at each of the time points noted.

4.6.11 Blood Lipid Analysis

Plasma was isolated by centrifugation from blood taken immediately post mortem, and frozen in liquid nitrogen before being shipped on dry ice to Vanderbilt for analyses.

4.6.12 Statistical analysis

GraphPad Prism 6 was used for calculating significance of fiber size differences and TUNEL staining results with unpaired student's T-tests and one-way ANOVA with a post-test Tukey's multiple-comparison test.

4.7 Figures

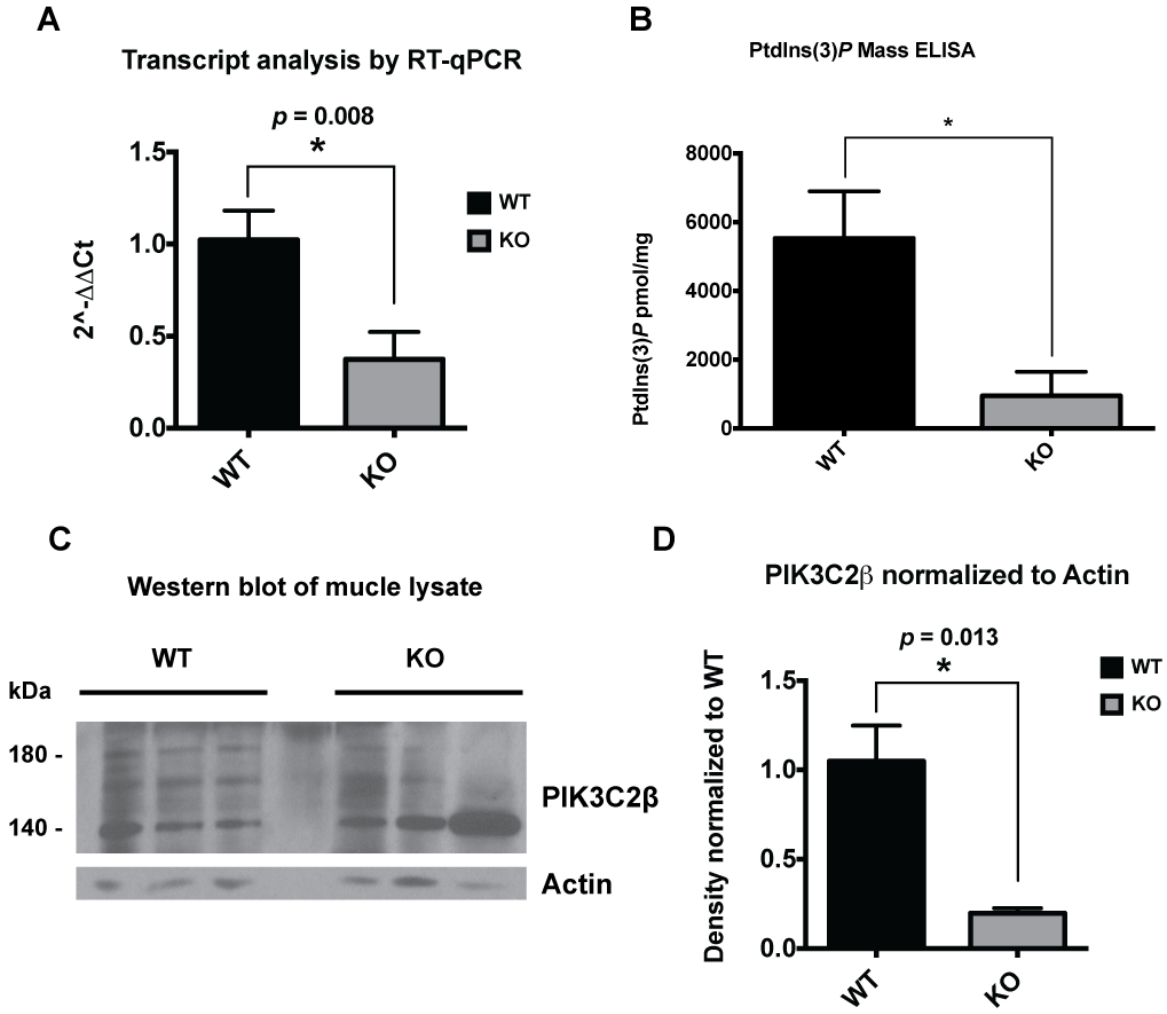

Figure 4.1 *Pik3c2b* knockout in muscle lysates is verified by molecular analyses.

(A) As measured by quantitative RT-PCR, a significant decrease in *Pik3c2β* transcript levels (37.4% ± 14.8%, n=3) was detected in skeletal muscle from knockout (KO) animals. Values were normalized to *Rpl4* transcript levels, with wild type (WT) average value set at 100% (± 16%, n=3). *:*p*=0.008. (B) PtdIns(3)*P* levels are reduced in KOs, as determined by using a PtdIns(3)*P* ELISA kit (purified lipid (pmol)/mass (mg) of muscle tissue) (WT: 5528 ± 1367, n=7; KO: 951 ± 699, n=4). *:*p*=0.017. (C) Evidence of reduction in expression of PIK3C2β by western blot. A band at the expected size of PIK3C2β can be seen at 180 kDa. (D) Quantification of western blot by densitometry shows significant reduction (85.2% ± 20.0%, n=3, *:*p*=0.013) in the intensity of the bands at 180 kDa. PIK3C2β is normalized internally to Actin, and KO normalized to WT. Error bars are presented as s.e.m.

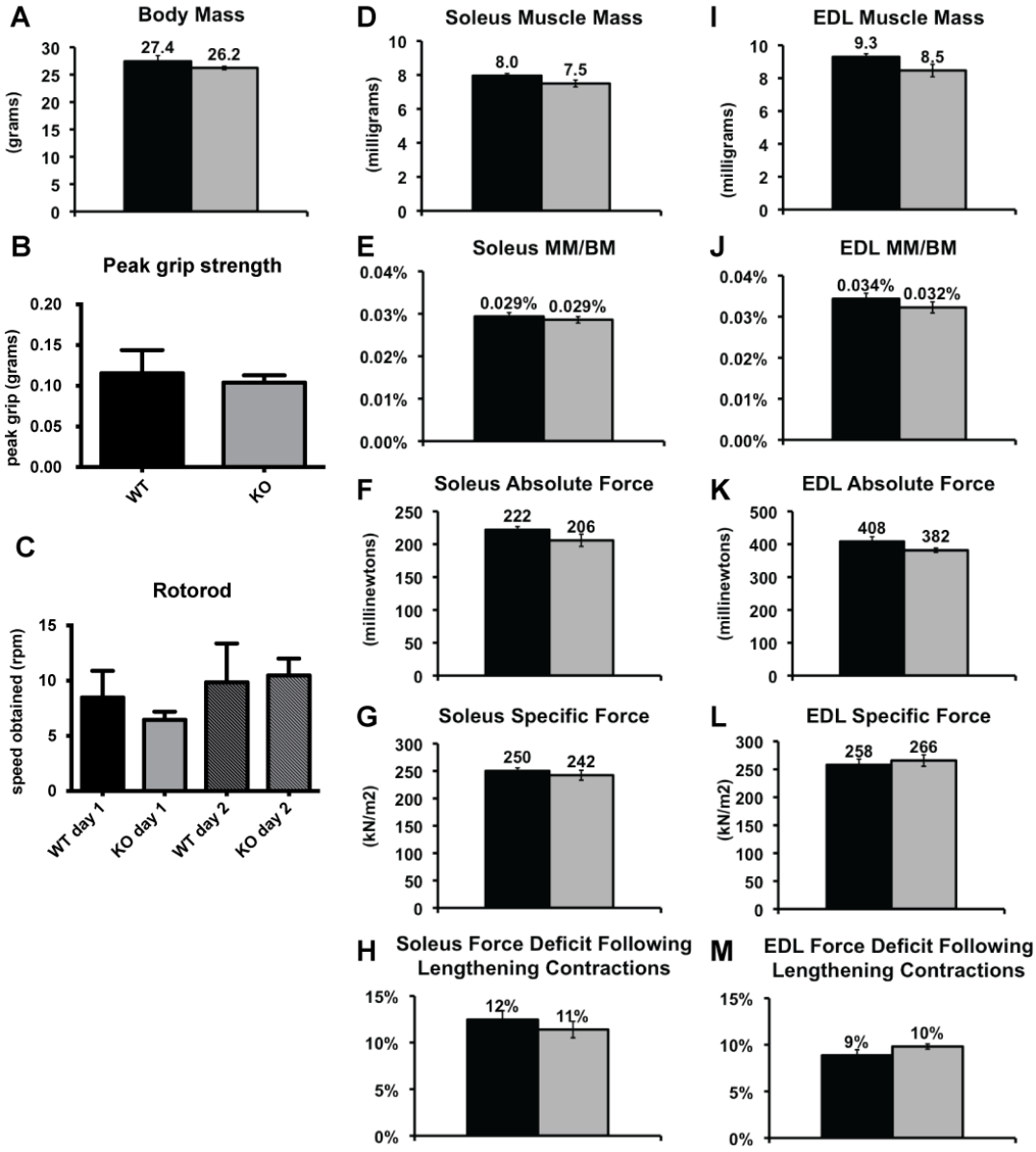

Figure 4.2 Physiological measurements of knockout animals show no differences from littermates.

(A) *Pik3c2β* knockout animals (KO, lighter bars) maintained stable growth and normal body mass compared with wild type littermate controls (WT) (n=4 WT; 4 KO). (B) Peak grip strength was measured in adult animals and was found to be very similar in WT and KO groups. (C) Animals (n = 4 per group) were placed on a stationary rod that rotated at a constant speed of 5 r.p.m. for 60 s and began accelerating at a rate of 0.1 r.p.m./s. The time each animal was able to stay on the rod beginning at rotation onset was recorded for three daily trials over 2 days. (D-M) Force measurement readings of isolated soleus (D-H) and EDL (I-M) muscles showed no significant differences between KO and WT groups regarding muscle mass (MM), muscle mass per body weight (MM/BW), absolute force, specific force or force deficit following lengthening contractions.

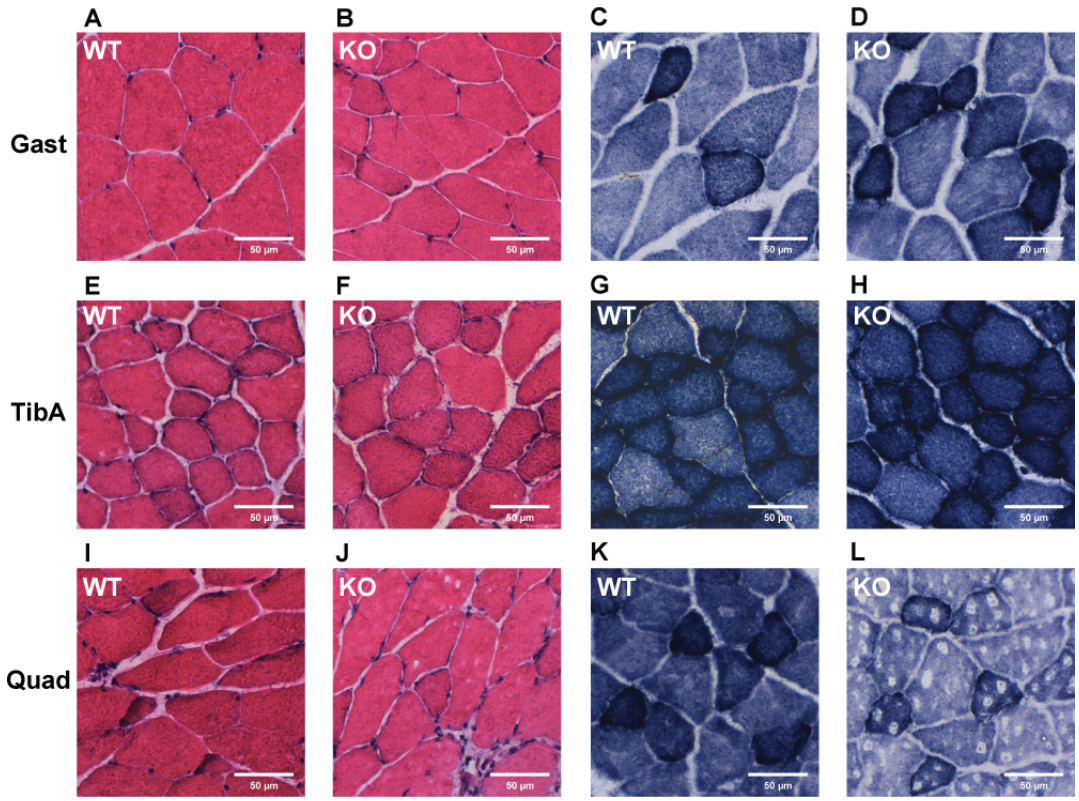

Figure 4.3 Basic histological analyses of *Pik3c2β*-cKO skeletal muscle show no aberrant features.

Representative cross-sectioned muscle from gastrocnemius (Gast, A-D), Tibialis anterior (TibA, E-H), and quadriceps (Quad, I-L) of adult female mice are shown above. Hematoxylin and eosin stains (H&E; left two columns) and succinic dehydrogenase reactivity (SDH; right two columns) show no patterns of aberrant or diseased muscle (spots in panel L are artifacts from freezing process). Scale bars are 50 µm.

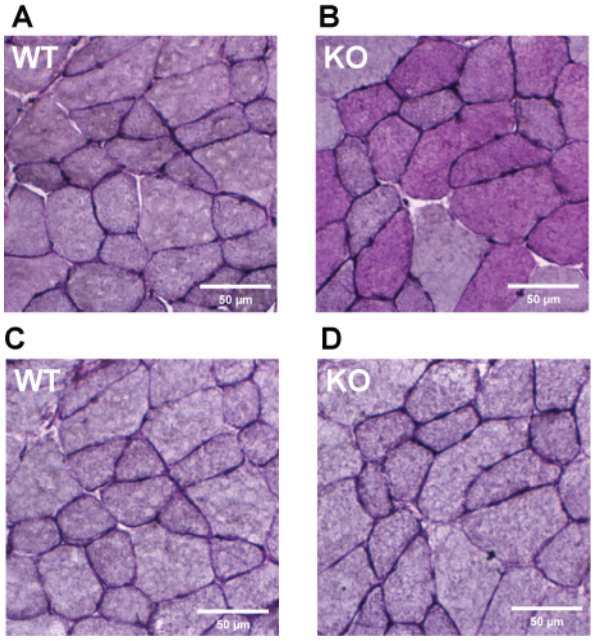

Figure 4.4 Analyses of *Pik3c2β*-cKO skeletal muscle show no aberrant glycogen accumulation.

Periodic Acid Schiff (PAS) staining of Tibialis anterior muscle in *Pik3c2β* knockout animals (KO) and wild type (WT) littermate controls reveals normal distribution of mucopolysaccharides. (A,B) Staining pattern of pararosaniline from Schiff's reagent (pink) is counterstained with hematoxylin (dark purple). (C,D) Prior to performing PAS stain, Diastase (α-Amylase) is used to clear polysaccharides as a control. Scale bars are 50 µm.

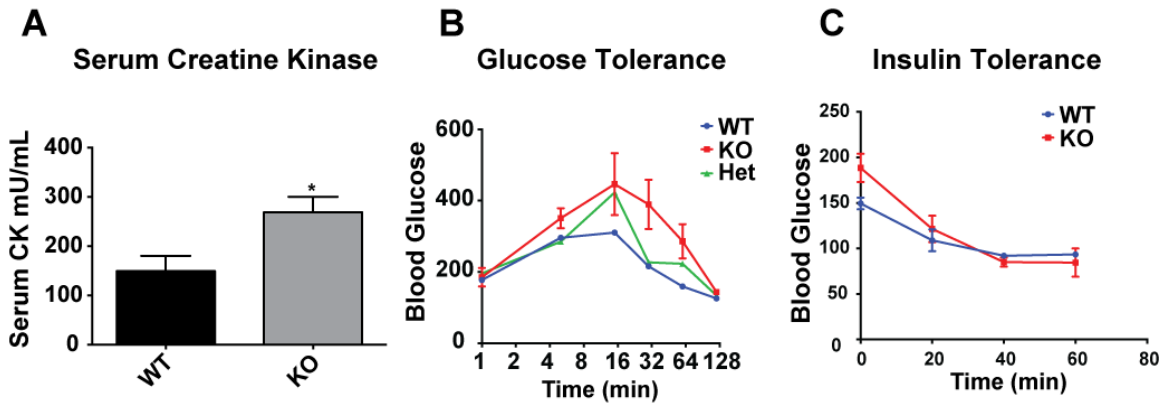

Figure 4.5 Metabolic processes

(A) Levels of serum creatine kinase were significantly elevated in rested animals. Animals were tested at 11 months of age, and PI3C2β knockout (KO) animals averaged 258 ± 38 mU/mL (n=4), compared with wild-type littermates (WT) that averaged 150 ± 18 mU/mL (n=4) *:p=0.04. (B) Blood glucose levels were measured over the course of time following acute injection of glucose (B) and 0.75 U/kg insulin (C), as a glucose tolerance test (GTT) and an insulin tolerance test (ITT), respectively. (B) Blood glucose was measured at 0, 5, 15, 30, 60 and 120 minutes following injection of glucose to measure disposal rates. There was a significant difference between the groups at 30 minutes post injection, KO = 390 ± 69 compared to WT = 216 ± 2 (*:p=0.018). Time points at 15 minutes (KO = 446 ± 87, WT = 311 ± 3) and 60 minutes (KO = 286 ± 48, WT = 160 ± 9) following glucose injection approached significance with p=0.056 and p=0.074, respectively (KO n=3, WT n=2). (C) Blood glucose levels following insulin injection dropped at approximately the same rate, starting at 189 ± 16 for KO and 150 ± 7 for WT (p=0.03, n=2), and ending at 85 ± 16 for KO and 94 ± 1 for WT after one hour. Error presented as s.e.m.

Chapter 5:
Conclusions and Future Directions

There is still much to be learned about the role of phosphatidylinositol (PtdIns) 3-phosphates in skeletal muscle, and the contributions of PtdIns3*P* kinases, phosphatases and effectors during development and muscle activity. The main premise of the work described in this dissertation is that the proper regulation of inter-conversion among the different PtdIns*P* isoforms in muscle, particularly between PtdIns(3)*P* and PtsIns(3,5)P_2, is important for maintaining muscle function and structural integrity, as deficiencies in the process result in diseases such as myotubular myopathy (MTM) and dystrophy, as seen in the *Pik3c3* conditional knockout mice. While this appears to be true in various contexts, dysregulation of the process can manifest in many outcomes.

5.1 Conclusions and future directions for knockout of *Fig4*

Null mutations of *Fig4* in mice (*plt*) cause numerous defects that ultimately result in rapidly progressive paralysis, including significant muscle atrophy, and early mortality (Chow, Zhang et al. 2007). Neuronal rescue of *Fig4* results in a correction of this disease, not only in the neurons in which FIG4 is present, but also results in rescue of phenotypes relating to glia and skeletal muscle, implying that the disease is primarily caused by impaired neuronal function (Figure 5.1) (Ferguson, Lenk et al. 2012). Results from the work outlined in chapter 2 (Reifler, Lenk et al. 2013) show a restoration of survival, muscle fiber size, muscle force, and overall health of animals.

The connection between FIG4 and the myotubularin protein family, specifically MTMR2, had previously been explored as a potential means of counterbalancing adverse effects from disruption of the interconversion between PtdIns(3)*P* and PtdIns(3,5)P_2 (Vaccari, Dina et al. 2011). Measurements of PtdIns(3)*P* in fibroblasts revealed no

significant differences among the different mutant groups. However, levels of PtdIns(3,5)P_2 from fibroblasts were significantly reduced relative to PtdIns(4,5)P_2 in *plt* mice, but had significant increases in *Mtmr2* KO mice (Vaccari, Dina et al. 2011). Fibroblasts from the *plt* mice had independently been demonstrated to have significant reduction in PtdIns(3,5)P_2 relative to total PtdIns*P* without significant changes to levels of PtdIns(3)*P* (Chow, Zhang et al. 2007). Muscle from *Mtm1* KO animals appeared to have significant increases in PtdIns(3)*P* based on measurements from ELISA, although PtdIns(3,5)P_2 was not examined in those samples (Pierson, Dulin-Smith et al. 2012). The key piece of information that hinted that *Fig4* KO might counteract effects seen in *Mtm1* mutations came from the Vaccari et al. paper. They showed that relative levels of PtdIns(3,5)P_2 were significantly reduced in fibroblasts from double knockout animals compared to levels in cells from *Mtmr2* KO mice, while mice heterozygous for one gene and null for the other had levels similar to *Mtmr2* KO levels. At the same time, they argued that perhaps the effect on levels of PtdIns(3,5)P_2 from haploinsufficiency of FIG4 would be below detection, because $Mtmr2^{-/-}Fig4^{+/-}$ animals showed reductions in myelin outfoldings compared with $Mtmr2^{-/-}$ mice. If features of MTM were due primarily to the buildup of PtdIns(3)*P* and/or PtdIns(3,5)P_2, then a double knockout of *Mtm1* and *Fig4* (or at least haploinsufficiency of *Fig4*) might have a positive effect on the *Mtm1* mutant phenotype. Our results did not confirm this hypothesis, although we were unable to measure levels of PtdIns(3,5)P_2 in muscle tissue to determine whether we had truly hit our intended target (Reifler, Lenk et al. 2013). Also, we did not have data from full double knockouts of *Fig4* and *Mtm1*.

It is possible that MTM1 functions in a different location within the cell than FIG4, or at least that the myopathy caused by the mutations is the result of enzymatic activity independent of FIG4/PIKfyve/VAC14. The very fact that neural rescue of *Fig4* results in healthy muscle tissue reveals at least that its dysregulation does not affect membrane integrity or triad formation.

There is one unexplored possibility that the mutational insertion in the *Fig4* gene of *plt* mice creates some alternately expressed form of *Fig4* in muscle, and that another product may be able to compensate for the loss of the full length protein in muscle and other cells, but not in neurons. This comes from preliminary observations of differential

expression in the levels of transcript able to be amplified by qRT-PCR using primer sets that target different parts of the message. Furthermore, some antibodies against FIG4 antigens reveal multiple bands that may represent the protein products of the alternate splicing. Of course, the existence of such products must be confirmed before any mechanistic conclusions are drawn.

Taking into account the results of muscle specific knockout of *Pikfyve*, it would be interesting to examine the affect of muscle specific knockout of *Fig4* (or Tg-NSE-*Fig4* rescued *plt*) on glucose tolerance and GLUT4 trafficking (Ikonomov, Sbrissa et al. 2013). As PIKfyve and FIG4 function in a tight complex, and elimination of FIG4 alone can alter the activity of PIKfyve, the *Fig4* KO animals could reinforce the importance of the equilibrium between PtdIns(3)*P* and PtdIns(3,5)P_2 as a regulator of glucose disposal through trafficking of GLUT4 in skeletal muscle (Ikonomov, Sbrissa et al. 2002, Berwick, Dell et al. 2004, Duex, Tang et al. 2006, Ikonomov, Sbrissa et al. 2007).

5.2 Conclusions and future directions for conditional knockout of *Pik3c3*

In our study of mice with conditional knockout of *Pik3c3*/*Vps34*, we determined that skeletal muscle of the mice resembled models of autophagic vacuolar myopathies and dystrophy. By the end of the second postnatal month, mice became sick and died, with highly elevated blood serum levels of creatine kinase (CK) along with defects in cardiac and skeletal muscle. Muscle membrane integrity was compromised based on the CK readings as well as Evans Blue dye (EBD) uptake and appearance of damaged muscle fibers from histological analyses. EBD was not as highly apparent in cardiac muscle, indicating that the dystrophic phenotype primarily manifested in skeletal muscle.

The analyses of cardiac disease matched previous studies of a similar knockout animal with targeted deletion of *Pik3c3* by another mutation, but with the same expression (using the Ckmm promoter to drive Cre recombinase) (Jaber, Dou et al. 2012). Both our results and theirs demonstrated significant hypertrophy in cardiac muscle, and accumulation of markers of autophagy, such as p62 and LC3. It is believed that the main cause of death in these animals is due to heart failure.

Our study expanded on the work done previously, and explored the defects seen in skeletal muscle. Another study that paralleled our own explored the effects of conditional knockout of the regulatory subunit of PIK3C3: PIK3R4/Vps15 (Nemazanyy, Blaauw et al. 2013). They used a Human Skeletal Actin promoter driving cre recombinase (*Acta1-Cre*) to selectively delete *Pik3r4* in skeletal muscle of mice. Their knockout mice reduced levels of PIK3C3, as well as PIK3R4, possibly by destabilizing the enzyme, to undetectable levels, or else eliminating auto-activation of the components of the complex. As seen in our mice, there was significant induction of p62 and LC3 (Figure 3.7).

Due to the fact that mice with deletions of autophagy genes such as *Atg7* do not present the same type of muscle disease, the question of whether complications from *Pik3c3* deletion arise from defective autophagy may be partially answered (Nemazanyy, Blaauw et al. 2013). The muscle from our knockout animals exhibited similar patterns of protein accumulation as seen in lysosomal trafficking diseases, termed autophagic vacuolar myopathies (AVMs) (Malicdan and Nishino 2012), also seen in the *Pik3r4* knockout mice (Nemazanyy, Blaauw et al. 2013).

One of the avenues that we were unable to follow to a satisfactory answer regards the specific mechanism for the loss of membrane integrity. We hypothesized that a mouse with extremely high serum CK readings would have some sort of defect in membrane repair. Therefore, we designed experiments to test the extent of membrane repair, by tracking the rate of fluorescent dye into isolated myofibers following injury from high intensity focal radiation. Unfortunately, results from the experiments did not adequately address the questions we wished to answer, as we had many technical complications, such as our difficulty in measuring levels of *Pik3c3* expression in any given cell (or ability to visualize the presence of Cre) in culture. There was high variability in responses to damage from some preparations, and we were unable to satisfactorily complete our investigations.

The search for a definitive mechanistic picture must work to identify the cause and disease mechanism of the high CK readings. One step that we have taken is to rederive the knockout line on a mouse background expressing Cre recombinase under the human skeletal actin (HSA or *Acta1*) promoter. This produces a mouse much more

similar to the one studied by Pende and colleagues, and may result in longer-lived mice with more identifiable deficiencies in skeletal muscle (Nemazanyy, Blaauw et al. 2013).

In regards to the *Pik3r4* mutant mouse, it would be of great interest to see whether effects of mutations in that line are caused by disturbances in physical interactions and associations between PIK3C3 and its regulatory subunit, or by direct interference in kinase activity. This could be accomplished by expressing constructs of *Pik3c3* in the knockout mice that contain point mutations in important domains of the protein.

5.3 Conclusions and future directions for mice with conditional knockout of *Pik3c2β*

I showed in my studies of the muscle specific *Pik3c2β* knockout mouse that it is possible to decrease levels of PtdIns(3)*P* in muscle without causing structural defects, and with only a minor impact on quality of life. These mice were not subjected to rigorous exercise or extreme dietary modification, and had free access to standard food rations. The major findings from my work showed modest increases in resting serum CK levels, and a deficiency in the ability of the mice to dispose of blood glucose. While basal levels of the glucose transporter type 4 (GLUT4) transcript and overall protein were unaffected as measured by qRT-PCR and Western blot analyses, there are more sophisticated assays available to test additional effects on the process. Some of the outstanding questions include the following:

If PtdIns(3)*P* is significantly reduced, is it only in a particular pool, or are levels changed only in a particular subcellular location? What could we learn through isolation of a portion of the internal membranes and analyses of the lipid composition, such as through fractionation experiments (Andrew, Roses et al. 1973, Smith and Appel 1977)? Do the different PI3Ks truly act on different pools of PtdIns to form PtdIns(3)*P*? Looking at comparisons with other animal models, was there any effect from knockout of *Pik3c3* on glucose transport?

In the continuation of this work, it would be interesting to see the effect of *Pik3c2β* cKO in regards to trafficking of GLUT4 to outer membranes by labeling the transporter and monitoring distribution over time following stimulation. Muscle is the

primary tissue responsible for postprandial glucose disposal. Previous work has shown that PIKfyve knockout in muscle causes impairment in glucose disposal in both oxidative (soleus) and glycolytic (EDL) muscles (Ikonomov, 2013). Specifically, basal glucose was normal, but insulin-stimulated blood glucose was significantly impaired. Inositol isoforms have been shown to generally cause an increase in plasma membrane trafficking of GLUT4 (Yamashita 2013). Since the muscle seems to be fairly healthy, it of utmost importance to have a clear picture of the overall PtdIns*P* dynamics.

In a previous study of *Pik3c2β* knockout, a null mutant of *Pik3c2β* was generated, and did not display any major disease phenotype, but the emphasis of the study was on epidermal cell development (Harada, Truong et al. 2005). It would be interesting to see whether metabolic defects are more apparent in another line that does not rely on the *Ckmm* promoter to produce targeted deletion of the gene. Finally, based on results from previous research (Razidlo, Katafiasz et al. 2011), one of the more interesting avenues of discovery will be the impact of *Pik3c2β* mutations on human disease, specifically, MTM.

Their study focused on phosphatases, myotubularin (MTM1) and the MTMR family, and the PI3Ks that regulate the equilibrium of PtdIns(3)*P* in HeLa cells and primary cultures of skeletal muscle myotubes (Razidlo, Katafiasz et al. 2011). Their findings indicated that MTM1 and PIK3C2β have a unique connection in the regulation of caspase 9 and PARP activation through Akt signaling, for while co-knockdown of MTM1 with PIK3C2β abrogated apoptotic effects, co-knockdown of other kinases with MTM1, including PIK3C2α and PIK3C3, did not have the same effect (Razidlo, Katafiasz et al. 2011). These data and others suggested a potential importance of PIK3C2β in muscle health, and characterization of an animal model with tissue-specific deletion of *Pik3c2β* on the background of MTM mice.

5.4 Future directions for the study of MTM1

In order to address the interactions between MTM1 and the other effectors, kinases and phosphatases targeting the same substrates and products, my first experiments with the *Mtm1* mutant mice focused on the potential of *Fig4* null or halplo-insufficiency to abrogate the deleterious effects of the disease (Reifler, Lenk et al. 2013).

While the results were not encouraging, we had begun a path with potentially high rewards. If we could restore the balance of PtdIns(3)*P* in the muscle, that might be enough to correct the features that are pathognomonic for MTM.

Therefore, we began crossing lines of mice that possessed *Mtm1* knockout with PI3K knockouts to attempt to rescue the MTM phenotype. Exciting preliminary data show that *Pik3c2β* KO may improve the disease phenotype of $Mtm1^{-/Y}$ by the following standards: The double knockout animals showed increases in survival, with mice heterozygous for *Pik3c2β* on the $Mtm1^{-/Y}$ background surviving slightly longer than $Mtm1^{-/Y}$ single knockouts; the double knockout animals showed an amelioration in appearance based on early histological analyses.

Assuming that deletion of *Pik3c2β* may provide some relief to skeletal muscle with mutations in *Mtm1*, it would be necessary to examine the time course of disease progression for treatment. If there is something like a critical window in muscle development in which cells rely on MTM1 activity to regulate accumulation of PtdIns(3)*P*, then it may be that inhibition of PI3 kinases would only be required temporarily, before their own activity drops to non-pathogenic levels on the $Mtm1^{-/o}$ background.

Pharmacologically targeted inhibition of PIK3C2β without inhibition of PI3K/AKT/mTOR pathway may be difficult, as many of the current small molecules have low specificity for individual PI3Ks, but it would be highly interesting to see the effects (Rodon, Dienstmann et al. 2013). If such an inhibitor could be developed, it would be important to test metabolic effects of diet as well, as there is a probability of complications similar to diabetes with impaired glucose disposal. Still, if the choice was between mortality within the first year of life or diabetic complications, diagnoses of *Mtm1* mutations may have a very plausible option for treatment.

5.5 Complications in the study of phosphatidylinositol phosphates

One of the great barriers in our understanding of PtdIns*P*s is the lack of sufficient tools for labeling and visualizing the dynamic inter-conversion among the phosphoisoforms. One of the more accurate ways in which the different phosphoisoforms

can be quantified relies on the introduction of radiolabeled inositol into the membranes of the cell, and normalization to total levels of PtdIns*P* (Zolov, Bridges et al. 2012). With current advances in technology, this has been accomplished by culturing large plates of dissociated cells for several days, first starving the cells of inositol, and then introducing the radioactively labeled inositol for the cells to metabolize. The cells are then processed for their lipid content, and passed through HPLC, for comparative analysis (specific isoform over total PtdIns*P* content). When optimized with high enough signal to noise, these results can provide very detailed information about the entire "PtdIns phosph-ome," with relative abundance of any given PtdIns*P*, assuming equal trafficking of the exogenous inositol throughout the membranes of the cell (Zolov, Bridges et al. 2012). Unfortunately, while there have been promising advances in treatment of primary cells from non-dividing neuronal cultures, our mouse models provide additional barriers, particularly as some of the lines do not even express Cre-recombinase until after muscle maturation. Additionally, these highly sensitive quantitative techniques do not provide information regarding subcellular localization, while being very difficult to apply towards mature tissue such as skeletal muscle.

Technological advances such as Surface Plasmon Resonance (SPR), isothermal titration calorimetry, and vesicle sedimentation approaches allow for more precise quantification of binding kinetics for recognition domains of specific PtdIns*P*s (Narayan and Lemmon 2006). Probes for individual PtdIns*P*s, commercially available from biotech companies such as Echelon, are marketed as being capable of detecting levels of PtdIns*P* in solubilized lipid extracts from tissue samples by indirect approaches such as in enzyme-linked immunosorbent assay (ELISA) (Pierson, Dulin-Smith et al. 2012) and other binding assays such as lipid dot blots (Yu, Mendrola et al. 2004), or even for visualizing the sub-cellular location of PtdIns*P*s *in situ* using indirect immuno-histological chemistry (IIHC) (Dowling, Vreede et al. 2009). When used as fusion proteins with easily identifiable or fluorescent tags, the recognition domains might potentially allow for visualization of the PtdIns*P*s and their intracellular localization in real time.

There are numerous caveats to many of the detection and quantification methods, and some techniques require expensive systems and large quantities of lipids. Many

techniques rely on non-native interactions between the lipids and the probes, that might result in technical artifacts (Narayan and Lemmon 2006). Furthermore, precise quantification of PtdIns*P* levels requires an understanding of the individual isoforms in relative terms to one another and possibly to the total levels of lipids and free Ins. This is in part because the interconversion among the different isoforms is so dynamic, and in part because there is evidence of auto-regulation of some of the kinases and phosphatases by levels of specific PtdIns*P*s.

Each detection method has its unique advantages and drawbacks, and it is important to bear the limitations in mind when attempting a description of the overall landscape of the PtdIns*P*s. It has been suggested that measurement of PtdIns*P*s should be performed by multiple detection methods, when possible, but certain tissues do pose greater barriers to some detection methods (Narayan and Lemmon 2006).

In order to identify subcellular localization of the individual phosphoisoforms in skeletal muscle, there are some options that could be used to varying effects. For general population analysis of cell organelles, fractionation experiments have been described using skeletal muscle from rodents (Smith and Appel 1977, Amoasii, Hnia et al. 2013), and could provide additional information on where the kinases, phosphatases and effector proteins localize. However, this uses the assumption that these proteins will remain relatively affixed to their target, and that the targets remain stable long enough for detection. Use of proteomic approaches, such as nano-liquid chromatography-tandem mass spectrometry, may give false positives while excluding some of the validated interactors (Tsujita, Itoh et al. 2010).

Alternative approaches to fractionation and proteomic analysis could include the use of labeled binding domains of proteins that specifically target individual PtdIns*P* isoforms, or what Echelon protocols refer to as “grip” proteins. Examples of these (sometimes proprietary) binding elements are the green fluorescent protein (GFP)-tagged constructs of tandem FYVE domains (labeling PtdIns(3)*P*), of tandem n-termini of the TRPML1 channel (labeling (PtdIns(3,5)P_2), of PH domains (labeling PtdIns(4,5)P_2), and others (Gillooly, Morrow et al. 2000, Lodhi, Bridges et al. 2008, Hertel, Switalski et al. 2011, Samie, Wang et al. 2013). There is still ongoing debate as to the specificity of some probes, and we must take on the challenge of visualizing some of the transient products

of highly dynamic processes that are of low relative abundance, while they are surrounded by hordes of energetic protein complexes. There is an additional worry that using these tagged probes for the purpose of visualization could also interfere with endogenous processes, producing unwanted artifacts.

While the focus of this dissertation is on muscle health, PtdIns*P*s regulate similar pathways in other environments, and are often regulated by the same enzymatic reactions. Many of the probes that are developed for visualization of PtdIns*P*s have been optimized in cell culture, and in organisms such as yeast. We need to optimize new, reproducible techniques for visualizing probes in healthy or diseased muscle, preferably *in vivo*, through transgenics and transiently expressed constructs. In addition to transfection or infection of fluorescent protein probes, morpholino technologies have also advanced and are capable of localizing to a variety of targets, although they are most useful in controlling expression of genes by binding RNA.

5.6 Overall conclusions

Enzymes that regulate or interact with PtdIns(3)*P* and other phosphoisoforms are involved in many cellular activities that directly affect muscle development and health. Due to the large network of proteins that interact with PtdIns(3)*P* it is not enough to simply describe diseases such as MTM or AVMs simply as displaying defective PtdIns*P* regulation, but may require a greater understanding of specificity in localization and of complicated protein to protein and protein complex to lipid dynamics. With advances in our ability to visualize and control smaller cellular elements, we will see a clearer picture of how the PtdIns*P*s are controlled, and how those lipids seem to control everything else around them.

5.7 Figures

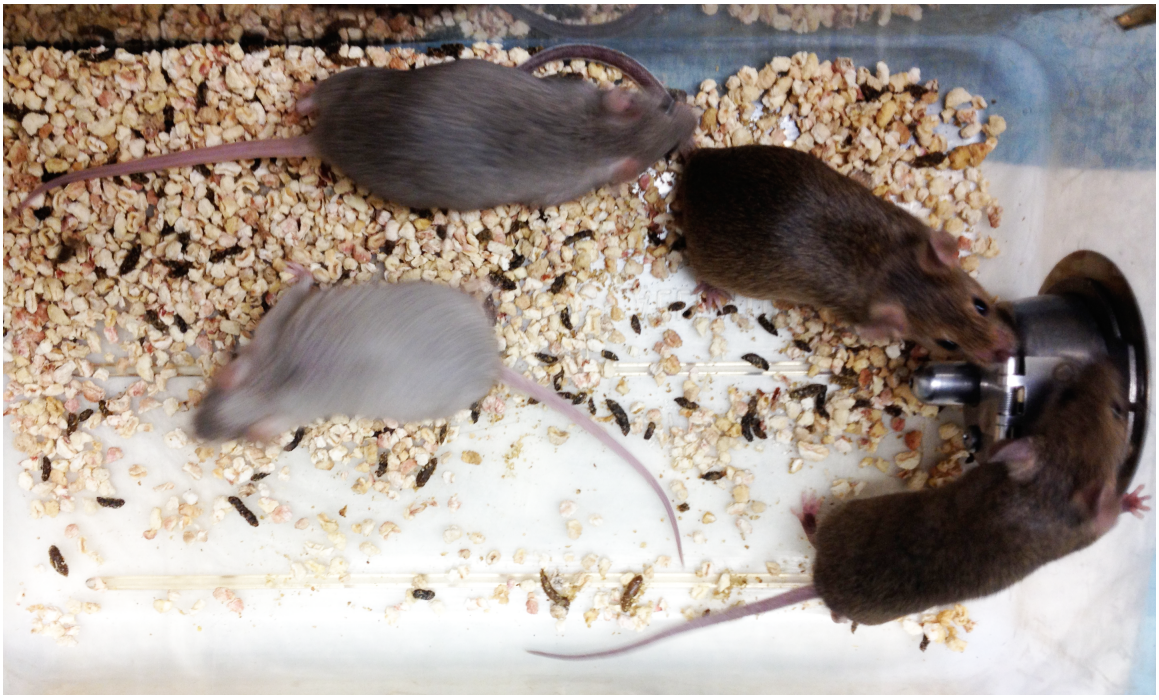

Figure 5.1 Photograph of *plt* mouse with transgenic rescue of FIG4 in neurons.

The *plt*;Tg(*NSE-Fig4*) mice do not suffer the same effects on muscle health as the *Fig4* null mice, but are easily distinguished by the color of their coat. Clockwise from top: $Fig4^{+/-}$ (heterozygous), $Fig4^{+/+}$ (wild type), $Fig4^{+/+}$ (wild type), $Fig4^{-/-}$ (null); all expressing transgenic FIG4 under the enolase (*NSE*) promoter. Mice were photographed at approximately 18 months of age.

References

Al-Qusairi, L., N. Weiss, A. Toussaint, C. Berbey, N. Messaddeq, C. Kretz, D. Sanoudou, A. H. Beggs, B. Allard, J. L. Mandel, J. Laporte, V. Jacquemond and A. Buj-Bello (2009). "T-tubule disorganization and defective excitation-contraction coupling in muscle fibers lacking myotubularin lipid phosphatase." Proc Natl Acad Sci U S A **106**(44): 18763-18768.

Amoasii, L., K. Hnia, G. Chicanne, A. Brech, B. S. Cowling, M. M. Muller, Y. Schwab, P. Koebel, A. Ferry, B. Payrastre and J. Laporte (2013). "Myotubularin and PtdIns3P remodel the sarcoplasmic reticulum in muscle in vivo." J Cell Sci.

Amoasii, L., K. Hnia and J. Laporte (2012). "Myotubularin phosphoinositide phosphatases in human diseases." Curr Top Microbiol Immunol **362**: 209-233.

Andrew, C. G., A. D. Roses, R. R. Almon and S. H. Appel (1973). "Phosphorylation of muscle membranes: identification of a membrane-bound protein kinase." Science **182**(4115): 927-929.

Arcaro, A., S. Volinia, M. J. Zvelebil, R. Stein, S. J. Watton, M. J. Layton, I. Gout, K. Ahmadi, J. Downward and M. D. Waterfield (1998). "Human phosphoinositide 3-kinase C2beta, the role of calcium and the C2 domain in enzyme activity." J Biol Chem **273**(49): 33082-33090.

Avila, G. and R. T. Dirksen (2001). "Functional effects of central core disease mutations in the cytoplasmic region of the skeletal muscle ryanodine receptor." J Gen Physiol **118**(3): 277-290.

Avila, G., J. J. O'Brien and R. T. Dirksen (2001). "Excitation--contraction uncoupling by a human central core disease mutation in the ryanodine receptor." Proc Natl Acad Sci U S A **98**(7): 4215-4220.

Backer, J. M. (2008). "The regulation and function of Class III PI3Ks: novel roles for Vps34." Biochem J **410**(1): 1-17.

Balla, T., M. Wymann and J. D. York (2012). Phosphoinositides. I, Enzymes of synthesis and degradation. Dordrecht ; London, Springer.

Banfic, H., D. Visnjic, N. Mise, S. Balakrishnan, S. Deplano, Y. E. Korchev and J. Domin (2009). "Epidermal growth factor stimulates translocation of the class II phosphoinositide 3-kinase PI3K-C2beta to the nucleus." Biochem J **422**(1): 53-60.

Bechtel, W., M. Helmstadter, J. Balica, B. Hartleben, B. Kiefer, F. Hrnjic, C. Schell, O. Kretz, S. Liu, F. Geist, D. Kerjaschki, G. Walz and T. B. Huber (2013). "Vps34 deficiency reveals the importance of endocytosis for podocyte homeostasis." J Am Soc Nephrol **24**(5): 727-743.

Beggs, A. H., J. Bohm, E. Snead, M. Kozlowski, M. Maurer, K. Minor, M. K. Childers, S. M. Taylor, C. Hitte, J. R. Mickelson, L. T. Guo, A. P. Mizisin, A. Buj-Bello, L. Tiret, J. Laporte and G. D. Shelton (2010). "MTM1 mutation associated with X-linked myotubular myopathy in Labrador Retrievers." Proc Natl Acad Sci U S A **107**(33): 14697-14702.

Berwick, D. C., G. C. Dell, G. I. Welsh, K. J. Heesom, I. Hers, L. M. Fletcher, F. T. Cooke and J. M. Tavare (2004). "Protein kinase B phosphorylation of PIKfyve regulates the trafficking of GLUT4 vesicles." J Cell Sci **117**(Pt 25): 5985-5993.

Blajecka, K., M. Marinov, L. Leitner, K. Uth, G. Posern and A. Arcaro (2012). "Phosphoinositide 3-kinase C2beta regulates RhoA and the actin cytoskeleton through an interaction with Dbl." PLoS One **7**(9): e44945.

Bodine, S. C., T. N. Stitt, M. Gonzalez, W. O. Kline, G. L. Stover, R. Bauerlein, E. Zlotchenko, A. Scrimgeour, J. C. Lawrence, D. J. Glass and G. D. Yancopoulos (2001). "Akt/mTOR pathway is a crucial regulator of skeletal muscle hypertrophy and can prevent muscle atrophy in vivo." Nat Cell Biol **3**(11): 1014-1019.

Bolino, A., A. Bolis, S. C. Previtali, G. Dina, S. Bussini, G. Dati, S. Amadio, U. Del Carro, D. D. Mruk, M. L. Feltri, C. Y. Cheng, A. Quattrini and L. Wrabetz (2004). "Disruption of Mtmr2 produces CMT4B1-like neuropathy with myelin outfolding and impaired spermatogenesis." J Cell Biol **167**(4): 711-721.

Bonangelino, C. J., N. L. Catlett and L. S. Weisman (1997). "Vac7p, a novel vacuolar protein, is required for normal vacuole inheritance and morphology." Mol Cell Biol **17**(12): 6847-6858.

Boss, W. F. and Y. J. Im (2012). "Phosphoinositide signaling." Annu Rev Plant Biol **63**: 409-429.

Bridges, D. and A. R. Saltiel (2012). "Phosphoinositides in insulin action and diabetes." Curr Top Microbiol Immunol **362**: 61-85.

Brooks, S. V. and J. A. Faulkner (1988). "Contractile properties of skeletal muscles from young, adult and aged mice." J Physiol **404**: 71-82.

Bruning, J. C., M. D. Michael, J. N. Winnay, T. Hayashi, D. Horsch, D. Accili, L. J. Goodyear and C. R. Kahn (1998). "A muscle-specific insulin receptor knockout exhibits features of the metabolic syndrome of NIDDM without altering glucose tolerance." Mol Cell **2**(5): 559-569.

Buj-Bello, A., V. Laugel, N. Messaddeq, H. Zahreddine, J. Laporte, J. F. Pellissier and J. L. Mandel (2002). "The lipid phosphatase myotubularin is essential for skeletal muscle maintenance but not for myogenesis in mice." Proc Natl Acad Sci U S A **99**(23): 15060-15065.

Cao, C., J. Laporte, J. M. Backer, A. Wandinger-Ness and M. P. Stein (2007). "Myotubularin lipid phosphatase binds the hVPS15/hVPS34 lipid kinase complex on endosomes." Traffic **8**(8): 1052-1067.

Chakrabarti, S., K. S. Kobayashi, R. A. Flavell, C. B. Marks, K. Miyake, D. R. Liston, K. T. Fowler, F. S. Gorelick and N. W. Andrews (2003). "Impaired membrane resealing and autoimmune myositis in synaptotagmin VII-deficient mice." J Cell Biol **162**(4): 543-549.

Chaussade, C., L. Pirola, S. Bonnafous, F. Blondeau, S. Brenz-Verca, H. Tronchere, F. Portis, S. Rusconi, B. Payrastre, J. Laporte and E. Van Obberghen (2003). "Expression of myotubularin by an adenoviral vector demonstrates its function as a phosphatidylinositol 3-phosphate [PtdIns(3)P] phosphatase in muscle cell lines: involvement of PtdIns(3)P in insulin-stimulated glucose transport." Mol Endocrinol **17**(12): 2448-2460.

Chen, J. K. (2013). "PIK3C3/VPS34, the class III PtdIns 3-kinase, plays indispensable roles in the podocyte." Autophagy **9**(6).

Chow, C. Y., J. E. Landers, S. K. Bergren, P. C. Sapp, A. E. Grant, J. M. Jones, L. Everett, G. M. Lenk, D. M. McKenna-Yasek, L. S. Weisman, D. Figlewicz, R. H. Brown and M. H. Meisler (2009). "Deleterious variants of FIG4, a phosphoinositide phosphatase, in patients with ALS." Am J Hum Genet **84**(1): 85-88.

Chow, C. Y., Y. Zhang, J. J. Dowling, N. Jin, M. Adamska, K. Shiga, K. Szigeti, M. E. Shy, J. Li, X. Zhang, J. R. Lupski, L. S. Weisman and M. H. Meisler (2007). "Mutation of FIG4 causes neurodegeneration in the pale tremor mouse and patients with CMT4J." Nature **448**(7149): 68-72.

Clague, M. J. and O. Lorenzo (2005). "The myotubularin family of lipid phosphatases." Traffic **6**(12): 1063-1069.

Codogno, P., M. Mehrpour and T. Proikas-Cezanne (2012). "Canonical and non-canonical autophagy: variations on a common theme of self-eating?" Nat Rev Mol Cell Biol **13**(1): 7-12.

Daimon, M., H. Sato, T. Oizumi, S. Toriyama, T. Saito, S. Karasawa, Y. Jimbu, K. Wada, W. Kameda, S. Susa, H. Yamaguchi, M. Emi, M. Muramatsu, I. Kubota, S. Kawata and T. Kato (2008). "Association of the PIK3C2G gene polymorphisms with type 2 DM in a Japanese population." Biochem Biophys Res Commun **365**(3): 466-471.

Das, S., J. Dowling and C. R. Pierson (2011). X-Linked Centronuclear Myopathy. GeneReviews™ [Internet]. A. M. Pagon RA, Bird TD, et al. Seattle (WA): University of Washington, Seattle; 1993-2013.

De Camilli, P., S. D. Emr, P. S. McPherson and P. Novick (1996). "Phosphoinositides as regulators in membrane traffic." Science **271**(5255): 1533-1539.

Di Paolo, G. and P. De Camilli (2006). "Phosphoinositides in cell regulation and membrane dynamics." Nature **443**(7112): 651-657.

Domin, J., L. Harper, D. Aubyn, M. Wheeler, O. Florey, D. Haskard, M. Yuan and D. Zicha (2005). "The class II phosphoinositide 3-kinase PI3K-C2beta regulates cell migration by a PtdIns3P dependent mechanism." J Cell Physiol **205**(3): 452-462.

Dominguez, V., C. Raimondi, S. Somanath, M. Bugliani, M. K. Loder, C. E. Edling, N. Divecha, G. da Silva-Xavier, L. Marselli, S. J. Persaud, M. D. Turner, G. A. Rutter, P. Marchetti, M. Falasca and T. Maffucci (2011). "Class II phosphoinositide 3-kinase regulates exocytosis of insulin granules in pancreatic beta cells." J Biol Chem **286**(6): 4216-4225.

Dove, S. K., F. T. Cooke, M. R. Douglas, L. G. Sayers, P. J. Parker and R. H. Michell (1997). "Osmotic stress activates phosphatidylinositol-3,5-bisphosphate synthesis." Nature **390**(6656): 187-192.

Dowling, J. J., R. Joubert, S. E. Low, A. N. Durban, N. Messaddeq, X. Li, A. N. Dulin-Smith, A. D. Snyder, M. L. Marshall, J. T. Marshall, A. H. Beggs, A. Buj-Bello and C. R. Pierson (2012). "Myotubular myopathy and the neuromuscular junction: a novel therapeutic approach from mouse models." Dis Model Mech **5**(6): 852-859.

Dowling, J. J., S. E. Low, A. S. Busta and E. L. Feldman (2010). "Zebrafish MTMR14 is required for excitation-contraction coupling, developmental motor function and the regulation of autophagy." Hum Mol Genet **19**(13): 2668-2681.

Dowling, J. J., A. P. Vreede, S. E. Low, E. M. Gibbs, J. Y. Kuwada, C. G. Bonnemann and E. L. Feldman (2009). "Loss of myotubularin function results in T-tubule disorganization in zebrafish and human myotubular myopathy." PLoS Genet **5**(2): e1000372.

Duex, J. E., F. Tang and L. S. Weisman (2006). "The Vac14p-Fig4p complex acts independently of Vac7p and couples PI3,5P2 synthesis and turnover." J Cell Biol **172**(5): 693-704.

Dyson, J. M., C. G. Fedele, E. M. Davies, J. Becanovic and C. A. Mitchell (2012). "Phosphoinositide phosphatases: just as important as the kinases." Subcell Biochem **58**: 215-279.

Falasca, M. (2012). Phosphoinositides and Disease. Dordrecht, Springer Netherlands : Imprint: Springer.

Falasca, M., W. E. Hughes, V. Dominguez, G. Sala, F. Fostira, M. Q. Fang, R. Cazzolli, P. R. Shepherd, D. E. James and T. Maffucci (2007). "The role of phosphoinositide 3-kinase C2alpha in insulin signaling." J Biol Chem **282**(38): 28226-28236.

Falasca, M. and T. Maffucci (2007). "Role of class II phosphoinositide 3-kinase in cell signalling." Biochem Soc Trans **35**(Pt 2): 211-214.

Ferguson, C. J., G. M. Lenk, J. M. Jones, A. E. Grant, J. J. Winters, J. J. Dowling, R. J. Giger and M. H. Meisler (2012). "Neuronal expression of Fig4 is both necessary and sufficient to prevent spongiform neurodegeneration." Hum Mol Genet **21**(16): 3525-3534.

Ferguson, C. J., G. M. Lenk and M. H. Meisler (2009). "Defective autophagy in neurons and astrocytes from mice deficient in PI(3,5)P2." Hum Mol Genet **18**(24): 4868-4878.

Fisher, S. K., J. E. Novak and B. W. Agranoff (2002). "Inositol and higher inositol phosphates in neural tissues: homeostasis, metabolism and functional significance." J Neurochem **82**(4): 736-754.

Foster, F. M., C. J. Traer, S. M. Abraham and M. J. Fry (2003). "The phosphoinositide (PI) 3-kinase family." J Cell Sci **116**(Pt 15): 3037-3040.

Funderburk, S. F., Q. J. Wang and Z. Yue (2010). "The Beclin 1-VPS34 complex--at the crossroads of autophagy and beyond." Trends Cell Biol **20**(6): 355-362.

Furuya, N., J. Yu, M. Byfield, S. Pattingre and B. Levine (2005). "The evolutionarily conserved domain of Beclin 1 is required for Vps34 binding, autophagy and tumor suppressor function." Autophagy **1**(1): 46-52.

Futter, C. E., L. M. Collinson, J. M. Backer and C. R. Hopkins (2001). "Human VPS34 is required for internal vesicle formation within multivesicular endosomes." J Cell Biol **155**(7): 1251-1264.

Gary, J. D., T. K. Sato, C. J. Stefan, C. J. Bonangelino, L. S. Weisman and S. D. Emr (2002). "Regulation of Fab1 phosphatidylinositol 3-phosphate 5-kinase pathway by Vac7 protein and Fig4, a polyphosphoinositide phosphatase family member." Mol Biol Cell **13**(4): 1238-1251.

Gibbs, E. M., E. L. Feldman and J. J. Dowling (2010). "The role of MTMR14 in autophagy and in muscle disease." Autophagy **6**(6): 819-820.

Gibbs, E. M., E. J. Horstick and J. J. Dowling (2013). "Swimming into prominence: the zebrafish as a valuable tool for studying human myopathies and muscular dystrophies." FEBS J **280**(17): 4187-4197.

Gillooly, D. J., I. C. Morrow, M. Lindsay, R. Gould, N. J. Bryant, J. M. Gaullier, R. G. Parton and H. Stenmark (2000). "Localization of phosphatidylinositol 3-phosphate in yeast and mammalian cells." EMBO J **19**(17): 4577-4588.

Glass, D. J. (2010). "PI3 kinase regulation of skeletal muscle hypertrophy and atrophy." Curr Top Microbiol Immunol **346**: 267-278.

Grounds, M. D. and T. Shavlakadze (2011). "Growing muscle has different sarcolemmal properties from adult muscle: a proposal with scientific and clinical implications: reasons to reassess skeletal muscle molecular dynamics, cellular responses and suitability of experimental models of muscle disorders." Bioessays **33**(6): 458-468.

Gumerson, J. D., C. S. Davis, Z. T. Kabaeva, J. M. Hayes, S. V. Brooks and D. E. Michele (2013). "Muscle-specific expression of LARGE restores neuromuscular transmission deficits in dystrophic LARGE(myd) mice." Hum Mol Genet **22**(4): 757-768.

Hakim, S., M. C. Bertucci, S. E. Conduit, D. L. Vuong and C. A. Mitchell (2012). "Inositol polyphosphate phosphatases in human disease." Curr Top Microbiol Immunol **362**: 247-314.

Hamilton, D. L., A. Philp, M. G. MacKenzie and K. Baar (2010). "A limited role for PI(3,4,5)P3 regulation in controlling skeletal muscle mass in response to resistance exercise." PLoS One **5**(7): e11624.

Han, B. K. and S. D. Emr (2011). "Phosphoinositide [PI(3,5)P2] lipid-dependent regulation of the general transcriptional regulator Tup1." Genes Dev **25**(9): 984-995.

Harada, K., A. B. Truong, T. Cai and P. A. Khavari (2005). "The class II phosphoinositide 3-kinase C2beta is not essential for epidermal differentiation." Mol Cell Biol **25**(24): 11122-11130.

Herman, P. K. and S. D. Emr (1990). "Characterization of VPS34, a gene required for vacuolar protein sorting and vacuole segregation in Saccharomyces cerevisiae." Mol Cell Biol **10**(12): 6742-6754.

Hertel, F., A. Switalski, E. Mintert-Jancke, K. Karavassilidou, K. Bender, L. Pott and M. C. Kienitz (2011). "A genetically encoded tool kit for manipulating and monitoring membrane phosphatidylinositol 4,5-bisphosphate in intact cells." PLoS One **6**(6): e20855.

Hnia, K., H. Tronchere, K. K. Tomczak, L. Amoasii, P. Schultz, A. H. Beggs, B. Payrastre, J. L. Mandel and J. Laporte (2011). "Myotubularin controls desmin intermediate filament architecture and mitochondrial dynamics in human and mouse skeletal muscle." J Clin Invest **121**(1): 70-85.

Hnia, K., I. Vaccari, A. Bolino and J. Laporte (2012). "Myotubularin phosphoinositide phosphatases: cellular functions and disease pathophysiology." Trends Mol Med **18**(6): 317-327.

Ho, C. Y., T. A. Alghamdi and R. J. Botelho (2012). "Phosphatidylinositol-3,5-bisphosphate: no longer the poor PIP2." Traffic **13**(1): 1-8.

Ikonomov, O. C., D. Sbrissa, K. Delvecchio, H. Z. Feng, G. D. Cartee, J. P. Jin and A. Shisheva (2013). "Muscle-specific Pikfyve gene disruption causes glucose intolerance, insulin resistance, adiposity, and hyperinsulinemia but not muscle fiber-type switching." Am J Physiol Endocrinol Metab **305**(1): E119-131.

Ikonomov, O. C., D. Sbrissa, K. Delvecchio, Y. Xie, J. P. Jin, D. Rappolee and A. Shisheva (2011). "The phosphoinositide kinase PIKfyve is vital in early embryonic development: preimplantation lethality of PIKfyve-/- embryos but normality of PIKfyve+/- mice." J Biol Chem **286**(15): 13404-13413.

Ikonomov, O. C., D. Sbrissa, R. Dondapati and A. Shisheva (2007). "ArPIKfyve-PIKfyve interaction and role in insulin-regulated GLUT4 translocation and glucose transport in 3T3-L1 adipocytes." Exp Cell Res **313**(11): 2404-2416.

Ikonomov, O. C., D. Sbrissa, J. Fligger, K. Delvecchio and A. Shisheva (2010). "ArPIKfyve regulates Sac3 protein abundance and turnover: disruption of the mechanism

by Sac3I41T mutation causing Charcot-Marie-Tooth 4J disorder." J Biol Chem **285**(35): 26760-26764.

Ikonomov, O. C., D. Sbrissa, K. Mlak, M. Kanzaki, J. Pessin and A. Shisheva (2002). "Functional dissection of lipid and protein kinase signals of PIKfyve reveals the role of PtdIns 3,5-P2 production for endomembrane integrity." J Biol Chem **277**(11): 9206-9211.

Itakura, E., C. Kishi, K. Inoue and N. Mizushima (2008). "Beclin 1 forms two distinct phosphatidylinositol 3-kinase complexes with mammalian Atg14 and UVRAG." Mol Biol Cell **19**(12): 5360-5372.

Itoh, T. and T. Takenawa (2002). "Phosphoinositide-binding domains: Functional units for temporal and spatial regulation of intracellular signalling." Cell Signal **14**(9): 733-743.

Jaber, N., Z. Dou, J. S. Chen, J. Catanzaro, Y. P. Jiang, L. M. Ballou, E. Selinger, X. Ouyang, R. Z. Lin, J. Zhang and W. X. Zong (2012). "Class III PI3K Vps34 plays an essential role in autophagy and in heart and liver function." Proc Natl Acad Sci U S A **109**(6): 2003-2008.

Jaber, N., Z. Dou, R. Z. Lin, J. Zhang and W. X. Zong (2012). "Mammalian PIK3C3/VPS34: the key to autophagic processing in liver and heart." Autophagy **8**(4): 707-708.

Jin, N., C. Y. Chow, L. Liu, S. N. Zolov, R. Bronson, M. Davisson, J. L. Petersen, Y. Zhang, S. Park, J. E. Duex, D. Goldowitz, M. H. Meisler and L. S. Weisman (2008). "VAC14 nucleates a protein complex essential for the acute interconversion of PI3P and PI(3,5)P(2) in yeast and mouse." EMBO J **27**(24): 3221-3234.

Johnson, E. E., J. H. Overmeyer, W. T. Gunning and W. A. Maltese (2006). "Gene silencing reveals a specific function of hVps34 phosphatidylinositol 3-kinase in late versus early endosomes." J Cell Sci **119**(Pt 7): 1219-1232.

Jungbluth, H., C. Wallgren-Pettersson and J. Laporte (2008). "Centronuclear (myotubular) myopathy." Orphanet J Rare Dis **3**: 26.

Jungbluth, H., H. Zhou, C. A. Sewry, S. Robb, S. Treves, M. Bitoun, P. Guicheney, A. Buj-Bello, C. Bonnemann and F. Muntoni (2007). "Centronuclear myopathy due to a de novo dominant mutation in the skeletal muscle ryanodine receptor (RYR1) gene." Neuromuscul Disord **17**(4): 338-345.

Katso, R. M., O. E. Pardo, A. Palamidessi, C. M. Franz, M. Marinov, A. De Laurentiis, J. Downward, G. Scita, A. J. Ridley, M. D. Waterfield and A. Arcaro (2006).

"Phosphoinositide 3-Kinase C2beta regulates cytoskeletal organization and cell migration via Rac-dependent mechanisms." Mol Biol Cell **17**(9): 3729-3744.

Kihara, A., T. Noda, N. Ishihara and Y. Ohsumi (2001). "Two distinct Vps34 phosphatidylinositol 3-kinase complexes function in autophagy and carboxypeptidase Y sorting in Saccharomyces cerevisiae." J Cell Biol **152**(3): 519-530.

Kukkonen, J. P. (2011). "A menage a trois made in heaven: G-protein-coupled receptors, lipids and TRP channels." Cell Calcium **50**(1): 9-26.

Laporte, J., F. Bedez, A. Bolino and J. L. Mandel (2003). "Myotubularins, a large disease-associated family of cooperating catalytically active and inactive phosphoinositides phosphatases." Hum Mol Genet **12 Spec No 2**: R285-292.

Laporte, J., L. J. Hu, C. Kretz, J. L. Mandel, P. Kioschis, J. F. Coy, S. M. Klauck, A. Poustka and N. Dahl (1996). "A gene mutated in X-linked myotubular myopathy defines a new putative tyrosine phosphatase family conserved in yeast." Nat Genet **13**(2): 175-182.

Lecompte, O., O. Poch and J. Laporte (2008). "PtdIns5P regulation through evolution: roles in membrane trafficking?" Trends Biochem Sci **33**(10): 453-460.

Leibiger, B., T. Moede, S. Uhles, C. J. Barker, M. Creveaux, J. Domin, P. O. Berggren and I. B. Leibiger (2010). "Insulin-feedback via PI3K-C2alpha activated PKBalpha/Akt1 is required for glucose-stimulated insulin secretion." FASEB J **24**(6): 1824-1837.

Lemmon, M. A. (2003). "Phosphoinositide recognition domains." Traffic **4**(4): 201-213.

Lenk, G. M., C. J. Ferguson, C. Y. Chow, N. Jin, J. M. Jones, A. E. Grant, S. N. Zolov, J. J. Winters, R. J. Giger, J. J. Dowling, L. S. Weisman and M. H. Meisler (2011). "Pathogenic mechanism of the FIG4 mutation responsible for Charcot-Marie-Tooth disease CMT4J." PLoS Genet **7**(6): e1002104.

Lenk, G. M. and M. H. Meisler (2013). "Mouse models with defects in PI(3,5)P2 and impaired endolysosome function." Methods Enzymol **in press**.

Lindmo, K. and H. Stenmark (2006). "Regulation of membrane traffic by phosphoinositide 3-kinases." J Cell Sci **119**(Pt 4): 605-614.

Lodhi, I. J., D. Bridges, S. H. Chiang, Y. Zhang, A. Cheng, L. M. Geletka, L. S. Weisman and A. R. Saltiel (2008). "Insulin stimulates phosphatidylinositol 3-phosphate production via the activation of Rab5." Mol Biol Cell **19**(7): 2718-2728.

Maffucci, T. (2012). "An introduction to phosphoinositides." Curr Top Microbiol Immunol **362**: 1-42.

Maffucci, T., A. Brancaccio, E. Piccolo, R. C. Stein and M. Falasca (2003). "Insulin induces phosphatidylinositol-3-phosphate formation through TC10 activation." EMBO J **22**(16): 4178-4189.

Maffucci, T., F. T. Cooke, F. M. Foster, C. J. Traer, M. J. Fry and M. Falasca (2005). "Class II phosphoinositide 3-kinase defines a novel signaling pathway in cell migration." J Cell Biol **169**(5): 789-799.

Malicdan, M. C. and I. Nishino (2012). "Autophagy in lysosomal myopathies." Brain Pathol **22**(1): 82-88.

Mammucari, C., G. Milan, V. Romanello, E. Masiero, R. Rudolf, P. Del Piccolo, S. J. Burden, R. Di Lisi, C. Sandri, J. Zhao, A. L. Goldberg, S. Schiaffino and M. Sandri (2007). "FoxO3 controls autophagy in skeletal muscle in vivo." Cell Metab **6**(6): 458-471.

Masiero, E., L. Agatea, C. Mammucari, B. Blaauw, E. Loro, M. Komatsu, D. Metzger, C. Reggiani, S. Schiaffino and M. Sandri (2009). "Autophagy is required to maintain muscle mass." Cell Metab **10**(6): 507-515.

McCartney, A., Y. Zhang and L. Weisman (2013). "Phosphatidylinositol 3,5-bis phosphate: low abundance, high significance." Bioessays **in press**.

Meijer, A. J. and D. J. Klionsky (2011). "Vps34 is a phosphatidylinositol 3-kinase, not a phosphoinositide 3-kinase." Autophagy **7**(6): 563-564.

Michell, R. H., V. L. Heath, M. A. Lemmon and S. K. Dove (2006). "Phosphatidylinositol 3,5-bisphosphate: metabolism and cellular functions." Trends Biochem Sci **31**(1): 52-63.

Millay, D. P., M. Maillet, J. A. Roche, M. A. Sargent, E. M. McNally, R. J. Bloch and J. D. Molkentin (2009). "Genetic manipulation of dysferlin expression in skeletal muscle: novel insights into muscular dystrophy." Am J Pathol **175**(5): 1817-1823.

Miller, S., B. Tavshanjian, A. Oleksy, O. Perisic, B. T. Houseman, K. M. Shokat and R. L. Williams (2010). "Shaping development of autophagy inhibitors with the structure of the lipid kinase Vps34." Science **327**(5973): 1638-1642.

Nance, J. R., J. J. Dowling, E. M. Gibbs and C. G. Bonnemann (2012). "Congenital myopathies: an update." Curr Neurol Neurosci Rep **12**(2): 165-174.

Narayan, K. and M. A. Lemmon (2006). "Determining selectivity of phosphoinositide-binding domains." Methods **39**(2): 122-133.

Nemazanyy, I., B. Blaauw, C. Paolini, C. Caillaud, F. Protasi, A. Mueller, T. Proikas-Cezanne, R. C. Russell, K. L. Guan, I. Nishino, M. Sandri, M. Pende and G. Panasyuk (2013). "Defects of Vps15 in skeletal muscles lead to autophagic vacuolar myopathy and lysosomal disease." EMBO Mol Med **5**(6): 870-890.

Nicholson, G., G. M. Lenk, S. W. Reddel, A. E. Grant, C. F. Towne, C. J. Ferguson, E. Simpson, A. Scheuerle, M. Yasick, S. Hoffman, R. Blouin, C. Brandt, G. Coppola, L. G. Biesecker, S. D. Batish and M. H. Meisler (2011). "Distinctive genetic and clinical features of CMT4J: a severe neuropathy caused by mutations in the PI(3,5)P(2) phosphatase FIG4." Brain **134**(Pt 7): 1959-1971.

Nicot, A. S. and J. Laporte (2008). "Endosomal phosphoinositides and human diseases." Traffic **9**(8): 1240-1249.

Nishida, Y., S. Arakawa, K. Fujitani, H. Yamaguchi, T. Mizuta, T. Kanaseki, M. Komatsu, K. Otsu, Y. Tsujimoto and S. Shimizu (2009). "Discovery of Atg5/Atg7-independent alternative macroautophagy." Nature **461**(7264): 654-658.

Nishino, I. (2003). "Autophagic vacuolar myopathies." Curr Neurol Neurosci Rep **3**(1): 64-69.

Nobukuni, T., S. C. Kozma and G. Thomas (2007). "hvps34, an ancient player, enters a growing game: mTOR Complex1/S6K1 signaling." Curr Opin Cell Biol **19**(2): 135-141.

North, K. (2008). "What's new in congenital myopathies?" Neuromuscul Disord **18**(6): 433-442.

Payrastre, B. (2004). "Phosphoinositides: lipid kinases and phosphatases." Methods Mol Biol **273**: 201-212.

Pierson, C. R., P. B. Agrawal, J. Blasko and A. H. Beggs (2007). "Myofiber size correlates with MTM1 mutation type and outcome in X-linked myotubular myopathy." Neuromuscul Disord **17**(7): 562-568.

Pierson, C. R., A. N. Dulin-Smith, A. N. Durban, M. L. Marshall, J. T. Marshall, A. D. Snyder, N. Naiyer, J. T. Gladman, D. S. Chandler, M. W. Lawlor, A. Buj-Bello, J. J. Dowling and A. H. Beggs (2012). "Modeling the human MTM1 p.R69C mutation in murine Mtm1 results in exon 4 skipping and a less severe myotubular myopathy phenotype." Hum Mol Genet **21**(4): 811-825.

Raben, N., V. Hill, L. Shea, S. Takikita, R. Baum, N. Mizushima, E. Ralston and P. Plotz (2008). "Suppression of autophagy in skeletal muscle uncovers the accumulation of ubiquitinated proteins and their potential role in muscle damage in Pompe disease." Hum Mol Genet **17**(24): 3897-3908.

Raben, N., A. Roberts and P. H. Plotz (2007). "Role of autophagy in the pathogenesis of Pompe disease." Acta Myol **26**(1): 45-48.

Rahimov, F. and L. M. Kunkel (2013). "The cell biology of disease: cellular and molecular mechanisms underlying muscular dystrophy." J Cell Biol **201**(4): 499-510.

Razidlo, G. L., D. Katafiasz and G. S. Taylor (2011). "Myotubularin regulates Akt-dependent survival signaling via phosphatidylinositol 3-phosphate." J Biol Chem **286**(22): 20005-20019.

Reifler, A., G. M. Lenk, X. Li, L. Groom, S. V. Brooks, D. Wilson, M. Bowerson, R. T. Dirksen, M. H. Meisler and J. J. Dowling (2013). "Murine Fig4 is dispensable for muscle development but required for muscle function." Skelet Muscle **3**(1): 21.

Robinson, F. L. and J. E. Dixon (2006). "Myotubularin phosphatases: policing 3-phosphoinositides." Trends Cell Biol **16**(8): 403-412.

Rodon, J., R. Dienstmann, V. Serra and J. Tabernero (2013). "Development of PI3K inhibitors: lessons learned from early clinical trials." Nat Rev Clin Oncol **10**(3): 143-153.

Romero-Suarez, S., J. Shen, L. Brotto, T. Hall, C. Mo, H. H. Valdivia, J. Andresen, M. Wacker, T. M. Nosek, C. K. Qu and M. Brotto (2010). "Muscle-specific inositide phosphatase (MIP/MTMR14) is reduced with age and its loss accelerates skeletal muscle aging process by altering calcium homeostasis." Aging (Albany NY) **2**(8): 504-513.

Rommel, C., B. Vanhaesebroeck, P. K. Vogt and SpringerLink (Online service) (2011). Phosphoinositide 3-kinase in Health and Disease Volume 1. Berlin, Heidelberg, Springer-Verlag Berlin Heidelberg.

Rozycka, M., Y. J. Lu, R. A. Brown, M. R. Lau, J. M. Shipley and M. J. Fry (1998). "cDNA cloning of a third human C2-domain-containing class II phosphoinositide 3-kinase, PI3K-C2gamma, and chromosomal assignment of this gene (PIK3C2G) to 12p12." Genomics **54**(3): 569-574.

Samie, M., X. Wang, X. Zhang, A. Goschka, X. Li, X. Cheng, E. Gregg, M. Azar, Y. Zhuo, A. G. Garrity, Q. Gao, S. Slaugenhaupt, J. Pickel, S. N. Zolov, L. S. Weisman, G. M. Lenk, S. Titus, M. Bryant-Genevier, N. Southall, M. Juan, M. Ferrer and H. Xu

(2013). "A TRP Channel in the Lysosome Regulates Large Particle Phagocytosis via Focal Exocytosis." Dev Cell.

Sandri, M. (2010). "Autophagy in skeletal muscle." FEBS Lett **584**(7): 1411-1416.

Sbrissa, D., O. C. Ikonomov, Z. Fu, T. Ijuin, J. Gruenberg, T. Takenawa and A. Shisheva (2007). "Core protein machinery for mammalian phosphatidylinositol 3,5-bisphosphate synthesis and turnover that regulates the progression of endosomal transport. Novel Sac phosphatase joins the ArPIKfyve-PIKfyve complex." J Biol Chem **282**(33): 23878-23891.

Shen, D., X. Wang and H. Xu (2011). "Pairing phosphoinositides with calcium ions in endolysosomal dynamics: phosphoinositides control the direction and specificity of membrane trafficking by regulating the activity of calcium channels in the endolysosomes." Bioessays **33**(6): 448-457.

Shen, J., W. M. Yu, M. Brotto, J. A. Scherman, C. Guo, C. Stoddard, T. M. Nosek, H. H. Valdivia and C. K. Qu (2009). "Deficiency of MIP/MTMR14 phosphatase induces a muscle disorder by disrupting Ca(2+) homeostasis." Nat Cell Biol **11**(6): 769-776.

Shin, J., M. M. Tajrishi, Y. Ogura and A. Kumar (2013). "Wasting mechanisms in muscular dystrophy." Int J Biochem Cell Biol.

Smith, P. B. and S. H. Appel (1977). "Isolation and characterization of the surface membranes of fast and slow mammalian skeletal muscle." Biochim Biophys Acta **466**(1): 109-122.

Soos, M. A., J. Jensen, R. A. Brown, S. O'Rahilly, P. R. Shepherd and J. P. Whitehead (2001). "Class II phosphoinositide 3-kinase is activated by insulin but not by contraction in skeletal muscle." Arch Biochem Biophys **396**(2): 244-248.

Srivastava, S., L. Di, O. Zhdanova, Z. Li, S. Vardhana, Q. Wan, Y. Yan, R. Varma, J. Backer, H. Wulff, M. L. Dustin and E. Y. Skolnik (2009). "The class II phosphatidylinositol 3 kinase C2beta is required for the activation of the K+ channel KCa3.1 and CD4 T-cells." Mol Biol Cell **20**(17): 3783-3791.

Stack, J. H., P. K. Herman, P. V. Schu and S. D. Emr (1993). "A membrane-associated complex containing the Vps15 protein kinase and the Vps34 PI 3-kinase is essential for protein sorting to the yeast lysosome-like vacuole." EMBO J **12**(5): 2195-2204.

Stein, M. P., C. Cao, M. Tessema, Y. Feng, E. Romero, A. Welford and A. Wandinger-Ness (2005). "Interaction and functional analyses of human VPS34/p150 phosphatidylinositol 3-kinase complex with Rab7." Methods Enzymol **403**: 628-649.

Strahl, T. and J. Thorner (2007). "Synthesis and function of membrane phosphoinositides in budding yeast, Saccharomyces cerevisiae." Biochim Biophys Acta **1771**(3): 353-404.

Taylor, G. S., T. Maehama and J. E. Dixon (2000). "Myotubularin, a protein tyrosine phosphatase mutated in myotubular myopathy, dephosphorylates the lipid second messenger, phosphatidylinositol 3-phosphate." Proc Natl Acad Sci U S A **97**(16): 8910-8915.

Tosch, V., H. M. Rohde, H. Tronchere, E. Zanoteli, N. Monroy, C. Kretz, N. Dondaine, B. Payrastre, J. L. Mandel and J. Laporte (2006). "A novel PtdIns3P and PtdIns(3,5)P2 phosphatase with an inactivating variant in centronuclear myopathy." Hum Mol Genet **15**(21): 3098-3106.

Touchberry, C. D., I. K. Bales, J. K. Stone, T. J. Rohrberg, N. K. Parelkar, T. Nguyen, O. Fuentes, X. Liu, C. K. Qu, J. J. Andresen, H. H. Valdivia, M. Brotto and M. J. Wacker (2010). "Phosphatidylinositol 3,5-bisphosphate (PI(3,5)P2) potentiates cardiac contractility via activation of the ryanodine receptor." J Biol Chem **285**(51): 40312-40321.

Tronchere, H., J. Laporte, C. Pendaries, C. Chaussade, L. Liaubet, L. Pirola, J. L. Mandel and B. Payrastre (2004). "Production of phosphatidylinositol 5-phosphate by the phosphoinositide 3-phosphatase myotubularin in mammalian cells." J Biol Chem **279**(8): 7304-7312.

Tsujita, K., T. Itoh, A. Kondo, M. Oyama, H. Kozuka-Hata, Y. Irino, J. Hasegawa and T. Takenawa (2010). "Proteome of acidic phospholipid-binding proteins: spatial and temporal regulation of Coronin 1A by phosphoinositides." J Biol Chem **285**(9): 6781-6789.

Vaccari, I., G. Dina, H. Tronchere, E. Kaufman, G. Chicanne, F. Cerri, L. Wrabetz, B. Payrastre, A. Quattrini, L. S. Weisman, M. H. Meisler and A. Bolino (2011). "Genetic interaction between MTMR2 and FIG4 phospholipid phosphatases involved in Charcot-Marie-Tooth neuropathies." PLoS Genet **7**(10): e1002319.

Vanhaesebroeck, B., J. Guillermet-Guibert, M. Graupera and B. Bilanges (2010). "The emerging mechanisms of isoform-specific PI3K signalling." Nat Rev Mol Cell Biol **11**(5): 329-341.

Vergne, I. and V. Deretic (2010). "The role of PI3P phosphatases in the regulation of autophagy." FEBS Lett **584**(7): 1313-1318.

Volpicelli-Daley, L. and P. De Camilli (2007). "Phosphoinositides' link to neurodegeneration." Nat Med **13**(7): 784-786.

Wang, L., K. Budolfson and F. Wang (2011). "Pik3c3 deletion in pyramidal neurons results in loss of synapses, extensive gliosis and progressive neurodegeneration." Neuroscience **172**: 427-442.

Weisman, L. S. (2006). "Organelles on the move: insights from yeast vacuole inheritance." Nat Rev Mol Cell Biol **7**(4): 243-252.

Wheeler, M. and J. Domin (2006). "The N-terminus of phosphoinositide 3-kinase-C2beta regulates lipid kinase activity and binding to clathrin." J Cell Physiol **206**(3): 586-593.

Whiteford, C. C., C. A. Brearley and E. T. Ulug (1997). "Phosphatidylinositol 3,5-bisphosphate defines a novel PI 3-kinase pathway in resting mouse fibroblasts." Biochem J **323 (Pt 3)**: 597-601.

Willinger, T. and R. A. Flavell (2012). "Canonical autophagy dependent on the class III phosphoinositide-3 kinase Vps34 is required for naive T-cell homeostasis." Proc Natl Acad Sci U S A **109**(22): 8670-8675.

Winters, J. J., C. J. Ferguson, G. M. Lenk, V. I. Giger-Mateeva, P. Shrager, M. H. Meisler and R. J. Giger (2011). "Congenital CNS hypomyelination in the Fig4 null mouse is rescued by neuronal expression of the PI(3,5)P(2) phosphatase Fig4." J Neurosci **31**(48): 17736-17751.

Workman, P. and R. L. van Montfort (2010). "Unveiling the secrets of the ancestral PI3 kinase Vps34." Cancer Cell **17**(5): 421-423.

Yamamoto, A., D. B. DeWald, I. V. Boronenkov, R. A. Anderson, S. D. Emr and D. Koshland (1995). "Novel PI(4)P 5-kinase homologue, Fab1p, essential for normal vacuole function and morphology in yeast." Mol Biol Cell **6**(5): 525-539.

Yan, Y. and J. M. Backer (2007). "Regulation of class III (Vps34) PI3Ks." Biochem Soc Trans **35**(Pt 2): 239-241.

Yu, J. W., J. M. Mendrola, A. Audhya, S. Singh, D. Keleti, D. B. DeWald, D. Murray, S. D. Emr and M. A. Lemmon (2004). "Genome-wide analysis of membrane targeting by S. cerevisiae pleckstrin homology domains." Mol Cell **13**(5): 677-688.

Zhou, X., J. Takatoh and F. Wang (2011). "The mammalian class 3 PI3K (PIK3C3) is required for early embryogenesis and cell proliferation." PLoS One **6**(1): e16358.

Zhou, X., L. Wang, H. Hasegawa, P. Amin, B. X. Han, S. Kaneko, Y. He and F. Wang (2010). "Deletion of PIK3C3/Vps34 in sensory neurons causes rapid neurodegeneration

by disrupting the endosomal but not the autophagic pathway." Proc Natl Acad Sci U S A **107**(20): 9424-9429.

Zolov, S. N., D. Bridges, Y. Zhang, W. W. Lee, E. Riehle, R. Verma, G. M. Lenk, K. Converso-Baran, T. Weide, R. L. Albin, A. R. Saltiel, M. H. Meisler, M. W. Russell and L. S. Weisman (2012). "In vivo, Pikfyve generates PI(3,5)P2, which serves as both a signaling lipid and the major precursor for PI5P." Proc Natl Acad Sci U S A **109**(43): 17472-17477.